Real-Time Imaging of Hippocampal Network Dynamics Reveals Trisynaptic Induction of CA1 LTP and "Circuit-Level" Effects of Chronic Stress and Antidepressants

Dissertation

der Fakultät für Biologie

der Ludwig-Maximilians-Universität

München

vorgelegt von Jens Stepan

München, 16. Juni 2014

Erstgutachter: Prof. Dr. Rainer Landgraf

Zweitgutachter: Prof. Dr. George Boyan

Tag der mündlichen Prüfung: 15. April 2015

Contents

Abbreviations

ACTH ..... adrenocorticotropic hormone, page 11
AD ..... antidepressant, page 1
AMPA ..... α-amino-3-hydroxy-5-methyl-4-isoxazolepoprionic acid, page 9
AMY ..... amygdala, page 7
ANOVA ..... analysis of variance, page 31
AXDs ..... anxiety disorders, page 1
BDNF ..... brain-derived neurotrophic factor, page 18
BIM ..... bicuculline methiodide, page 24
c/a ..... commissural/associational, page 7
CA ..... cornu ammonis, page 3
CCD ..... charged coupled device, page 25
CIS ..... chronic immobilization stress, page 72
CMS ..... chronic mild stress, page 72
CORT ..... corticosterone, page 12
CRH ..... corticotropin releasing hormone, page 11
CSDS ..... chronic social defeat stress, page 22
CTRL ..... control, page 49
CUS ..... chronic unpredictable stress, page 72
CVS ..... chronic variable stress, page 72
DG ..... dentate gyrus, page 3
DGS ..... dentate gyrus supra, page 28
DMSO ..... dimethyl sulfoxide, page 24
EC ..... entorhinal cortex, page 3
EPSP ..... exitatory postsynaptic potential, page 9
FDS ..... fast depolarization-mediated signal, page 27
fEPSP ..... field exitatory postsynaptic potential, page 24
FLUO ..... fluorescein, page 29
FST ..... forced swim test, page 74
GABA ..... gamma aminobutyric acid, page 7
GC ..... glucocorticoids, page 11
GCL ..... granule cell layer, page 4
GPCRs ..... G-protein-coupled receptors, page 12
GR ..... glucocorticoid receptor, page 12

HCN1 ..... hyperpolarization-activated cyclic nucleotide-gated 1 channels, page 74
HF ..... hippocampal formation, page 3
HIP ..... hippocampus, page 2
HPA ..... hypothalamic-pituitary-adrenal, page 11
HTC ..... hippocampal trisynaptic circuit, page 24
LEC ..... lateral entorhinal cortex, page 4
LTD ..... long-term depression, page 8
LTP ..... long-term potentiation, page 2
MAO ..... monoamine-oxidase, page 17
MAOI ..... monoamine-oxidase inhibitor, page 17
MD ..... major depression, page 1
MEC ..... medial entorhinal cortex, page 4
mEPSC ..... miniature excitatory postsynaptic current, page 69
MF ..... mossy fiber, page 6
ML ..... molecular layer, page 4
MPIP ..... Max Planck Insitute of Psychiatry, page 22
MR ..... mineralocorticoid receptor, page 12
NET ..... norepinephrine transporter, page 16
NGF ..... nerve growth factor, page 19
NMDA ..... N-Methyl-D-Aspartate, page 9
PARA ..... parasubiculum, page 3
PCL ..... pyramidal cell layer, page 5
PFC ..... prefrontal cortex, page 10
PL ..... polymorphic layer, page 4
PP ..... perforant pathway, page 4
PRE ..... presubiculum, page 3
PVN ..... paraventricular nucleus of the hypothalamus, page 11
ROI ..... region of interest, page 27
SC ..... Schaffer collateral, page 6
SERT ..... serotonine transporter, page 16
SH ..... steroid hormones, page 11
SL ..... stratum lucidum, page 5
SLM ..... stratum lacunosum-moleculare, page 5
SNRI ..... selective noradrenaline reuptake inhibitor, page 17
SO ..... stratum oriens, page 5
SR ..... stratum radiatum, page 5
SRPDs ..... stress-related psychiatric disorders, page 1
SSNRI ..... selective serotonine noradrenaline reuptake inhibitor, page 17
SSRE ..... selective serotonine reuptake enhancer, page 18
SSRI ..... selective serotonine reuptake inhibitor, page 17

SUB ..... subiculum, page 3
TCA ..... tricyclic antidepressants, page 16
Trk ..... tyrosine related kinase, page 19
USA ..... United States of America, page 16
VSDI ..... voltage-sensitive dye imaging, page 21

List of Tables

List of Figures

Real-Time Imaging of Hippocampal Network Dynamics Reveals Trisynaptic Induction of CA1 LTP and "Circuit-Level" Effects of Chronic Stress and Antidepressants

Abstract

Today's pervasive presence of stress renders stress-related psychiatric disorders (SRPDs), a relevant global health problem. Memory impairment is a major symptom likely mediated by the hippocampus (HIP), a limbic brain region highly vulnerable to stress. Recent evidence suggests that information processing problems within specific neuronal networks might underlie SRPDs. However, the precise functional neurocircuitry that mediates hippocampal CA1 long-term potentiation (LTP), a putative correlate of mammalian learning and memory, remains unknown at present. Furthermore, valuable assays for studying stress and drug effects on polysynaptic activity flow through the classical input/output circuit of the HIP are missing.

To engage a circuit-centered approach, voltage-sensitive dye imaging was applied in mouse brain slices. Single pulse entorhinal cortex (EC) to dentate gyrus (DG) input, evoked by perforant path stimulation, entailed strong neuronal activity in the DG, but no distinct neuronal activity in the CA3 and CA1 subfield of the HIP. In contrast, a theta-frequency (5 Hz) stimulus train induced waves of neuronal activity percolating through the entire hippocampal trisynaptic circuit (HTC-waves). Spatially restricted blocking of glutamate release at CA3 mossy fiber synapses caused a complete disappearance of HTC-waves, suggesting frequency facilitation at DG to CA3 synapses the pivotal gating mechanism. In turn, non-theta frequency stimulations (0.2/1/20 Hz) proved much less effective at generating HTC-waves.

CA1 long-term potentiation (CA1 LTP) is the best understood form of synaptic plasticity in the brain, but predominantly at the monosynaptic level. Here, HTC-waves comprise high-frequency firing of CA3 pyramidal neurons (>100 Hz), inducing NMDA receptor-dependent CA1 LTP within a few seconds. Detailed examination revealed the existence of an induction threshold for LTP. Consequently, baseline recordings with a reduced number of HTC-waves were carried out to test the effects of memory enhancing drugs and HPA axis hormones on hippocampal network dynamics. Bath application of caffeine (5 μM), corticosterone (100 nM) and corticotropin-releasing hormone (5 & 50 nM) rapidly boosted HTC-waves.

Cognitive processes taking place within the HIP are challenged by stress exposure, but whether and how chronic stress shapes "net" neuronal activity flow through the HIP remains elusive. The HTC-wave assay, refined for group comparisons, revealed that chronic stress markedly lowers the strength of evoked neuronal activity propagation

through the hippocampal trisynaptic circuit. In contrast, antidepressants (ADs) of several classes, the mood stabilizer lithium, the anesthetic ketamine, and the neurotrophin brain-derived neurotrophic factor amplified HTC-waves. An opposite effect was obtained with the antipsychotic haloperidol and the anxiolytic diazepam. The tested ADs exert this effect at low micromolar concentrations, but not at 100 nM, and nearly always, also not at 500 nM. Furthermore, the AD fluoxetine was found to facilitate LTP of HTC-waves. Finally, pharmacological blockade of the tyrosine-related kinase B receptor abolished fluoxetine effects on HTC-waves.

These results highlight a circuit-centered approach suggesting evoked synchronous theta-rhythmical firing of EC principal cells as a valuable tool to investigate several aspects of neuronal activity flow through the HIP. The physiological relevance is emphasized by the finding that the resulting HTC-waves, which likely occur during EC theta oscillations, evoke NMDA receptor-dependent CA1 LTP within a few seconds. Furthermore, HTC-waves allow to integrate molecular, cellular and structural adaptations in the HIP, pointing to a monoaminergic neurotransmission-independent, "circuit-level" mechanism of ADs, to balance the detrimental effects of chronic stress on HIP-dependent cognitive abilities.

Real-Time Imaging of Hippocampal Network Dynamics Reveals Trisynaptic Induction of CA1 LTP and "Circuit-Level" Effects of Chronic Stress and Antidepressants

Eidesstattliche Erklärung

Ich versichere hiermit an Eides statt, dass die vorgelegte Dissertation von mir selbständig und ohne unerlaubte Hilfe angefertigt ist.

Jens Stepan
München, den 01.06.2014

Erklärung

Hiermit erkläre ich, dass die Dissertation nicht ganz oder in wesentlichen Teilen einer anderen Prüfungskommission vorgelegt worden ist und ich mich anderweitig einer Doktorprüfung ohne Erfolg nicht unterzogen habe.

Jens Stepan
München, den 01.06.2014

Acknowledgments

First and foremost, I would like to express my sincere respect to Dr. M. Eder. I am very much thankful that he guided me through my time as a PhD student. His comprehensive knowledge, stimulating suggestions and encouragement helped me throughout my entire period of research and during the writing of the thesis.

I would like to express my gratitude to Prof. Dr. G. Boyan, Prof. Dr. G. Grupe and Prof. Dr. R. Landgraf without whose support it would not have been possible to do this dissertation at the faculty of biology at the University of Munich.

I want to thank Prof. Dr. Dr. F. Holsboer for affording me access to the excellent research facilities at the Max Planck Institute of Psychiatry.

Special thanks go to C. Avrabos, B. Hauger, D. Hilberer, C. Hilf, N. Olah, J. Weeger, G. von Wolff and all other colleagues at the Max Planck Institute of Psychiatry, whose vital support greatly contributed to the success of this work.

Jens Stepan

Munich, June 2015

Chapter 1

Introduction

Modern society is faced with ubiquitous and universally pervasive stress (Chrousos, 2009). Stressors may be broadly defined as any physiological or emotional stimuli that overwhelm homeostatic systems of an organism (Radley, 2012). Multiple strands of evidence have established a robust and causal association between higher levels of significant stressors and stress-related psychiatric disorders (SRPDs) (Hammen, 2005; Sapolsky et al., 1986; McEwen and Gianaros, 2011).

Most common among SRPDs is major depression (MD). Meta-analysis of epidemiological surveys found that the lifetime prevalence of MD is in the range of 10-15%, affecting over 340 million people worldwide (Lépine and Briley, 2011; Slattery et al., 2004). The World Health Organization estimates that MD will become the leading cause of burden of disease by the year 2030, even before ischemic heart disease (WHO, 2004). However, modern pharmacological treatment regimes with antidepressant (AD) drugs largely depend on substances discovered more than half a century ago, and response rates are considerably low, leaving about 20-30% of patients without effect. Even if treated by mental-health specialists and remission is achieved, MD is rarely accompanied by a total disappearance of all symptoms (Berton and Nestler, 2006; Duman and Aghajanian, 2012; Kallarackal et al., 2013; Lépine and Briley, 2011; Ressler and Mayberg, 2007; Trivedi et al., 2006).

Equally common are anxiety disorders (AXDs) including extremely debilitating diseases like post-traumatic stress disorder, panic disorder, and phobias. They are frequently diagnosed with a combined lifetime risk of over 28%, raising a similar socioeconomic burden compared to that of MD paralleled by considerably low response rates to pharmacological intervention (Ressler and Mayberg, 2007; Shin and Liberzon, 2010).

In this thesis, SRPDs are pooled together for the following reasons: (i) High comorbidity between SRPDs (e.g., up to 90% between AXDs and depressive episodes); (ii) SRPDs share a variety of symptoms impeding the diagnostic classification; (iii) a highly overlapping fashion of neurocircuits considered to be involved; (iv) similar pharmacological (ADs) and psychological (cognitive behavioral therapy) treatment strategies (Holsboer et al., 2012; Ressler and Mayberg, 2007).

A vital factor that a coherent cause or cure for SRPDs is non-existing might be the heterogeneous character of these brain disorders, likely resulting from a complex interplay of

environmental and genetic factors (Holsboer, 2008). Due to the lack of specific tests and markers, their diagnosis is still clinical based with the aid of core signs and symptoms (e.g., MD; depressed mood, anhedonia, changed appetite and weight, sleep disturbances, feelings of helplessness and thoughts about death and suicide; Duric and Duman, 2013; Richelson, 2001).

Although it is increasingly thought that much of the phenomenology of SRPDs is attributable to problems of information processing within distinct neuronal networks (Castrén, 2005), there is an incomplete understanding of circuit-level mechanisms associated with the pathophysiology and pharmacotherapy of these disorders (Karayiorgou et al., 2012).

The hippocampus (HIP), a temporal lobe structure, is one brain region intimately linked to the pathophysiology of SRPDs. Multiple strands of evidence suggest a critical role for the HIP in the acquisition and retention of new information, a process that is often associated with theta (3-8 Hz) activity in the entorhinal-parahippocampal network (Burgess et al., 2002; Buzsàki, 2002; Gruart et al., 2006; Mitchell et al., 1982; Morris et al., 1986; Rutishauser et al., 2010; Stepan et al., 2012; Tsien et al., 1996; Whitlock et al., 2006; Winson, 1978; Zola-Morgan et al., 1986). Although a decline in cognitive functions is strongly associated with SRPDs, it is not known how polymodal sensory information is gated through the hippocampal network for subsequent storage (MacQueen and Frodl, 2011; McEwen and Gianaros, 2011). Extensive research to find cellular surrogates for learning and memory was done over the last 50 years, but, due to the lack of suitable methods, this happened predominantly at the monosynaptic level. Consequently, the neuronal network dynamics that lead to polysynaptic induction of CA1 long-term potentiation (LTP) at the hippocampal CA3 to CA1 synapse, a widespread experimental model for studying the cellular underpinnings of learning and memory remain elusive (Bliss and Collingridge, 1993).

Beyond its role in synaptic plasticity, the HIP is both, a key contributor to the neuroendocrine stress response and severely damaged by prolonged stress exposure. This dual function potentially promotes a self-amplifying dysregulation of stress response, likely mediating alterations in behavior and emotions that are characteristic for SRPDs (Kim and Diamond, 2002; Sapolsky et al., 1986). Numerous studies conducted on the micro- (e.g., single-cell recordings, (epi-)genetics) and macro-scale (fMRI, clinical studies) yield valuable insight into possible mechanism of disregulated stress response. However, the underlying disordered electrical signaling patterns in specific brain circuits are poorly understood (McEwen and Gianaros, 2011).

ADs have been shown to counterbalance detrimental effects of stress and especially the HIP is suggested to be a possible side of their action (Krishnan and Nestler, 2008). However, ADs represent a heterogeneous group of drugs showing a high variability of effectiveness according to specific subtypes of SRPDs, likely mediated by the induction of multifarious molecular, cellular and structural changes upon treatment (Berton and Nestler, 2006; Duric and Duman, 2013). Consequently, it seems difficult to integrate all

these mechanism for prediction of the outcome on the neuronal circuit level or even behavior. Therefore, more circuit-centered electrophysiological approaches might be suited to elucidate convergent processes of AD drug action at the level of input/output relationships in the HIP (Karayiorgou et al., 2012).

1.1 The hippocampal formation

The dentate gyrus (DG), the ammon's horn (cornu ammonis (CA), with its subregions CA3, CA2 and CA1), the subiculum (SUB), the presubiculum (PRE), the parasubiculum (PARA), and the entorhinal cortex (EC), are summarized under the term hippocampal formation (HF) (Amaral and Witter, 1989). Beyond this shared anatomical identity, they comprise six cytoarchitectonically distinct brain regions, considered as integral components of the medial temporal lobe system (Figure 1.1; Amaral and Witter, 1989).

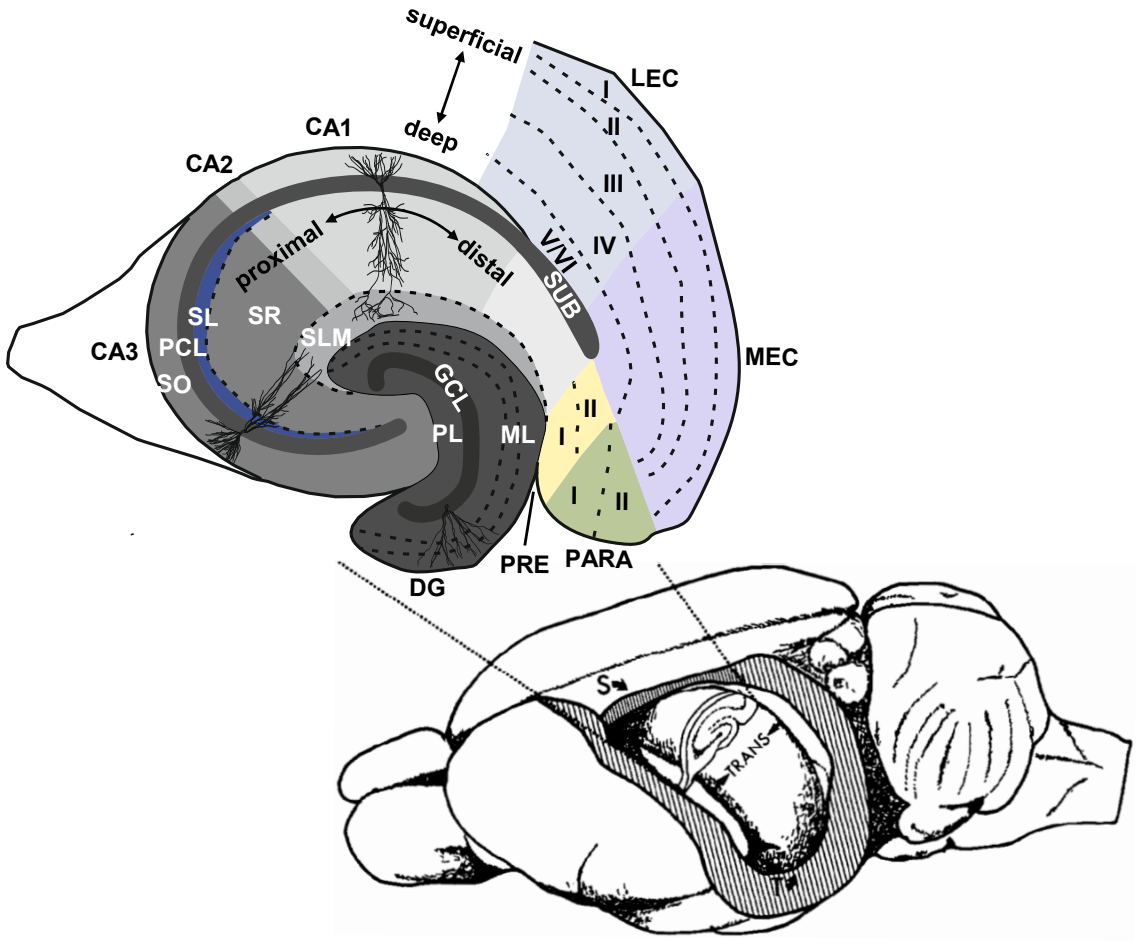

Fig. 1.1. Anatomy of the hippocampal formation. *Expansion of the c-shaped HIP from the septal nuclei (S) to the temporal lobe (T) in the rodent brain (adapted from Amaral and Witter, 1989). The outtake depicts a cross-section through the transverse axis (TRANS) of the HIP which is oriented perpendicular to the septotemporal axis.*

The rodent HIP (here: DG and CA-subregions) appears as an elongated, banana-shaped structure situated in the caudal part of each brain hemisphere with a long or septotemporal axis running from the septal nuclei rostrally to the temporal cortex ventrocaudally

(Figure 1.1; Amaral, 1993; Amaral and Witter, 1989; Andersen et al., 2006). Connectivity patterns, gene expression profiles and behavioral studies support a functional segmentation of the HIP along its rostral/caudal axis into three subdivisions: dorsal/rostral (septal pole), intermediate, and ventral/caudal (temporal pole). Although clear borders are difficult to draw, the dorsal part is often associated with cognitive functions, whereas the ventral part is related to stress, emotion and affect (Fanselow and Dong, 2010). CA-subregions and the DG share a characteristic three-layered appearance with largely unidirectional connectivity. Contrarily, the SUB, PRE, PARA, and EC are characterized by reciprocal connectivity and more than three layers, although discrimination between layers is sometimes difficult (Watson et al., 2011; van Strien et al., 2009).
A highly topographical organization along its septotemporal- and transverse axis is characteristic for the HF and connectivity between its different parts is mediated via specific fiber bundles. Examples include the angular bundle, which is made up by axons connecting the EC with all other fields of the HF or the fimbria-fornix pathway, mediating connectivity between the HF and the basal forebrain, hypothalamic nuclei, and the brain stem (Figures 1.1, 4.16; Watson et al., 2011; Andersen et al., 2006).

1.1.1 Cytoarchitecture of the hippocampal formation

The EC closely resembles the standard six layer scheme, which is characteristic for the neocortex with five cell body layers and a superficial molecular layer. However, principle cell distribution is different from the neocortex. The most prominent excitatory cells are stellate cells and pyramidal cells, situated predominantly in layers II and III. Layers I-III usually refer to external and layers IV-V to internal principal layers. Due to differences in cytoarchitecture, connectivity, and function, the EC can be subdivided into a medial entorhinal cortex (MEC) and a lateral entorhinal cortex (LEC) (Figure 1.1; Andersen et al., 2006; Patton and McNaughton, 1995; Watson et al., 2011).
The DG is not divided into subregions but differs remarkably in its shape along the longitudinal axis with a more "U"-shaped anatomy in ventral, and a more "V"-shaped anatomy in dorsal parts. It has been reported that functional differences may be present along the transverse axis of the granule cell layer (Witter, 2007). Therefore, it is useful to refer to a particular transverse portion of the DG. The part situated between area CA1 and CA3, is referred to as suprapyramidal or inner blade and the part inferior to area CA3 as the infrapyramidal or outer blade. The region linking the two blades (at the kink of the "V" or "U") is called the crest (Figure 1.1; Amaral et al., 2007; Claiborne et al., 1986; Patton and McNaughton, 1995).
The DG is composed of three layers. The deep layer (adjacent to CA3) is called hilus or polymorphic layer (PL) and contains mixed fibers and interneurons. The principal cell layer or granule cell layer (GCL) predominantly contains densely packed granule cells. The molecular layer (ML) represents the most superficial layer and is cell free apart from a few interneurons. The granule cell layer and molecular layer together are sometimes referred to as the fascia dentata. The major components of the ML are the axons of the perforant pathway (PP) (part of the angular bundle), which originates in the EC and

the dendrites of the dentate granule cells. In addition, a variety of subcortical inputs establish synapses on dendrites in this layer (Figure 1.1; Amaral et al., 2007; Patton and McNaughton, 1995; Claiborne et al., 1986; Watson et al., 2011; Witter, 2007).
Comparatively, the first two layers of the CA region are composed of a deep layer called stratum oriens (SO), containing basal dendrites followed by pyramidal cell layer (PCL), the principle cell layer. The basic organization is completed by the ML. This most superficial layer is divided into a number of sublayers in the CA subregions. The stratum lucidum (SL) only exists in areas CA2 and CA3 and contains proximal apical dendrites of pyramidal cells. The stratum radiatum (SR) is situated in the middle and contains the distal apical dendrites of the pyramidal neurons followed by stratum lacunosum-moleculare (SLM) adjacent to the hippocampal fissure, comprising the pyramidal neurons apical tufts of the apical dendrites (Figure 1.1; van Strien et al., 2009; Andersen et al., 2006).

1.1.2 Connection matrix of the hippocampal formation

The EC constitutes the major gateway between the HF and the rest of the brain. Its neurons represent the main entry point for polymodal (sensory) information routed to the DG and HIP, and it relays processed sensory information from the HF back to a variety of brain regions. Thus, the EC is the beginning and the end of a highly topologically arranged loop of information flow through the HF. The EC relays cortical and subcortical information via three parallel excitatory inputs, summarized as the so-called PP, to DG granule cells, CA3/CA1 pyramidal neurons, and interneurons in both fields. By far, the most prominent input arises from EC layer II stellate cells to the entire transverse extent of the DG converging onto the apical dendrites of dentate principal cells and interneurons. Specifically, the LEC (via lateral PP), projects to the outer third of the molecular layer of the DG, and the MEC (via medial PP) projects to the middle third. In addition, there is a slight projection from EC layer II cells onto distal apical dendrites of CA3 pyramidal cells in SLM, with a comparable convergence of MEC/LEC inputs. The origin of the main projection from the EC to SLM of area CA1 lies in layer III, also known as temporoamonic pathway forming synapses on distal apical dendrites of CA1 pyramidal cells (Figures 1.1, 4.1; Andersen et al., 2006; Boeijinga and Van Groen, 1984; Patton and McNaughton, 1995; van Groen et al., 2003; van Strien et al., 2009). Although these connections are well established, recent studies point out strain differences. It was reported that layer II stellate cells in C57BL/6J mice project exclusively to the DG and that projections to CA3 originate from EC layer III cells (van Groen et al., 2003).

1.1.2.1 The entorhinal cortex layer II stellate cell

Stellate cells constitute the dominant cell type in layer II of the EC. They received this name from their star-shaped arborization and spanning, with numerous dendrites radiating out from the soma. The most striking physiological features of layer II stellate cells are rhythmical changes in network activity at 3-10 Hz, as observed in local field

potential recordings. These theta oscillations occur in response to subthreshold depolarizations, and recent work suggests them being the key contributor to theta rhythm generation in the EC-hippocampal network (Alonso and Llinás, 1989; Andersen et al., 2006; Mizuseki et al., 2009; Mitchell et al., 1982; Quilichini et al., 2010). The role of EC theta oscillations in animal cognition is well established. Their elimination results in deficits of spatial memories, and layer II stellate cells are selectively impaired in their function in animal models of Alzheimer's disease (Mitchell et al., 1982; Stranahan and Mattson, 2010). In comparison to excitatory cells in other layers, layer II stellate cells show strong modulation of their spiking to specific phases of theta oscillations and include the highest fraction of significantly theta-modulated neurons (Quilichini et al., 2010). A subset of layer II stellate cells in the dorsocaudal medial EC represents a specific example for modulation of spike patterns. These cells form a topographically organized neuronal map of the spatial environment. These so-called grid cells fire whenever the animal's position coincidences with any vertex of a regular grid of equilateral triangles spanning the surface of an environment and were found in all mammals including humans (Fyhn et al., 2008; Hafting et al., 2005; Jacobs et al., 2013). Grid cells exhibit phase modulation of their spikes to specific spacial cues (e.g., when the rat runs through the receptive field of a subset of neurons), suggesting an important computation mechanism in the EC. Overall, phase modulation of stellate cell spiking by theta oscillations provides a possible mechanism by which the EC entails sequences of theta-rhythmical spiking in EC layer II cells, thereby effectively routing sensory information to the HIP (Alonso and Llinás, 1989; Burgalossi et al., 2011; Mizuseki et al., 2009).

1.1.3 The trisynaptic pathway of the hippocampus

The DG receives its major input from the EC via the PP. Granule cells of the DG, the only cells that give rise to axons (mossy fiber (MF)) leaving this structure (syn.: principle cell), synapse on pyramidal neurons in area CA3. These neurons in turn, pass electrical signals on pyramidal cells in area CA1 via their so-called Schaffer collateral (SC)s. This set of synapses is referred to as the classical trisynaptic circuit of the HIP (Figures 1.1, 4.1; Amaral and Witter, 1989; Amaral, 1993; van Strien et al., 2009).

1.1.3.1 The mossy fiber to CA3 synapse

The synaptic contact formed between DG granule cells and CA3 pyramidal cells is rather unique in having morphological, pharmacological, and physiological features, not usually observed in cortical synapses (Andersen et al., 2006; Henze et al., 2000). It is the second synapse of the classical trisynaptic pathway and conveys input on proximal dendrites of CA3 pyramidal cells (Figure 1.1). Each granule cell of the rodent DG gives rise to a single unmyelinated axon, known as MF. Immediately after leaving the granule cell layer of the DG, the main MF gives rise to numerous small filopidal extensions which synapse on dendrites of polymorphic neurons in the hilus. Afterwards, the main MF leaves the hilus, establishing synaptic contacts (large MF boutons) in SL on the dendritic tree of various CA3 principle cells with a limited degree of septotemporal divergence

(Henze et al., 2000; Amaral and Witter, 1989). Synapses on pyramidal cells show some distinct features. The total number of mossy terminals along the granule cell axon is relatively small, with very limited convergence ($\approx$ 50 granule cells per pyramidal cell) and divergence ($\approx$ 10-18 pyramidal cells per granule cell). This sparse connection pattern is not seen elsewhere in the brain (Andersen et al., 2006; Henze et al., 2000; Henze et al., 2002; Watson et al., 2011). DG granule cells provide their main input onto gamma aminobutyric acid (GABA)ergic interneurons in SL (via small filopidal extensions), perfectly positioned to disynaptically inhibit CA3 pyramidal cells following MF activation, which adds onto the sparse coding between granule cells and CA3 pyramidal cells. This connection pattern is associated with a net inhibition of CA3 pyramidal cells after MF activation (Henze et al., 2000; Mori et al., 2004). However, an important aspect in this circuitry is the remarkable frequency facilitation specifically at MF to CA3 synapse (up to 1000 %; Nicoll and Schmitz, 2005; Toth et al., 2000), in response to (theta)-rhythmical synaptic input (Mori et al., 2004; Toth et al., 2000), accompanied by a switch from net inhibition to net excitation in the CA3 network.

1.1.3.2 Extrinsic inputs/outputs of the hippocampus

Compared to the EC, DG granule cells receive only minor input from other cortical regions. Köhler (1985) reports a variable projection from the PRE and PARA that ramifies in the molecular layer. Subcortical inputs arise from the septal nuclei, supramammillary area, hypothalamic nuclei, and the brain stem. The inner third of the molecular layer receives a projection that originates exclusively from ipsilateral and contralateral neurons in the polymorphic layer (mossy cells). There are no axons originating from DG granule cells other than MF (Andersen et al., 2006; Watson et al., 2011). One prominent extrinsic input to area CA3 neurons arises from axons of other CA3 neurons. These commissural/associational (c/a) inputs are numerous and originate from CA3 neurons on both sides of the brain. CA3 neurons also have connections with cholinergic neurons in the medial septal nucleus and the nucleus of the diagonal band of Broca, which synapse mainly in SO. There are no backprojections from the DG or area CA3 to the EC. Therefore, the main input region of HIP has no influence on EC activity (Andersen et al., 2006; Watson et al., 2011). CA1 pyramidal cells receive extrinsic input via c/a fibers from the contralateral hemisphere. Inputs from the nucleus reuniens of the thalamus and the basolateral nucleus of the amygdala (AMY) innervate CA1 neurons via synapses on their distal apical dendrites. CA1 pyramidal cells represent an important output region of the HIP. They are heavily connected with the subiculum and layer IV/V of the EC. Via the fimbria/fornix pathway various regions constitute targets of the CA1 principle cells (Andersen et al., 2006). Furthermore, there are remarkable differences in projection patterns of hippocampal neurons depending on their specific position on the septotemporal- and transversal axis (Amaral and Witter, 1989; Andersen et al., 2006).

1.2 Synaptic plasticity in the hippocampus

The mammalian brain is composed of a trillion of neurons and a quadrillion of chemical synapses. This enormous connectivity gives rise to tremendously complex neuronal networks. Electrical activity in the these networks not only shapes behavior, it also triggers remarkable dynamic modifications and rewiring. The ability to respond to naturally occurring and artificial stimulation patterns with changes in synaptic efficacy is called synaptic plasticity (Bliss and Collingridge, 1993; Ho et al., 2011). Synaptic plasticity plays a decisive role in the development and homeostasis of brain function. Different patterns of stimulation elicit changes in synaptic strength on various time-scales. Here, the focus is on long-lasting forms of cellular plasticity. Specifically, an enhancement of synaptic response at excitatory glutamatergic synapses represents a widespread phenomenon of experience-dependent changes in the mammalian brain (Andersen et al., 2006; Ho et al., 2011). Synaptic plasticity is a prominent feature of hippocampal synapses, and lesions of the HIP negatively affect the acquisition and storage of new episodic and spatial information (Neves et al., 2008), resulting in a rare unifying hypothesis in contemporary neuroscience: *"Memories might be stored by alterations in the strength of synaptic connections between neurons in the CNS"* (Byrne et al., 2008, p.296).
In 1949, the Canadian psychologist Donald Hebb formulated the first hypothesis, suggesting that the acquisition and retention of new information (learning and memory) might take place at the cellular level. He proposed that a synapse that links two neurons is strengthened if the cells are active at the same time (Hebb, 2002, p.62). Strong experimental evidence for this theory originated in 1973 by Bliss and Lømo, who were the first to record a long-lasting enhancement of synaptic transmission in the HIP. They showed that brief tetanic stimulations of the PP in anesthetized rabbits, induce a sustained increase of the population response recorded in granule cells of the DG and titled this phenomenon long-term potentiation (LTP; Bliss and Lømo, 1973. Subsequently, it has been shown that additional forms of activity-dependent plasticity exist (e.g., long-term depression (LTD), spike timing dependent plasticity) and that synapses in the majority of brain regions can undergo long lasting changes in synaptic response, such as the AMY, motor cortex, sensory cortex and spinal cord (Andersen et al., 2006; Bliss and Collingridge, 1993). The early studies on LTP were carried out *in vivo*. After the introduction of the more feasible hippocampal slice preparation, most researchers turned towards the HIP as a model system to study the cellular and molecular underpinnings of synaptic plasticity. Specifically, a vast amount of studies was conducted on LTP at the hippocampal CA3 to CA1 synapse (CA1 LTP), resulting in a sophisticated understanding of monosynaptic induction and expression mechanisms underlying LTP at central synapses (Andersen et al., 2006; Byrne et al., 2008; Ho et al., 2011).

1.2.1 The role of NMDA receptors in LTP

Further experimental evidence for Hebb's so-called "neurophysiological postulate" was supplied by Wigström and Gustafsson (1986), showing that simultaneous presynaptic

transmitter release and postsynaptic depolarization induce a glutamate receptor blocker sensitive form of LTP. Consequently, it was suggested that ionotropic glutamate receptors play a central role in the induction, expression, and maintenance of LTP at hippocampal SC to CA1 synapses. Several different types of glutamate receptors are known and distinguished by functional and pharmacological properties, but two types - N-Methyl-D-Aspartate (NMDA) and α-amino-3-hydroxy-5-methyl-4-isoxazoleproprionic acid (AMPA) receptors are of particular interest. These receptors are ligand-gated, non-selective cation channels that allow the flow of K^+, Na^+, and in some cases Ca^{2+} upon opening. Activation of the AMPA receptors is triggered by the release of glutamate rendering them permeable to K^+ and Na^+ and resulting in an exitatory postsynaptic potential (EPSP). The NMDA receptor adds another dimension and subserves induction of LTP, whereas AMPA receptors are important for its expression and maintenance. The NMDA receptor channel pore is blocked by Mg^{2+} at rest. For channel opening two concomitant events have to take place. The binding of glutamate (and the co-agonist glycine) and the relief of the Mg^{2+}-block by a sufficient depolarization of the postsynaptic membrane. Subsequently, the channel also conducts Ca^{2+} ions, which can enter the postsynaptic cell. Thereby, the NMDA channel acts as a coincidence detector, allowing a unique contribution to information processing at the molecular level, in a manner analogous to the model proposed by Hebb (2002) for associative learning (Bliss and Collingridge, 1993; Byrne et al., 2008; Ho et al., 2011; Wigström and Gustafsson, 1986). Out of several types of LTP which have been reported so far, the best understood is NMDA receptor-dependent LTP, that received its name because D-APV (see Appendix 8.1) and MK-801, two highly specific antagonist of the NMDA receptor, block its induction while having almost no effect on basic synaptic transmission. The discovery by Morris et al. (1986) that D-APV injected into rodent HIP severely impairs spatial memory acquisition, and two recent studies reporting LTP-like synaptic changes in the HIP following learning support the necessity of LTP for information storage (Gruart et al., 2006; Morris et al., 1986; Whitlock et al., 2006).

The Ca^{2+} entrance into the postsynaptic compartment through NMDA receptors seems to be an absolutely necessary trigger for the induction of NMDA receptor-dependent LTP (Malenka and Bear, 2004). The intracellular Ca^{2+} concentration is tightly regulated with very low intracellular (0,0002 mM) and relatively high extracellular (2 mM) concentrations, whereby small changes trigger profound alterations in intracellular signaling. First evidence that Ca^{2+} is a central mediator connecting extracellular events with intracellular signaling cascades came from Lynch et al. (1983). They injected the calcium chelator ethyleneglycol-bis-(-aminoethylether)-N,N,N',N',-tetraacetic acid, into CA1 pyramidal cells and thereby blocked the induction of CA1 LTP. Moreover, Malenka et al. (1988) showed that chemically induced release of Ca^{2+} in the postsynaptic cell is sufficient to induce CA1 LTP. Several postsynaptic mechanisms involved in the expression and maintenance of CA1 LTP have been identified so far and following several decades of controversy the contribution of presynaptic changes and glia cells are now considered to be essential partners (Ho et al., 2011; Malenka and Bear, 2004). The Ca^{2+}-dependent AMPA

trafficking at the postsynaptic plasma membrane (by lateral diffusion and exocytosis; removal by endocytosis) and activation of postsynaptic kinases (e.g., calcium/calmodulin-dependent protein kinase II) and phosphatases (e.g., protein phosphatase 1) are believed to regulate downstream targets important for LTP expression and maintenance (Byrne et al., 2008; Ho et al., 2011).

1.2.2 Hippocampal plasticity during theta oscillations

Comparable to the situation in the EC, theta oscillations (3-10 Hz) represent a prominent network pattern in the HIP of mammals and are often associated with the formation of episodic and spatial memories (Axmacher et al., 2006; Berry and Thompson, 1978; Buzsàki, 2002; Rutishauser et al., 2010; Winson, 1978). The extracellular currents underlying theta oscillations are believed to be mainly of extrinsic origin, generated by an interplay between inhibitory (medial septum) and excitatory (via PP) inputs (Pernía-Andrade and Jonas, 2014; Buzsàki, 2002). However, recent evidence suggests that several intrinsic theta generators exist in area CA1 (Goutagny et al., 2009). Many cells in the HIP exhibit a rhythmical pattern of firing that is related to theta, and the onset of stimuli causes ongoing theta to reset so that it becomes phase-locked to the stimuli (McCartney et al., 2004). Therefore, theta-frequency oscillations might provide a framework how sequential binding of cell assemblies over a temporal metric brings about synaptic modification (Goutagny et al., 2009; Hasselmo, 2005). The most prominent theta oscillations are observed in CA1 and the relationship between discharge of pyramidal cells and fluctuations in membrane potentials are best understood. Several studies report that the induction of LTP is optimal when several high-frequency pulses were applied every 200ms (theta-burst stimulation). Moreover, stimulations at specific phases of the theta cycle induce distinct effects. Activation on the peak of theta, recorded locally in stratum radiatum of CA1, causes LTP, while stimulation on the trough causes LTD. This seems to depend on phasic changes in pyramidal cell depolarization during theta rhythm, priming them for synaptic plasticity (Buzsàki, 2002; Capocchi et al., 1992; Hasselmo, 2005; Stäubli and Lynch, 1987). Interestingly, single hippocampal neurons in freely behaving rats fire normally at the peak of ongoing theta activity (McCartney et al., 2004). Furthermore, several lines of evidence suggest that synchronization of theta activities between HIP and other brain regions (AMY, prefrontal cortex (PFC)) improves neuronal communication during region specific memory tasks (Seidenbecher et al., 2003; Siapas et al., 2005).

1.3 Neurocircuitry of stress

Homeostasis and, thus, survival of all organisms is permanently challenged by physiological (systemic) and emotional (neurogenic, psychogenic) adverse effects, termed stressors. Physiological stressors like hypoxia or hemorrhage are believed to exceed selective homeostatic systems. In contrast, emotional stressors require an anticipatory response that is initiated by comparison of the stimuli with innate programs or memories (Chrousos, 2009; de Kloet et al., 2005; Jankord and Herman, 2008). Such an anticipatory response likely involves several highly intersected limbic brain structures (e.g., HIP, AMY, PFC), rendering the response greatly influenced by the organism's ability to predict and control the presence or intensity of the stressor. Consequently, the individual's appraisal and coping strategy is highly variable (Jankord and Herman, 2008; Kim and Diamond, 2002). When stress is overwhelming or perceived to be so, a cascade of neuroendocrine adaptive responses is initiated to re-establish homeostasis (de Kloet et al., 2005; McEwen, 2007; Raison and Miller, 2003). Adaptive responses engage the so-called stress system which is situated in the central nervous system (e.g., hypothalmaus, pituitary, spinal cord) and in several peripheral organs (e.g., adrenals, liver), mediating a fast and relatively stereotopic response to maintain physiological integrity even in life threatening situations (Figure 1.2; Ulrich-Lai and Herman, 2009). Next to the autonomic nervous system, which engages very rapid alterations in physiological functions, the hypothalamic-pituitary-adrenal (HPA) axis constitutes a central hub in the neurocircuitry of stress, orchestrating an appropriate regulatory response according to the characteristics and physiological impact of the stressor (Chrousos, 2009; de Kloet et al., 2005; Radley, 2012). Upon activation, which is reflected by a peripheral release of steroid hormones (SH), including glucocorticoids (GC), but also the local release of neurotransmitters (e.g., glutamate, noradrenaline, serotonine) and neuropeptides (corticotropin releasing hormone (CRH), adrenocorticotropic hormone (ACTH)), a wide array of organ systems is activated and integrated by central and peripheral feedback to the brain (Figure 1.2; de Kloet et al., 2005; Joëls et al., 2009; Maras and Baram, 2012; McEwen, 2007). Beyond rapid activation of the HPA axis for adaptive coping, there exists substantial evidence that excessive or prolonged activation damages brain structures (especially the HIP; Figure 1.3). The resultant excess in stress hormones is widely implicated in the onset of SRPDs (Chrousos and Gold, 1992; de Kloet et al., 2005; Holsboer, 2000; Radley, 2012).

1.3.1 Activation of the HPA axis

Endocrine systems are constantly active to maintain the integrity of the organisms homeostasis. However, intense excitation of the HPA axis occurs in response to any external or internal challenge that overwhelms the individual's ability to adapt and cope. Physiological stimuli engage regulatory processes by ascending brainstem systems or circumventricular organs (visceral and sensory stimuli) projecting directly to the parvocellular divisions of the paraventricular nucleus of the hypothalamus (PVN), whereas psychogenic

stimuli, mediated by the limbic system, converge indirectly onto this structure (McEwen and Gianaros, 2011; Popoli et al., 2012).

Upon activation, parvocellular neurons produce CRH. Together with simultaneously released arginine vasopressine, CRH induces the release of ACTH from the pituitary gland via the portal circulation. ACTH enters the blood stream and triggers the release of SHs from the zona fasciculata of the adrenal glands. Among these, GCs (cortisol in humans and corticosterone (CORT) in rodents) are often associated with SRPDs (Figure 1.2; Jankord and Herman, 2008; Smith and Vale, 2006).

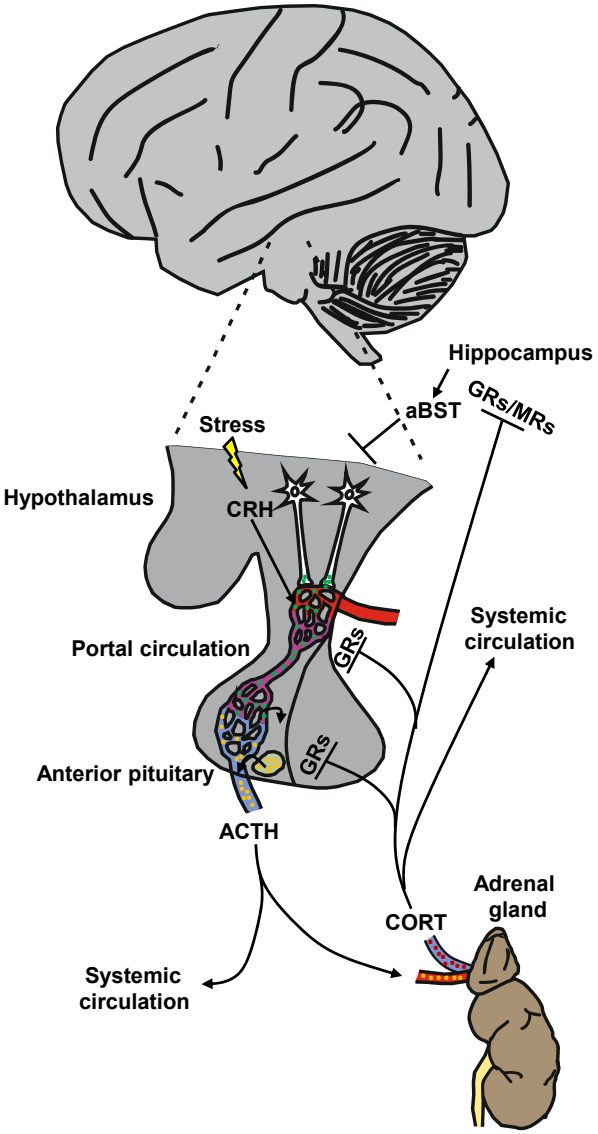

Fig. 1.2. Schematic illustration of the HPA axis. *In response to stress, CRH is released into hypophysial portal vessels by neurons localized in the PVN of the hypothalamus. CRH subsequently cause ACTH release from the anterior pituitary. ACTH stimulates SH production in the adrenals and secretion into the systemic circulation. SHs, including CORT modulate several targets and inhibit further HPA axis activation via MRs and GRs, that are widely distributed throughout the brain (modified from Myers et al., 2012).*

GCs readily overcome the blood brain barrier and bind to two types of receptors, the mineralocorticoid receptor (MR) and the glucocorticoid receptor (GR). These receptors are ligand driven transcription factors. Most of them reside in the cytoplasm and binding of corticosteroids triggers translocation of the receptor complex to the nucleus. Here, the SH receptor complex changes gene transcription directly through binding to recognition sites in the DNA or indirectly via interactions with other transcription factors. The MR is highly expressed in limbic brain areas and has a approximately tenfold higher affinity to GCs than the GR. This high affinity renders the MR activated, even through the absence of stress. A common theory is that the MR is important for basal GC tone and stress response initiation, whereas the more ubiquitously expressed GR (except for area CA3) is only activated by large amounts of GCs, pointing to a more reactive role in stress response including the termination of HPA axis activation (de Kloet et al., 2008; Groeneweg et al., 2011; Karst et al., 2005).

Recent evidence suggests the existence of an additional family of membrane bound MRs and GRs that are coupled to G-protein-coupled receptors (GPCRs), exerting rapid

effects on the excitability and activation of neurons via nongenomic pathways. Despite their different location, these receptors are known to differ by their molecular structure, their affinities to CORT, and their mode of action (Groeneweg et al., 2011; Maggio and Segal, 2010). This is thought to partially explain the observation of a fast and delayed feedback inhibition of the HPA axis by circulating GCs. This regulation likely occurs via GRs and MRs, expressed in structures of the HPA axis (PVN, pituitary) or indirectly via GRs or MRs, expressed in brain regions with afferent connections (direct or indirect) onto PVN neurons (HIP, AMY, PFC; Figure 1.2; Jankord and Herman, 2008; Smith and Vale, 2006).

Beside SHs, CRH has been increasingly recognized to mediate stress-induced alterations in the HIP. It is now well established that several brain regions contain CRH-expressing neurons, including the HIP (Maras and Baram, 2012). Its release upon stress constitutes the starting point of HPA axis activation, and the neuropeptide modulates diverse brain functions via two GPCRs: CRH receptor types 1 ($CRHR_1$) and 2 ($CRHR_2$). Especially CRH-$CRHR_1$ interaction seems to be important in the modulation of neuronal excitability of hippocampal neurons. The receptor is expressed on neurons in all subfields of the HIP but most abundant on the somata and dendrites of CA1 pyramidal cells, which is consistent with its proposed modulation of glutamatergic signaling and synaptic plasticity. The mechanisms by which CRH modulates synaptic plasticity have been shown to be highly dose- and time-dependent, however, knowledge about the underlying molecular and cellular mechanisms is still sparse (for overview see Maras and Baram, 2012).

Overall, peripherally and centrally released SHs mediate complex acute and chronic effects throughout the body including the brain. Locally released neurotransmitters and neuropeptides provide a spatially restricted modulation of hippocampal physiology and actions within a time frame of milliseconds. Furthermore, stress mediators are not secreted to the same amount throughout the day. For example, stress triggers the release of large bursts of GCs, which are superimposed on a basal pulsatile and circadian secretion mode. These diverse functions of HPA axis-related hormones and transmitters along a continuum of spatial and temporal domains illustrate the complex interplay between stress, mediators of the stress system and hippocampal physiology (Figure 1.2; Joëls et al., 2009; Maras and Baram, 2012).

1.3.1.1 Role of the hippocampus in stress integration

Multifarious afferent projections modulate neurons in the PVN. Major projections arise from four distinct brain regions: brain stem neurons, cell groups of the lamina terminalis, extra-hypothalamic nuclei, and forebrain limbic structures (HIP, AMY, PFC). Not all of these cell groups provide direct innervation of the PVN. However, information from a wide array of sensory modalities converge onto PVN neurons, influencing expression and release of CRH from parvocellular neurons (Radley, 2012; Smith and Vale, 2006).

The HF has been implicated as a key contributor in the inhibitory regulation of the HPA

axis and in the termination of the stress response. After chronic stress, there is a remarkable downregulation of GC receptors on hippocampal neurons. Forebrain specific downregulation of GC receptors causes an increase of basal CORT secretion and a resistance to the dexamethasone-mediated, negative feedback inhibition of the HPA axis. Furthermore, lesions in the HIP under basal conditions and following stress disrupt the circadian GC rhythm and produce elevated basal levels of circulating mediators of the HPA axis. These lesion experiments also showed that the response to particular stressors was changed. The reaction to physiological stressors remains largely unaffected, while the response to emotional stressors (e.g., restraint, open field) was prolonged, indicating a specific role for stimulus modality. In turn, stimulation of hippocampal neurons *in vivo* reduces ACTH and CORT release (Jankord and Herman, 2008; Herman and Mueller, 2006; Radley, 2012; Roozendaal et al., 2001; Smith and Vale, 2006).
Nevertheless, the HIP possesses no direct connections with CRH producing neurons in the hypothalamus. But how does the predominant excitatory glutamatergic projection from the HIP (specifically ventral subiculum) exerts inhibitory drive onto the HPA axis? The transformation is thought to be mediated by disynaptic projections to other brain regions with direct projections onto parvocellular neurons, like the infralimbic cortex and the anterior bed nucleus of the stria terminalis. The latter renders excitatory output from the HIP inhibitory, likely contributing to the fast GC-mediated feedback inhibition of the HPA axis. Interestingly, hyperactivity and loss of negative feedback occur in more than 50% of depressed patients (Figure 1.2; de Kloet et al., 2005; Duman and Aghajanian, 2012; Jankord and Herman, 2008; Herman and Mueller, 2006; Radley, 2012; Smith and Vale, 2006; Tasker et al., 2006).

1.3.2 Effects of stress in the hippocampus

Studies performed in the human and animal HIP have revealed various mechanisms how acute and chronic stress exposure alters hippocampal function, including: (i) Molecular alterations: e.g., enhanced glutamate and GC release, decreased expression of neurotrophins; (ii) cellular effects: e.g., enhanced cell loss and neuronal atrophy, decreased synaptic plasticity; (iii) morphological changes: e.g., decreased hippocampal volume, altered neuronal network connectivity. Initial molecular and cellular effects of stress can progress to severe structural modifications of neurons of the HIP and other limbic brain regions. On longer timescales, these molecular and cellular refinements can lead to morphological changes, characterized by deficiencies in neuronal function and neuronal network connectivity (Figure 1.3; Duric and Duman, 2013; Kim and Diamond, 2002; Maras and Baram, 2012; Radley, 2012; Sousa et al., 2000). Acute stress and low to moderate rises in CORT levels in the HIP are paralleled by enhanced neurotransmission, likely mediated by nongenomic pathways upon activation of membrane bound MRs. The best understood mechanism is a rise of extracellular glutamate levels, causing a rapid and reversible enhancement of miniature excitatory postsynaptic current frequency in area CA1, accompanied by an increased probability of postsynaptic action potential induction (Joëls, 2006; Karst and Joëls, 2005; Popoli et al., 2012; Sandi, 2011).

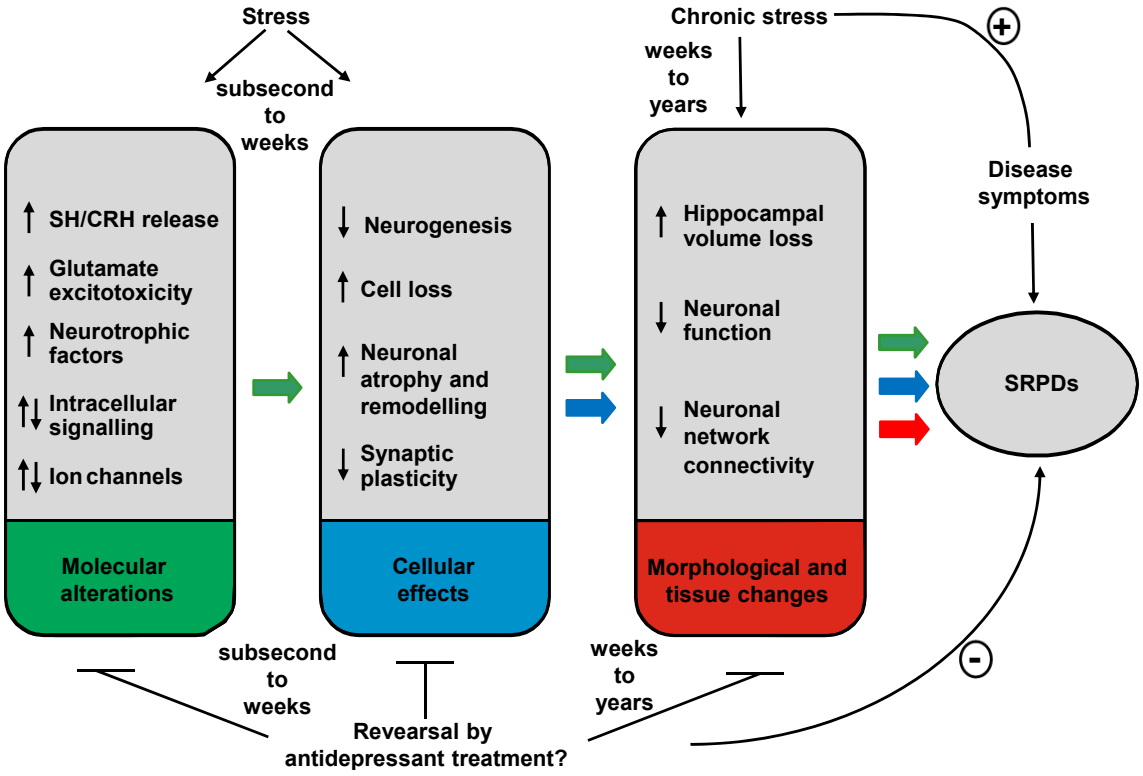

Fig. 1.3. Stress and ADs bidirectionally modulate hippocampal physiology. *Diverse molecular, cellular and morphological modifications in the HIP are driven by stress and AD treatment in a time-dependent manner (modified from Duric and Duman, 2013).*

The effects of chronic stress and high levels of CORT on basal neurotransmisson in the HIP are less well understood. Basal glutamate release seems to be unaffected, but synaptic plasticity is profoundly impaired (Popoli et al., 2012). First experimental evidence came from Foy et al. (1987), showing that adult rats receiving restraint tailshock stress exert marked impairments of CA1 LTP *in vitro*. Comparable effects on LTP induction were obtained with administration of high doses of CORT *in vivo* and *in vitro* (Maggio and Segal, 2010). Subsequent studies revealed a link to the HPA axis, showing that LTP impairment after acute inescapable stress is prevented by GR blockers and protein synthesis anatagonists (Xu et al., 1997; Xu et al., 1998).

The effects of CRH reported from *in vitro* and *in vivo* experiments in the HIP mostly resemble the effects of CORT. Acute stress and low concentration of CRH enhance neuronal excitability and potentiate synaptic plasticity, whereas chronic stress and high CRH concentrations exert opposing effects (Maras and Baram, 2012; von Wolff et al., 2011).

Today, it is well established that stress has strong effects on synaptic transmission and synaptic plasticity in the HIP, including a dose-dependent relationship between CORT concentration and cellular effects. The often proposed inverted U-shaped relationship of circulating GCs on cellular functions is likely accomplished by differential activation (time, concentration) of co-expressed GRs and MRs in the HIP (de Kloet et al., 2005; Diamond et al., 1992; Joëls, 2006; Joëls et al., 2009; Maggio and Segal, 2010).

Overall, the two co-existing roles of the HIP - learning and memory, and regulation of HPA axis activity - seem to be dramatically affected by stress. In addition, chronic stress

triggers a reorganization of the stress control circuitry (Ulrich-Lai and Herman, 2009). On this basis, Sapolsky et al. (1986) formulated the "glucocorticoid cascade hypothesis" of hippocampal aging, outlining that a damage of brain structures important to HPA axis restraint engage a feed forward circuit enabling ongoing stressors to render GC overproduction indefinitely. Dysfunction of neuronal excitability and synaptic plasticity may aggravate this "viscious circle" by preventing an individual's ability to adapt to new situations and to make decisions about how to deal with new challenges or stressors (McEwen and Gianaros, 2011; Raison and Miller, 2003; Sapolsky et al., 1986).

1.4 Pharmacology of antidepressants

Although SRPDs cause severe individual and socioeconomic burden, current pharmacological therapies remain unsatisfactory, requiring several weeks of administration to produce a clinical benefit, while leaving a demanding amount of patients resistant to drug treatment. Furthermore, the cellular processes underlying therapeutic effects of ADs remain elusive (Duman and Aghajanian, 2012; Krishnan and Nestler, 2008). Nevertheless, ADs are the first-line medication to counterbalance the detrimental effects of SRPDs (Olfson and Marcus, 2009; Pratt et al., 2011). It was reported that the rate of prescribed medication in the United States of America (USA) increased from 5.84% in 1996 to 10.12% in 2005 with a concomitant decreased likelihood of patients to undergo psychotherapy (Olfson and Marcus, 2009). Based on this study and findings from the USA Health and Nutrition Examination Surveys (2005-2008) (Pratt et al., 2011), it was estimated that 11% (27 million people) of the US American population older than 12 took AD medication between 2005 and 2008 (Olfson and Marcus, 2009; Pratt et al., 2011).

1.4.1 Classification of antidepressants

The serendipitous discovery of the first ADs resulted from clinical observations in the 1960s. Iproniazid and imipramine, two non-psychiatric drugs, exert potent antidepressant effects in humans, and a more detailed examination revealed that they enhance synaptic serotonin and noradrenaline transmission (Berton and Nestler, 2006; Krishnan and Nestler, 2008). On that template, various compounds with AD properties were developed, rendering the group of AD drugs quite heterogeneous. In contrast, these drugs are characterized by only a few known functional effects, that are possibly associated with their therapeutic efficiency. Therefore, their classification based on functional characteristics might be more useful than a structural one (Richelson, 2001).
The first group of drugs inhibits the reuptake of monoamines by blocking the serotonine transporter (SERT), norepinephrine transporter (NET), and dopamine transporter nonspecifically (tricyclic antidepressants (TCA) e.g., amitriptyline or clomipramine; Krishnan and Nestler, 2008; López-Muñoz and Alamo, 2009; Wrobel, 2007).
The second group of drugs block the destruction of monoamine neurotransmitters by the

enzyme monoamine-oxidase (MAO) (monoamine-oxidase inhibitor (MAOI), e.g., tranylcypromine, isocarboxazid). Two isoforms of MAO exist: MAO-A / MAO-B and this group can be further subdivided depending on whether the blockade is isoform-selective and reversible or not (Yamada and Yasuhara, 2004).
With the introduction of fluoxetine in 1988 (Wrobel, 2007), the well established "first-generation" ADs have been extended by a third group, the so-called "second-generation" ADs which are characterized by a more specific inhibition of SERT and NET. According to their effects on specific transporters, they are further classified into distinct groups. These include ADs selective for serotonine (selective serotonine reuptake inhibitor (SSRI) (e.g., fluoxetine, citalopram), noradrenaline (selective noradrenaline reuptake inhibitor (SNRI) (e.g., desipramine, reboxetine) or a combination of both (selective serotonine noradrenaline reuptake inhibitor (SSNRI); e.g., venlafaxine, duloxetine; Berton and Nestler, 2006; López-Muñoz and Alamo, 2009; Wrobel, 2007).
The actual selection of specific ADs for a patient depends on various factors including the patient's prior experience with medication, actual symptoms and medication, severeness of disease, etiopathology, receptor affinity of the drug, comorbidity, genetic polymorphisms in stress-related genes, age and adverse side effects (Bauer et al., 2007; Binder et al., 2004; Richelson, 2001). The latter are predominantly caused by a relatively high affinity of most ADs to biogenic amine-receptors (α_1-adrenergic, dopamine D_2, histamine H_1, muscarinergic acetylcholine and 5-HT_{2a}), mediating symptoms like dry mouth, sweating, sedation, sexual dysfunction, orthostatic hypotension or weight gain. Unfortunately, the adverse side effects usually occur more rapidly than beneficial ones, a fact that is often considered as the leading cause for the low compliance seen in patients under AD medication (Bauer et al., 2007; Binder et al., 2004; Bylund, 2007; Richelson, 2001).
Overall, meta-analyses failed to reveal substantial differences in efficacy between first- and second-generation ADs, rendering the latter ones lower affinity to the biogenic amine receptors the possible advantage over first-generation ADs (Anderson, 2000; Cipriani et al., 2009; Gartlehner et al., 2011; Richelson, 2001; Schatzberg, 2002).

1.4.2 Theories of antidepressant drug action

The discovery that iproniazid (MAOI) and imipramine (TCA) target monoamine neurotransmission set the foundation of the so-called catecholamine and serotonin hypotheses of depression (Berton and Nestler, 2006; Holsboer, 2000). It was postulated that altered production, release, turnover or function of monoamine neurotransmitters (especially serotonin (5-hydroxitryptamine or 5-HT) and norepinephrine) or altered function of their GPCRs (except serotonin 5-HT_3 receptor; Millan et al., 2008) in certain brain areas might underlie depression, and that ADs are able to reverse the underlying synaptic deficit (Foord et al., 2005; Holsboer, 2000; Luscher et al., 2011; López-Muñoz and Alamo, 2009; Nutt, 2002). This was a tremendous advantage in neuropsychopharmacology, equipping researchers and physicians with a cellular correlate for depression and other SRPDs for the first time. However the drawback is that research has been canalized onto this

particular neurotransmitter system, hampering research on non-monoamine-based ADs (Berton and Nestler, 2006; López-Muñoz and Alamo, 2009). After the development of more selective compounds for the noradrenergic- (e.g., desipramine, SNRI), and the serotonergic system (e.g., clomipramine, SSRI), drugs that are selective for two monoamine transporters were developed (e.g., venlafaxine). Although there was a lack of clinical evidence, it has been suggested that balanced or dual reuptake inhibitors may be superior to single re-uptake inhibitors (Berton and Nestler, 2006; López-Muñoz and Alamo, 2009; Wrobel, 2007).

However, the monoamine hypothesis is challenged by several inherent inconsistencies, the main one being the delayed onset of the clinical AD effect (several weeks) of most drugs, although monoamine reuptake inhibition occurs immediately following drug administration (due to K_i values in the low nanomolar range), and the finding that several cellular processes assumed to be important for ADs efficiency, are activated rapidly (Berton and Nestler, 2006; Holsboer et al., 2012; Holsboer, 2000; Krishnan and Nestler, 2008; Rantamäki et al., 2011). Furthermore, tianeptine, a selective serotonine reuptake enhancer (SSRE) exerts AD effects (McEwen et al., 2010; Sanacora et al., 2012). Complicating the picture, dietary tryptophan, which diminishes serotonin levels in the brain, does not significantly affect mood in healthy volunteers and patients suffering from MD (Castrén, 2005). Moreover, by means of various methodological approaches, including genetically altered mice which display depression-related behavior (Cryan et al., 2002), various mechanisms of AD drug action have been identified so far. This includes the aforementioned monoaminergic system, the glutamatergic system, the GABAergic system, ion channels, neurotrophins like brain-derived neurotrophic factor (BDNF), and components of the HPA axis. Several of these targets are modulated by AD drug concentrations much higher than those required for serotonin/norepinephrine reuptake inhibition, supporting the idea of monoaminergic-independent effects occurring with brain concentrations of ADs in the high nanomolar/low micromolar range (Duman and Aghajanian, 2012; Holsboer and Barden, 1996; Jang et al., 2009; López-Muñoz and Alamo, 2009; Luscher et al., 2011; Méndez et al., 2012; Rammes and Rupprecht, 2007; Saarelainen et al., 2003). In line with this, magnetic resonance spectroscopy studies in humans revealed fluoxetine and fluvoxamine brain concentrations in the low micromolar range after a few weeks of drug administration. Interestingly, the appearance of such concentrations match with the time point of symptom alleviation (Bolo et al., 2000; Strauss et al., 1997).

These observations point to cellular adaptions and morphological changes triggered by ADs far from a simple increase of the synaptic availability of monoamines. Additional changes in intracellular signal transduction cascades and synaptic connectivity are likely to occur (Castrén, 2005; López-Muñoz and Alamo, 2009). Accordingly an alternative hypothesis to the chemical view of SRPDs and the action of ADs has emerged in recent years (Castrén, 2005; Leistedt and Linkowski, 2013). The network hypothesis argues that information processing disturbance within distinct neuronal networks represents the common final pathway of SRPDs and that AD drugs induce changes in neuronal plasticity and connectivity that, when treated chronically, gradually lead to improvements in

neuronal information processing and healing of the disorder (Figure 1.3; Castrén, 2005). However, contradicting evidence comes from the observation that AD medication has often to be taken for several years and a termination of drug intake after symptom alleviation leads to a relapse to disease in a high percentage of patients (Castrén, 2005; Leistedt and Linkowski, 2013; Castrén, 2013). Nevertheless, an increasing amount of data highlights the effects of ADs on the plasticity of neuronal networks. Imaging studies in patients with MD have revealed that reduced gray matter in the HIP is to some degree reversed by ADs (Castrén, 2005). Highly recognized evidence for the network hypothesis comes from the observation that chronic stress decreases and ADs increase the production and/or turnover of new neurons in the rodent HIP (Castrén, 2005; Duric and Duman, 2013). Interestingly, the increased neurogenesis facilitated by chronic AD treatment coincidences with the behavioral effects produced by ADs. It is thought that ADs restore or facilitate synaptic plasticity, reminiscent to the situation during development and thereby alleviate adaptions in neuronal connectivity (Castrén, 2005; Leistedt and Linkowski, 2013; Maya Vetencourt et al., 2008).

1.4.2.1 Role of neurotrophic factors and their receptors in the pharmacology of antidepressants

Neurotrophins, which include nerve growth factor (NGF), BDNF, NT-3, NT-4/5, and NT-6 are critical regulators of the formation and plasticity of neuronal networks and are produced in an activity-dependent manner (Castrén et al., 2007; Jang et al., 2009; Poo, 2001). The physiological actions of neurotrophins are mediated through two classes of receptors: high-affinity tyrosine related kinase (Trk) receptors and a low-affinity pan-neurotrophin-receptor (p75NTR). The Trk receptors are members of a transmembrane tyrosine kinase family (TrkA, TrkB, and TrkC). NGF predominantly binds and activates TrkA, BDNF, and NT-4/5 mainly interact with TrkB, and NT-3 predominantly associates with TrkC, while having lower affinity to TrkA and TrkB receptors. Binding of neurotrophins to Trk receptors initiates receptor homodimerization, autophosphorylation of cytoplasmic tyrosine residues on the receptors, and a cascade of cell signaling events including Ras/Raf/MAP kinase, PI3K/Akt, and PLC-γ1 (Jang et al., 2009; Poo, 2001). In addition to long-term effects of neurotrophins like gene regulation, the cytoplasmic effectors activated by neurotrophins have been also implicated in a wide range of more rapid actions, most notably modulation of neuronal excitability and synaptic transmission (Berton and Nestler, 2006; Poo, 2001). Chronic stress is widely used as a model of SRPDs. Chronic stress decreases expression of BDNF in the HIP of rodents and a common finding is, if administered chronically but also acutely, most ADs induce autophosphorylation of TrkB receptors in the HIP, which is sufficient to ameliorate the detrimental effects of stress on behavior (Berton and Nestler, 2006; Poo, 2001; Saarelainen et al., 2003). Moreover, reduced levels of BDNF have been found in patients suffering from MD and AD drug therapy restores brain BDNF levels to the normal range (Castrén et al., 2007).
However, it is important to note that BDNF and other neurotrophic factors do not control mood and no single hypothesis of AD action is valid by oneself (Castrén, 2005;

Leistedt and Linkowski, 2013). Rather, the different adaptive system seem to be orchestrated in response to AD treatment. The synthesis and release of several important neuromodulators and neurotransmitters is regulated by neuronal activity and changes in activity patterns produce changes in the concentrations of these signaling molecules. Although the initial effects of ADs are obviously chemical, subsequent adaptive changes in the concentrations of these signaling molecules are tightly linked to the structure of neuronal networks and may be a consequence of altered information processing rather than its cause (Leistedt and Linkowski, 2013). According to this view, it is more likely that AD treatment rapidly modulates several molecular and cellular targets, which activate neurotrophic factor systems, thereby re-establishing normal activity patterns in the hippocampal neurocircuitry and ultimately in behavior (Figure 1.3; Castrén et al., 2007; Duman and Aghajanian, 2012). Therefore, analyzing endophenotypes of specific brain circuits might help bridging the gap between molecular/cellular processes and behavioral outcome under AD treatment.

Chapter 2

Aims of the thesis

Extensive research in humans and rodents has shown that cognitive deficits and a disturbance of the neuroendocrine stress response are frequently associated with stress-related psychiatric disorders (SRPDs), but also provided substantial evidence that these symptoms are likely mediated by malfunction of information processing within distinct neuronal networks, including the hippocampus (HIP; Airan et al., 2007; Castrén, 2005).
Classical electrophysiology has gained valuable insights regarding the contribution of single cells and small neuronal populations in the pathophysiology of SRPDs. However, this "sparse world view" provides a limited and possibly distorted picture of how large-scale neuronal networks respond to a constantly changing environment in real time (Lewis and Lazar, 2013). Accordingly, a more intensive use of circuit-centered approaches in psychiatric research is highly recommended (Karayiorgou et al., 2012). Within this framework, the present dissertation intended to address three major questions:

1. First, which activity pattern in perforant path fibers is capable of evoking polysynaptic activity flow through the HIP *in vitro*?

2. Second, is this circuit-centered approach suited to address a long standing question in hippocampal physiology: How do brain systems afferent to the HIP initiate the formation of CA1 LTP?

3. Third, is this circuit-centered approach suited to investigate whether and how chronic stress and acute application of various drugs alter neuronal network dynamics in the HIP?

To address these questions, field potential recordings and voltage-sensitive dye imaging (VSDI) were applied to mouse brain slices. VSDI allows the analysis of neuronal activity on a millisecond time-scale, with a micrometer-range spatial resolution and, most notably, a scope spanning the entire HIP (Airan et al., 2007; von Wolff et al., 2011).

Chapter 3

Material and Methods

3.1 Animals

CD1 male breeders (12-24 week-old, Charles River; Erkrath; Germany) were used as "resident" mice within the chronic social defeat stress (CSDS) paradigm. All other animals comprise adult (8-12 week-old) male C57BL/6N mice (MPI of Neurobiology; Martinsried; Germany). Animals that underwent the CSDS paradigm were single-housed, all other mice were housed one to five per standard cage (25 x 19 cm) at the animal facility of the Max Planck Insitute of Psychiatry (MPIP) in Munich. The animals received food and water *ad libitum* and temperature and humidity were maintained constant (22 °C ± 1 °C; relative humidity 55% ± 10%) with a 12 h light/dark cycle (lights on from 7:00 A.M. to 7:00 P.M.). All experimental procedures were approved by the Committee of Animal Health and Care of the local governmental body and were performed in strict compliance with the guidelines for the care and use of laboratory animals set by the European Community.

3.1.1 Chronic social defeat stress paradigm

The CSDS paradigm was carried out by *Andrés Uribe* (RG M.V. Schmidt) at the MPIP. In brief, male CD1 mice served as resident mice, which were held under the conditions described above. They were allowed to habituate to a standard cage for 1 week and afterwards to the social defeat cage (45 cm x 25 cm) for 5 to 7 days prior to the experiment. For the CSDS, an experimental C57BL/6N mouse was placed into the defeat cage of a physically superior resident CD1 mouse for approximately 1 min. During this period the C57BL/6N mouse was physically defeated by the CD1 mouse. The physical contact was carried out between 9 a.m. and 5 p.m. in a random manner to avoid habituation to a fixed schedule of defeat. After physical interaction, the CD1 and experimental mouse were maintained in sensory contact for 24h, using a perforated metal partition dividing the defeat cage in two. The experimental mice were exposed to an unfamiliar CD1 mouse defeat cage for 19 consecutive days and VSDI recordings were conducted between day 15 to 20. On the day of data acquisition the animals were not exposed to a CD1 mouse.

All mice were handled daily, and weight and fur status was assessed. Injured animals were discarded from the experiments (Berton et al., 2006; Wang et al., 2011).

3.2 Preparation and staining of brain slices

Initial experiments revealed that brain slice quality is paramount for optical recordings of polysynaptic activity flow in the HIP. Thus, the most crucial steps of brain slice preparation are described in detail. The brain should be removed rapidly from the cranium, but handled as gently as possible to avoid damage. Mice were anesthetized with isoflurane (see Appendix 8.1) and decapitated at the level of the cervical spinal cord using an animal guillotine. All following steps were done in ice-cold sucrose-based saline (Bischofberger et al., 2006). The fractionally frozen physiological saline was crushed with a hand blander to a homogenizate, thereby avoiding damage of the brain by ice crystals or concentration gradients. The saline (pH 7.4) was saturated with carbogen gas (95% O_2/5% CO_2) using microfilter candles and consisted of (in mM): 87 NaCl, 2.5 KCl, 25 $NaHCO_3$, 1.25 NaH_2PO_4, 0.5 $CaCl_2$, 7 $MgCl_2$, 25 glucose, and 75 sucrose. After decapitation, the brain was transferred into a petri dish and the brain was rapidly removed from the cranial cavity including the following steps:

1. Removal of the scalp by a sagittal incision from caudal to frontal
2. Sagittal incision (median) of the cranium, beginning at the level of the foramen magnum to frontal
3. Two small incisions on each side of the cranium perpendicular to the previous one at the level of bregma
4. Swinging open the skull on each side with a butt forceps
5. Gentle removal of the brain from the cranial cavity from frontal to caudal with a slim spatulum
6. Transfer of the brain with a flat spatulum for storage in carbogenated cutting solution (30sec.).

Next, the brain was separated into its hemispheres and the right hemisphere was prepared for the slicing procedure by a special transversal cut, which is sometimes called "magic cut" (Bischofberger et al., 2006). These cuts were done on a standard filter paper to simplify the cutting procedure. Cutting the hemisphere at this specific angle optimizes the conservation of the intrahippocampal axonal projections along its septotemporal axis (Bischofberger et al., 2006). To remove excessive saline, a standard filter paper was used. Accordingly, the brain was glued at the "magic cut" side on the cooled tissue block with a tissue adhesive produced from enbucrilate (Histoacryl®; Aesculap AG; Tuttlingen; Germany). As soon as the hemisphere adhered to the tissue block, a few drops of ice-cold saline were dripped onto the brain with a pipette. This avoids that glue creeps up, covers the surface of the brain and aggravates the movement of the razor blade (Bischofberger et al., 2006). Then the tissue block was immediately placed in the cutting dish of the

vibratome (HM650V, Freq.: 66, Ampl.: 0.9, V=8; Thermo Scientific; Waltham; USA). Subsequently, 350 μm-thick horizontal slices containing the HIP were cut with a cleaned (acetone, ethanol) razor blade (Dreaming; Goldhand mbH; Düsseldorf; Germany). According to Bischofberger et al. (2006), the angle between blade and horizontal plane was set at $\sim 17^\circ$. When the respective slice was cut, the vibratome was stopped and the slice was removed with a needle by two cuts perpendicular to each other through the surrounding tissue. Afterwards, slices were transferred into a maintenance chamber, where they were placed upside-down in contrast to the original orientation during the slicing procedure. This orientation should be maintained through all following steps until the end of VSDI measurements. After preparation, slices were incubated in carbogenated sucrose-based saline for 30 min at 34 °C. Subsequent staining of slices with the voltage-sensitive dye Di-4-ANEPPS (see 8.1; Tominaga et al., 2000; Airan et al., 2007; Refojo et al., 2011; von Wolff et al., 2011), dissolved in dimethyl sulfoxide (DMSO) to a 20.8 mM stock solution was carried out at room temperature ($23 - 25\,^\circ$C). For staining, slices were transferred to a 60 x 15mm petri dish and kept for 15 min in carbogenated physiological saline containing Di-4-ANEPPS (7.5 g/ml; <0.1% DMSO; Refojo et al., 2011; von Wolff et al., 2011). The physiological saline (pH 7.4) consisted of (in mM): 125 NaCl, 2.5 KCl, 25 $NaHCO_3$, 1.25 NaH_2PO_4, 2 $CaCl_2$, 1 $MgCl_2$, and 25 glucose. Afterwards, slices were transferred back to the maintenance chamber and stored at room temperature for a minimum of 30 min in Di-4-ANEPPS-free, but bicuculline methiodide (BIM)-containing (0.6 μM) carbogenated physiological saline (only exception, Figure 4.23).

3.3 Brain slice experiments

VSDI and field exitatory postsynaptic potential (fEPSP) recordings were conducted at room temperature on a vibration-cushioned table (TMC; Peabody; USA), equipped with a Faraday cage (TMC; Peabody; USA) to minimize extraneous electrical noise. In the submerged recording chamber, slices were fixed with a custom made platinum frame/nylon string harp ("grid") and continuously superfused with BIM (0.6 μM), containing carbogenated physiological saline (4-5 ml/min flow rate). The circulation was established by using a combination of a gravity system (for influx) and a peristaltic pump (Ismatec; Glattburg; Germany; for outflow). Thus, vibrations at the surface of the superfusion medium were avoided. These settings minimize motion artifacts during recordings which is indispensable for VSDI experiments. Figure (3.1A) depicts one representative slice that was cut at a distance between 2.3 and 3.0 mm ($\pm$ 0.1 mm) from the ventral base of the brain. Pilot experiments revealed that hippocampal trisynaptic circuit (HTC)-waves can be most reliably evoked in these particular slices. According to the "ventral/dorsal HIP hypothesis" (Maggio and Segal, 2007; Fanselow and Dong, 2010), experiments were conducted in the dorsal HIP or in the intermediate zone. EC/DG-input was evoked by electrical stimulation of the PP, which also contains fibers that directly innervate the most distal apical dendrites of CA3 pyramidal neurons (Steward, 1976; Andersen et al., 2006). After fixation of the slice, but before placing stimulation or recording electrodes, these fibers

were cut at the tip of the suprapyramidal blade, the point where they exit the DG (Figure 3.1A). Temporoammonic projections (Andersen et al., 2006) were likewise functionally inactivated by a cut, ranging from the hippocampal fissure to the cortical surface (Figure 3.1A). The deafferentations were accomplished by means of a tapered scalpel blade and a custom-made "microknife" (approximately 100 μm blade length; Figure 3.1B).

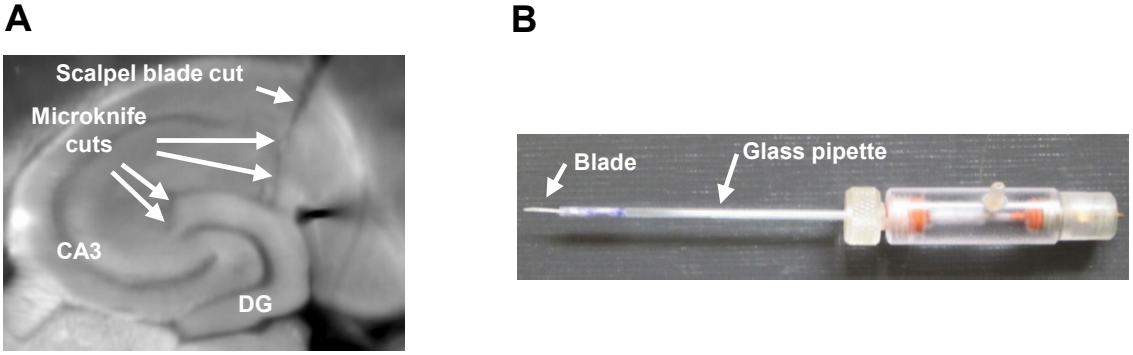

Fig. 3.1. Deafferentiations performed in hippocampal brain slices. ***(A)*** *Illustration of deafferentiations performed with a scalpel blade and the microknife in hippocampal brain slices.* ***(B)*** *Custom made microknife used for cutting direct cortical inputs to areas CA3 and CA1 (**A**, modified from Stepan et al., 2012).*

The scalpel blade was used for a first, rough cut on the tissue block directly following the slicing procedure. The "microknife" was made by breaking out small pieces from a standard razor blade. Under a microscope, the quality of the "microknife" was checked. When the respective "microknife" quarried out, it was glued into a shortened 1.5 mm borosilicate glass pipette (Harvard Apparatus; Edenbridge; UK). This construction was then coupled to a microelectrode holder. Thereby, the "microknife" could be utilized to precisely round out the "pre-cut" generated by the scalpel blade (Figure 3.1A,B).

3.4 Voltage-sensitive dye imaging (VSDI)

VSDI and data analysis were performed using the MiCAM02 hard- and software package (BrainVision; SciMedia Ltd.; Costa Mesa; USA). The tandem-lens fluorescence microscope was equipped with the MiCAM02-HR camera (charged coupled device (CCD) camera) and a 2x and 1x lens at the objective and condensing side, respectively (Figure 3.2).

By means of a halogen light source (MHAB; 150W; Moritex Corp.; Tokyo; Japan), an excitation filter (530 nm pass) and a dichroic mirror (520 $\sim$ 560 nm reflect (>90%), 600 nm (>85%) pass), light with a specific wavelength was reflected towards the objective lens to illuminate the brain slice, stained with Di-4-ANEPPS (Tominaga et al., 2000). It is well known that fluorophores (e.g., Di-4-ANEPPS) absorb light energy (photons), a process that sometimes can move an electron into a different orbital, the so-called exited state (within fs). Fluorescence emission is one way how a fluorophore returns to its low-energy ground state. Due to energy loss in the excited state, the emitted light has a longer wavelenght. The difference between the exciting and emitted wavelengths is known as Stokes shift (Lichtman and Conchello, 2005). Accordingly, emitted photons (fluorescence)

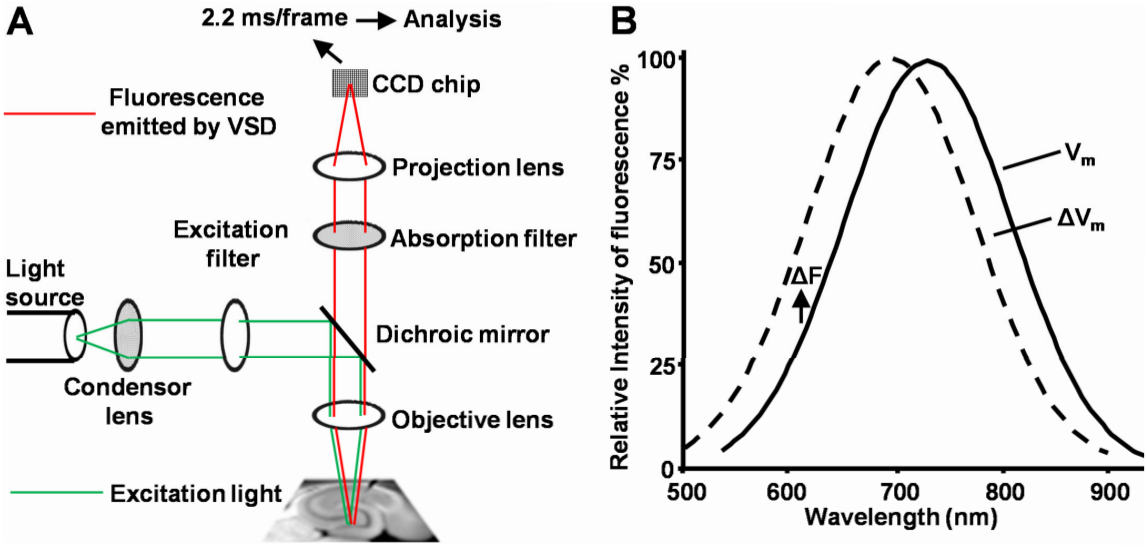

Fig. 3.2. Voltage-sensitive dye imaging. ***(A)*** *Components used for imaging of neuronal activities, by means of fluorescence emitted from voltage-sensitive dyes, recorded with a CCD camera.* ***(B)*** *Electrochromic voltage-sensitive dyes, are believed to sense voltage via the Stark effect. Upon depolarization, the emission spectrum of Di-4-ANEPPS shifts to shorter wavelengths (eletrochromatic effect; dotted line), with a concomitant decrease of the area under the curve (△F) of integrated wavelengths > 590nm. (**B**, modified from Canepari and Zecevic, 2010, p.16). Abbreviations: △F, change in fluorescence; V_m, membrane voltage; VSD, voltage-sensitive dye.*

were collected and projected onto the CCD sensor through an emission filter (> 590nm; Figure 3.2; Tominaga et al., 2000).

The fast styryl dye used here, interacts directly with the electric field and the charge distribution over the molecule depends on the membrane voltage which additionally displays a linear relationship to the amount of photons emitted (Fluhler et al., 1985; Loew, 1992; Miller et al., 2012). One hypothesis is that excitation of the dye with a simultaneously occurring change of the membrane potential alters the excited state molecular dipole (electrochromic effect, within ns) shifting its emission spectrum to longer (excited state molecular dipole is stabilized = hyperpolarization) or shorter (the charge shift inverted state is destabilized = depolarization) wavelengths (Stark effect; △F). These bathochromic or hypsochromic shifts are accompanied by a concomitant decrease or increase of the area under the curve. This allows to differentiate between excited and/or unexcited tissue and to calculate the fractional change of fluorescence (% △F/F) for each pixel, thus reflecting a direct measurement of neuronal activity (Figure 3.2; Canepari and Zecevic, 2010; Loew, 1992; Miller et al., 2012; Tominaga et al., 2000). Because the electric field and the energy levels of the fluorophore directly interact, the kinetics of voltage sensing occur on a timescale commensurate with absorption and emission, resulting in ultrafast spectral emission shifts (fs to ps) many orders of magnitude faster than required to resolve action potentials in neurons (Miller et al., 2012). Typical values for changes of △F in neuronal tissue stained with Di-4-ANEPPS range around 10% per 100 mV. Unless noted otherwise, standard settings of the MiCAM02-HR camera system were as follows: 88 x 60 pixels frame size, 36.4 x 40.0 μm pixel size, and 2.2 ms sampling time.

3.5 Processing and quantification of VSDI data

From recorded VSDI signals, % $\triangle$F/F for wavelengths $>$ 590 nm was calculated. For all quantifications, % $\triangle$F/F values were spatially and temporally smoothed, using a 3 x 3 x 3 average filter. VSDI signals presented in images were smoothed with a 5 x 5 x 3 average filter. To attenuate slow signal components produced from bleaching of the voltage-sensitive dye (Carlson and Coulter, 2008) and a slight summation of 5 and 20 Hz neuronal responses, a weak high-pass filter of the MiCAM02 software was applied (τ= 220 ms) to the imaging data afterwards. Pixelation of images was reduced by the interpolation function of the MiCAM02 software.

For analysis of neuronal population activity in hippocampal subregions, three standardized region of interest (ROI) were manually set according to anatomical landmarks. The circular CA3-ROI (r = 4 pixels) was placed into the CA3 region close to the DG, but not overlapping with it. The circular CA1-ROI (r = 4 pixels) was positioned into the CA1 subfield at a distance of $\sim$ 200 μm from the visually identified distal end of the stratum lucidum. The CA3-ROI spanned the stratum oriens, stratum pyramidale, and stratum lucidum/radiatum (Figure 4.2A).

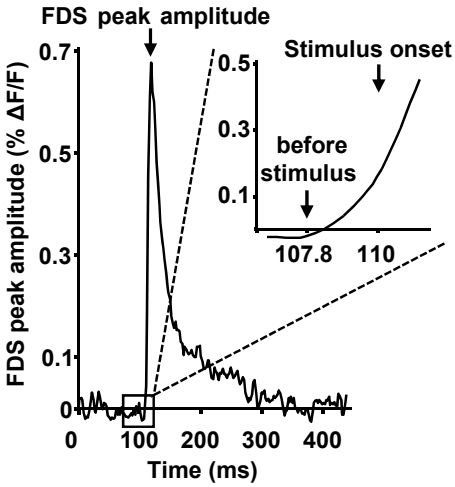

Fig. 3.3. Quantification of the fast, depolarization-mediated VSDI signal. *To quantify FDSs, the value (% $\triangle$F/F) before stimulus onset (107.8 ms) was subtracted from the value at FDS peak amplitude (110 ms).*

This was also the case for the CA1-ROI, with the exception of the LTP experiments, where it only covered the stratum radiatum (r = 2 pixels; Figure 4.18A). The polygon DG-ROI (composed of $\sim$ 450 pixels) enclosed the outer two layers of the DG (without the hilus) and was created by the polygon-drawing function of the MiCAM02 software (Figure 4.18A). The average of smoothed % $\triangle$F/F values within a particular ROI served as final measure of neuronal population activity. For further analysis in BrainVision, the peak amplitude of the fast depolarization-mediated signal (FDS) was corrected (Figure 3.3), to avoid that background fluorescence (noise) biased FDS values during LTP- and pharmacological experiments. From all data presented in absolute values (only for illustration of results) the peak amplitude was determined in Excel (Version 2003; Microsoft; Redmond; USA) without applying the correction procedure.

3.5.1 HTC-wave assay adjustments for group comparisons

The voltage range (15-35 V), to generate comparable CA1-FDSs (0.1 to 0.3 % $\triangle$F/F) during baseline recordings in pharmacological experiments was quite limited (see Results, 4.1.4). However, to minimize variance in the input signal, the HTC-wave assay was

further adapted for cross-slice and animal comparisons (Figures 4.1, 4.27A,B). This normalization is supposed to be prerequisite for evaluating functional meanings of changes caused by chronic stress. Instead of fixed voltage intensities, the levels of FDSs within a specific DG-ROI were used. This polygon dentate gyrus supra (DGS)-ROI (composed of $\sim$ 150 pixels) covered the outer two-third of the DG suprapyramidal ML (corresponding to the synaptic input field of the PP; Figure 4.27B; Andersen et al., 2006). Single-pulse EC/DG-input served to adjust activity levels within the DGS-ROI. Pilot experiments revealed that DGS-FDS activity levels of 0.35/0.45/0.55 % $\triangle$F/F (default DGS-FDS) covered nearly the complete dynamic range of input signals, which were capable of inducing HTC-waves without producing epileptic-like activity (Figure 4.28). Furthermore, increasing the FDS within this particular ROI was associated with a linear increase in subsequent CA3-, and CA1-FDSs (Figure 4.28). On each adjusted intensity level, 15 stimuli at 5 Hz were applied to the PP. The first FDS in the DGS-ROI and the mean of the last three FDSs in areas CA3 and CA1 were used as final measure of neuronal activity (Figure 4.28). Recordings were obtained from 2 to 3 slices per animal and subsequent statistical analysis was performed on individual animal basis.

3.6 Field potential recordings

Field potentials in the CA3 stratum lucidum and CA1 stratum radiatum were recorded using borosilicate glass pipettes (Harvard Apparatus; Edenbridge; Kent; UK) (1 MΩ open-tip resistance) that were filled with BIM (0.6 μM) containing physiological saline. Recorded data was low-pass filtered at 1 kHz and digitized at 5 kHz. Recorded signals were stored (Macintosh 7100; Apple Inc.; Cupertino; USA) and fEPSPs and population spikes were analyzed using the Pulse Software and macros written in Igor Pro (Version 6.12a; WaveMetrics Inc.; Lake Oswego; USA).

3.7 Electrical stimulation techniques

In all experiments, neuronal activity was evoked by square pulse electrical stimuli (200 μs pulse width), delivered through custom-made monopolar tungsten electrodes (Teflon-insulated to the tip of 50 μm diameter). These electrodes enabled a very precise placement into the neuronal tissue at the stimulation site and did not interfere with the imaging process (e.g., by producing irritating shadows as observed with other electrodes). A highly localized electrical stimulation was achieved by placing the indifferent electrode far away from the slice in the recording chamber. During recordings which required two stimulation electrodes (CA1 LTP experiments), the currently unused electrode was uncoupled from the stimulation device in order to avert an indirect application of voltage to the inactive electrode. The electrode used for evocation of EC/DG-input was placed under a binocular on the visually identified PP at distance of 40 μm ($\pm$ 10 μm) away from its entry zone into the DG, to avoid direct stimulation of neurons and their dendrites within the ML (Figure 4.18A). Baseline recordings in stratum radiatum were done to

monitor putative alterations in the strength of neurotransmission at SC to CA1 synapses in LTP experiments. Using stimulation of the SC-commissural pathway near the CA3 averted boundary of the CA1-ROI, a large fraction of the CA3 to CA1 synapses was antidromically (Bliss and Collingridge, 1993) activated under both conditions, during baseline recordings and after LTP induction. This approach recruited commissural fibers just as SCs which were cut somewhere in the CA3 or CA1 region during preparation of brain slices. Low stimulation intensities evoke neuronal activity within the CA1-ROI that may be overlaid with signals resulting from activation of such "irrelevant" fibers. To minimize the probability of interference, a stimulation intensity which produced a strong fEPSP and, thus, a concomitant population spike was used (Figure 4.18; Stepan et al., 2012). For analysis of VSDI experiments neither the peak amplitude nor the slope of CA1-FDS could be used as proper measure of changes in the strength of neurotransmission at CA3 to CA1 synapses. This is due to the fact that in contrast to field potential recordings, VSDI displays action potentials and EPSPs always as signals exhibiting the same deflection course (Carlson and Coulter, 2008). To overcome this problem and thereby render LTP experiments via VSDI possible, the amplitude of a later CA1-FDS component was used as such a measure (frame 13, 28.6 ms after the stimulation pulse (FDS_{F13}); Stepan et al., 2012). By means of simultaneous VSDI and field potential recordings, Stepan et al. (2012) showed that the FDS_{F13} value reflects the amplitude of the glutamatergic fEPSP during its decaying phase. Using the FDS_{F13} amplitude with a value in the range between 60-80 % of the CA1-FDS peak amplitude revealed that increasing the stimulation intensity or adding the AMPA receptor potentiator cyclothiazide (100 μM; Eder et al., 2003; Stepan et al., 2012) further increased the FDS_{F13} signal in field potential and VSDI recordings (Figure 4.18). Moreover, the induction of populations spikes with high stimulation intensities showed that at this particular point of time, fEPSPs do not mingle with action potentials fired by CA1 pyramidal neurons anymore (Stepan et al., 2012). Further evidence supporting the use of the FDS_{F13} amplitude in the LTP experiments comes again from VSDI combined with field potential recordings. 5 Hz EC/DG-input for 6 s, which evoked CA1 LTP as measured with VSDI, caused a long-lasting increase in the slope and the amplitude of fEPSPs, 28.6 ms after the stimulation pulse (Figure 4.18C).

3.8 Fluorescein-guided administration of drugs to brain slices

For local application of DCG-IV (see Appendix 8.1) and D-APV to hippocampal subfields CA3 and CA1, a non-invasive pressure application was used. All following steps were visually guided under a binocular. After baseline recordings, the camera unit was removed and a borosilicate glass pipette (0.2-0.3 MΩ open-tip resistance) mounted on a micromanipulator was positioned in the neuronal tissue beyond the HIP. The glass pipette was filled with physiological saline containing BIM (0.6 μM), fluorescein (FLUO) (10 μM) and the drug to be applied. The filling was done just before pressure application to avoid blinding of the tip. Subsequently, the tip of the pipette was slightly moved into the brain tissue and pulled out of the slice again with a defined number of steps using

the micromanipulator. This procedure ensured an appropriate and comparable position of the tip of the pipette in relation to the surface of the slice for all experiments. To avoid damage of neuronal tissue by the pressure ejected fluid, the horizontal end-position was set somewhat above the region of interest. FLUO, whose fluophoric characteristics were triggered by means of light emitted from a UV diode (Conrad; Hirschau; Germany; 405 nm), served to visually guide the spread of the pressure ejected fluid (Figure 4.14A). Pilot experiments revealed that a spatially restricted drug application on the region of interest could be achieved by thoroughly setting the following parameters (Figure 4.14A):

- The resistance of the glass pipette (size of the aperture)
- Capitalization of the ejected fluid on the stream of the superfusion medium through the recording chamber
- Appropriate adjustment of the strength of pressure applied to the electrode
- The distance of the tip of the pipette in relation to the slice surface (see above)
- The specific orientation of the slice within the recording chamber to exclusively cover the region of interest.

In the FLUO-guided experiments, somewhat higher concentrations of drugs were used than typically bath-applied to reach the maximum pharmacological effect. This was done since drugs (DCG-IV and D-APV) had to rapidly penetrate the neuronal tissue by diffusion and, second, the application duration was restricted to a few seconds. Pilot experiments revealed that excessive application of FLUO increases the VSDI signal above baseline. Therefore, both, the period of application and the concentration of FLUO were kept as low as possible. A FLUO concentration of 10 μM and application times of approx. 60" were suited to avoid effects on the VSDI signal (Figure 4.22). Nevertheless, control applications of FLUO alone were carried out in all sets of experiments. The spatial restriction of the FLUO-guided drug administration on the region of interest was verified by bath application of DCG-IV at a concentration of 1 μM (Kew et al., 2002; Nicoll and Schmitz, 2005). DCG-IV decreased evoked neuronal activity in the DG, consistent with its inhibitory effect on glutamatergic neurotransmission at PP synapses (Figure 4.14B; Kew et al., 2002). If DCG-IV was specifically applied to area CA3, this effect was not observed (Figure 4.15). Next, a set of control experiments was done to determine which concentration of pressure applied D-APV leads to a complete block of NMDA receptors. Different pressure-applied concentrations of D-APV were compared to bath application of D-APV at the standard concentration of 50 μM (Avrabos et al., 2013). These control experiments revealed that D-APV, pressure applied for 1 min at a concentration of 200 μM, reduced the FDS_{F13} amplitude of CA1-FDSs to nearly the same extent as bath applied D-APV at 50 μM (Figure 4.22).

3.9 Chemicals

See Table (8.1).

All salts for the physiological saline solutions were purchased from Sigma-Aldrich. For chemicals not solved in artificial cerebrospinal fluid, the corresponding amount of solvent was added during baseline recordings. Corticosterone was dissolved in ethanol, which was present at a concentration of 0.009% during experiments. Diazepam and Haloperidol were dissolved in DMSO, which was present at a maximum concentration of $\leq 0.001\%$ and $\leq 0.02\%$, respectively.

3.10 Statistics

For statistical comparisons between groups, the data were checked for normality distribution and equal variance. If the criteria where met, statistical significance was assessed by paired t-est, unpaired t-tests or analysis of variance (ANOVA) when appropriate; when the criteria were not met, a Mann-Whitney U-test or a Kruskal-Wallis ANOVA on ranks were used. Analysis of stimulation strength intensities was performed using one-way ANOVA for repeated measures. ANOVAs were followed by the appropriate *post-hoc* test (see figure legends). All tests were run in SigmaStat (Systat Software; Chicago; USA) and differences were considered significant if $p < 0.05$. Data are given as mean $\pm$ s.e.m.

Chapter 4

Results

The results are organized in the following way: The first section examines the characteristics of polysynaptic activity flow through the trisynaptic circuit of the HIP, sections two and three assess how this phenomenon is influenced by chronic stress and antidepressant drugs.

4.1 Polysynaptic activity flow in the hippocampus

Previous work shows that VSDI is suited to monitor disynaptic activity propagation within the HIP by direct stimulation of DG granule cells (von Wolff et al., 2011). Here, non-synaptic activation of hippocampal neurons was avoided by electrical stimulation of the PP, which constitutes the main axon bundle conveying information from the EC to the HIP (Figure 4.1, 4.2A).

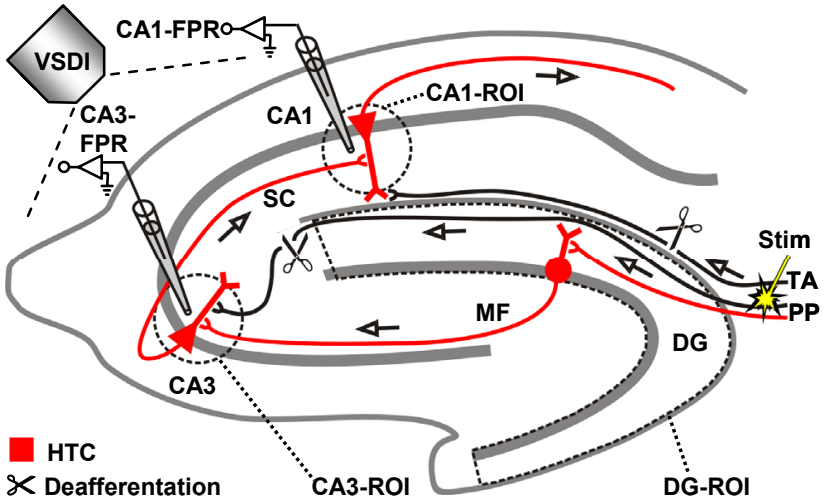

Fig. 4.1. Experimental setup for recordings of polysynaptic activity flow in the HIP. *Arrangement used for investigations shown in Figures (4.3 - 4.11). Abbreviations: FPR, field potential recording; MF, mossy fiber; SC, Schaffer collateral; Stim, extracellular electrical stimulation; TA, temporoammonic pathway (adapted from Stepan et al., 2012).*

This EC/DG-input opens the possibility to investigate manifold aspects of trisynaptic activity flow through the HIP. DG granule cells give rise to the anatomically most prominent non-commissural/associational innervation of CA3 pyramidal cells. This may also render EC/DG-input the major trigger for physiological phenomenons like CA1 LTP. Consequently, PP fibers that directly innervate areas CA3 and CA1 (temporoammonic pathway) were micro-dissected via surgical cuts in all following experiments to ensure that hippocampal activity solely arises from EC/DG-input (Figures 4.1, 3.1A). As VSDI measure of neuronal activity, "regions of interest" (ROIs)-extracted fast, depolarization-mediated imaging signals (FDSs) were used (Figures 4.1, 4.2A, 4.3; Airan et al., 2007; Refojo et al., 2011; Tominaga et al., 2000; von Wolff et al., 2011).

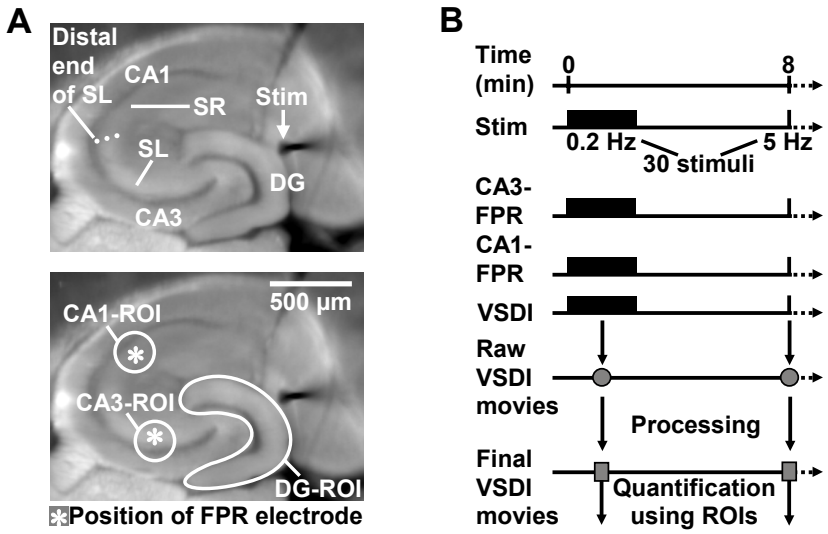

Fig. 4.2. Anatomical position of ROIs and experimental protocol. ***(A)*** *Illustration of the position of ROIs in relation to important landmarks in the HIP.* ***(B)*** *Experimental protocol used for investigations shown in Figures (4.3 - 4.11). Abbreviations: SL, stratum lucidum; SR, stratum radiatum (**A,B**, adapted from Stepan et al., 2012).*

After staining of brain slices Di-4-ANEPPS, every neuronal membrane contributes to the resulting fluorescent signal, but the exact contribution of each part of the neuron (dendrites, soma, axon) and neuronal signal components (action potentials, EPSPs) has not been conclusively answered until now (Chemla and Chavane, 2010; Carlson and Coulter, 2008). Thus, it is rational to state that stimulus-evoked FDSs in hippocampal slice preparations represent a multi-component signal, reflecting neuronal action potentials as well EPSPs of all neurons monitored in a given ROI. Consequently, FDSs are abolished or at least strongly diminished by voltage-gated Na^+ channel blockers or ionotropic glutamate receptor antagonists and lowered extracellular Ca^{2+} concentrations, respectively (Airan et al., 2007; Carlson and Coulter, 2008; Chemla and Chavane, 2010; Tominaga et al., 2000).

4.1.1 Evoked theta-rhythmical activity in the perforant pathway

It is well established that the hippocampal theta rhythm (3-8 Hz) represents the "on-line" state of the HIP and the induction of specific memories is associated with theta activity in

the entorhinal-hippocampal system (Axmacher et al., 2006; Berry and Thompson, 1978; Buzsàki, 2002; Rutishauser et al., 2010; Winson, 1978). Using brain slices, optimized for preservation of intrahippocampal connections, it was first tested whether repeated theta-rhythmical (5 Hz) EC/DG-input triggers hippocampal network dynamics which, except for their rate of occurrence, differ from those elicited by non-theta (0.2 Hz) EC/DG-input (Figure 4.2B).

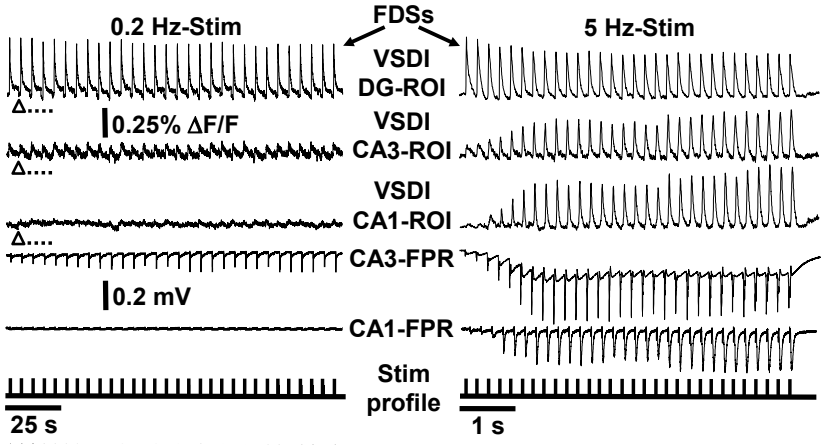

*Fig. 4.3. **Hippocampal activities in response to 0.2 and 5 HZ EC/DG-input.** Open triangles symbolize an interruption of VSDI for 4.34 s. Stimulus artifacts in FPR traces were truncated for clarity (adapted from Stepan et al., 2012).*

Repetitive (0.2 Hz) EC/DG-input triggered prominent neuronal activity in the DG, but only slight neuronal activity in the CA3 region, and no detectable neuronal activity in area CA1 (Figures 4.3, 4.4). These experiments also revealed that unlike direct stimulation of DG granule cells (von Wolff et al., 2011), single pulses applied to the PP are not capable of triggering trisynaptic activity flow through the HIP (Figures 4.3, 4.4).

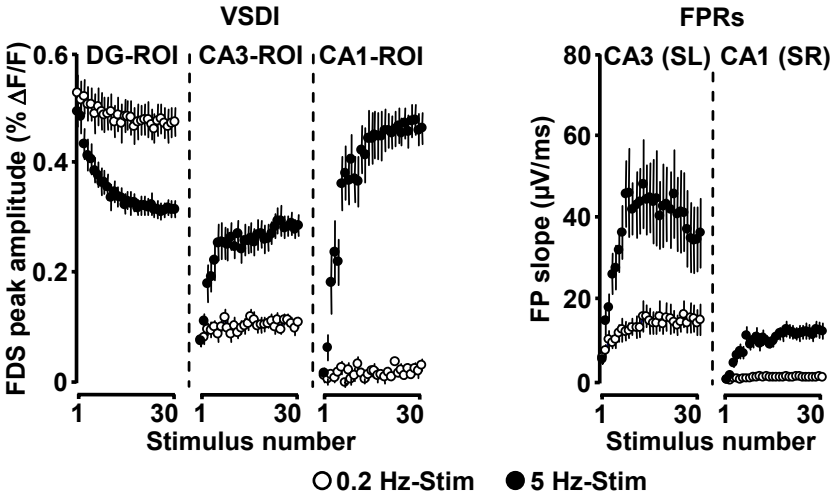

*Fig. 4.4. **Quantification of neuronal activities in hippocampal subregions.** Neuronal activity was monitored using voltage-sensitive dyes and FPRs (N = 9 slices/5 mice) (adapted from Stepan et al., 2012).*

In contrast to non-theta low frequency pulses, 5 Hz EC/DG-input reliably generated waves of neuronal activity which propagated through the entire trisynaptic circuit of

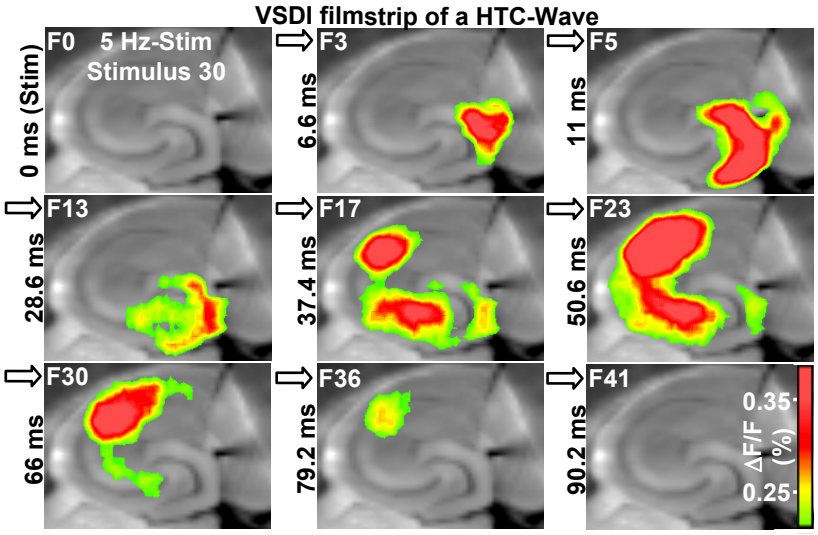

Fig. 4.5. Illustration of hippocampal activities in response to 5 Hz EC/DG-input. *Subfigures depict neuronal activity within the HIP at different timepoints during the 30th stimulus (adapted from Stepan et al., 2012).*

the HIP (HTC-waves; Figures 4.3, 4.4, 4.5, 4.6A). This polysynaptic activity flow started to appear in an initially progressive manner, with complete percolations from approximately the third stimulus on. This corresponds to 600 ms after initiation of EC/DG-input. HTC-waves precisely followed the input rhythm. FDSs in the DG occurred $\sim$ 4 ms after PP stimulation and in CA3 and CA1 with a delay of $\sim$ 12.5 ms and $\sim$ 20 ms, respectively (Figures 4.3, 4.4, 4.6A).

Further analysis of FDSs and fEPSPs revealed that neuronal activity in the DG slightly decreased during 5 Hz EC/DG-input (Figures 4.3, 4.4) .This reduction presumably results from a known habituation process that involves GABAergic neurotransmission and the preferential recruiting of inhibitory interneurons in the DG after focal PP stimulation (Ewell and Jones, 2010; Teyler and Alger, 1976). A pharmacological blockade of ionotropic glutamate receptors completely abolished HTC-waves (Figure 4.6B).

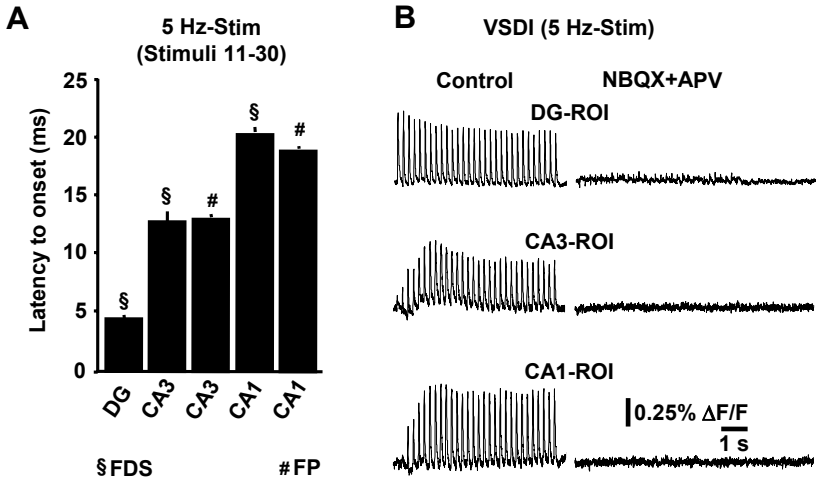

Fig. 4.6. Characteristics of neuronal activities in response to 5 Hz EC/DG-input. (A) *The latency to onset after electrical stimulation of PP axons in hippocampal subfields from experiments depicted and quantified in Figures 4.3 - 4.5* ***(B)*** *Bath application of the AMPA/kainate receptor blocker NBQX (5µM) and the NMDA receptor antagonist D-APV (50 µM) to slices, fully inhibited neuronal activity in the HIP (**A**, N = 9 slices/5 mice) (**A,B**, adapted from Stepan et al., 2012).*

4.1.1.1 HTC-waves involve high-frequency firing of CA3 pyramidal neurons

A closer examination of the CA3 (SL) field potential recordings suggests that HTC-waves involve high-frequency firing of CA3 pyramidal neurons. Here, multiple population spikes, which represent the synchronous firing of several neurons, accompanied the typically fast rising MF fEPSPs (Figure 4.7; Nicoll and Schmitz, 2005; Toth et al., 2000). Both, the rate and the number of these population spikes (173 $\pm$ 19 Hz; Figure 4.7) correspond to the characteristics of physiological burst firing of CA3 pyramidal neurons (Andersen et al., 2006, p.157). This resulted in a prominent SC fEPSP as reflected by pop-spikes that were also interlaced in this signal (Figure 4.7). This indicates that HTC-waves likely elicit action potentials in CA1 pyramidal neurons, which provide a major source of excitatory output of the HIP targeting numerous brain regions, including the EC (Figure 4.7; Andersen et al., 2006).

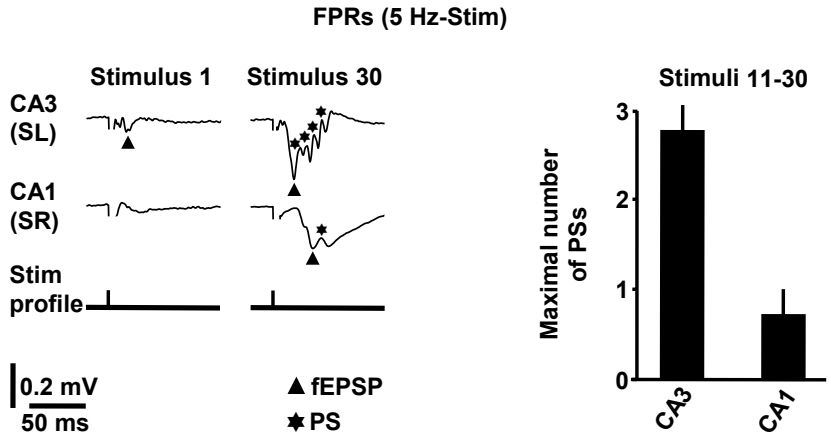

Fig. 4.7. Burst-firing of CA3 pyramidal neurons in response to 5 Hz EC/DG-input. *Pop-spike (PS) initiation and quantity in CA3 and CA1 pyramidal neurons in response to 5 Hz EC/DG-input (N = 9 slices/5 mice) (adapted from Stepan et al., 2012).*

4.1.1.2 Non-theta frequency stimulations are much less effective in inducing HTC-waves

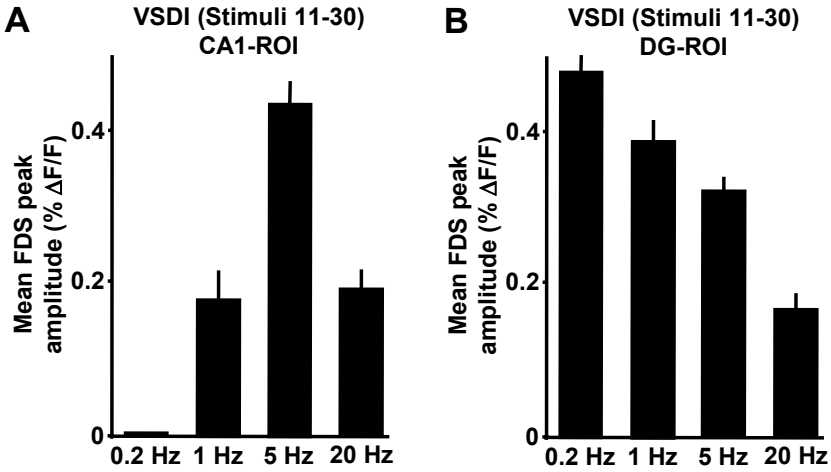

Fig. 4.8. Induction of HTC-waves by non-theta frequency EC/DG-input. (A,B) *Quantification of CA1 and DG neuronal activity in the HIP obtained from non-theta EC/DG-input markedly differs from 5 Hz EC/DG-input (**A,B**; 0.2/5 Hz: N = 9 slices/5 mice, 1 Hz: N = 9 slices/6 mice, 20 Hz: N = 11 slices/6 mice) (**A,B**, adapted from Stepan et al., 2012).*

Several lines of evidence suggest that DG granule cell activity may be subject to a tightly regulated, frequency-dependent inhibitory control (Andersen et al., 1966; Mott and Lewis, 1992). To potentially corroborate this notion, it was determined whether and how effectively non-theta (1 and 20 Hz) EC/DG-input generates activity percolations through the HTC. Neuronal activity was triggered reliably in all three subfields, but activity propagations were considerably less strongly pronounced than those produced by 5 Hz EC/DG-input (Figure 4.8A). Furthermore, these experiments revealed that the aforementioned decline of DG activity was more distinct during 20 Hz EC/DG-input. The opposite scenario was observed for 0.2 and 1 Hz EC/DG-input with a markedly lower decrease of DG activity levels (Figure 4.8B).

4.1.1.3 Rationale for the use of bicuculline methiodide

Pilot experiments revealed that a minimum experimental variability in HTC dynamics can be achieved when brain slice stimulations were carried out in the presence of bicuculline methiodide (BIM). If not stated otherwise, 0.6 μM (BIM) was added to all salines after staining the brain slices with Di-4-ANEPPS. The improvement for initiation of HTC-waves critically depends on concentration of the $GABA_A$ receptor antagonist, since excessive increases of BIM can cause hyperexcitability of the hippocampal network (Figure 4.9; Swann et al., 2007).

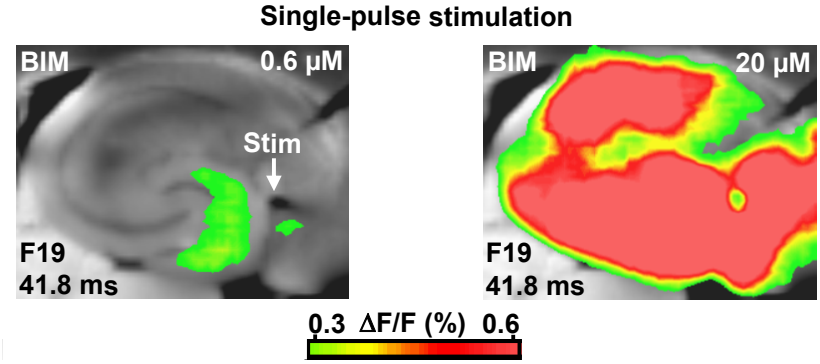

***Fig. 4.9. High concentration of BIM causes epileptiform activity in the HIP**. Single-pulse activation of EC/DG-input causes moderate, spatially restricted neuronal activity in the HIP in BIM (0.6 μM)-treated slices. A subsequent increase to 20 μM led to enormous epileptiform activity in all hippocampal subfields (adapted from Stepan et al., 2012).*

A weakly blocking dose is justified for the following reasons: First, specific excitatory interneurons in the HIP (e.g., mossy cells) heavily cross the transverse axis. Thus, it is likely that the intact brain contains more excitatory circuitry than slices (Jackson and Scharfman, 1996). Second, the relatively long axons of principal neurons are cut to a greater extent during preparation of slices, than the short projections of hippocampal GABAergic interneurons (Andersen et al., 2006). These considerations point to an unproportional enhancement of inhibition in large-scale hippocampal circuits *in vitro* (e.g., (Iijima et al., 1996). And third, recent evidence suggests that the voltage-sensitive dye used here (Di-4-ANEPPS) slightly potentiates $GABA_A$ receptor function (Mennerick et al., 2010). BIM at the considerably low concentration of a 0.6 μM almost never led to epileptiform activity in the hippocampal subfields under investigation (Figure 4.9). Nevertheless, every experiment was analyzed with respect to such activity and, in the rare cases in which epileptiform like activity was observed ($<$1% of experiments; Figure 4.9), slices were discarded from subsequent analysis. Although less strongly pronounced, EC/DG-input in the absence of BIM also reliably triggered HTC-waves (Figure 4.10B).

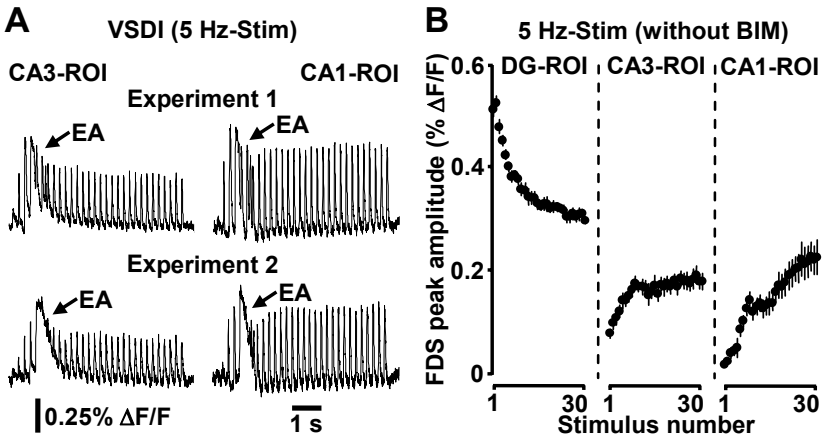

Fig. 4.10. Impact of BIM on polysynaptic activity flow in the HIP. (A) *Examples of epileptiform activity (EA) induced by EC/DG-input.* ***(B)*** *5 Hz EC/DG-input evoked HTC-waves also in the absence of BIM (**B**, N = 10 slices/6 mice) (**A,B**, adapted from Stepan et al., 2012).*

4.1.1.4 Level of HTC-waves depends on stimulation intensity

Because the VSDI signals can be very small, relatively high stimulation intensities were used to evoke EC/DG-inputs. This ensures both, a proper signal-to-noise ratio in combination with utilization of BIM, a minimum experimental variability in HTC dynamics.

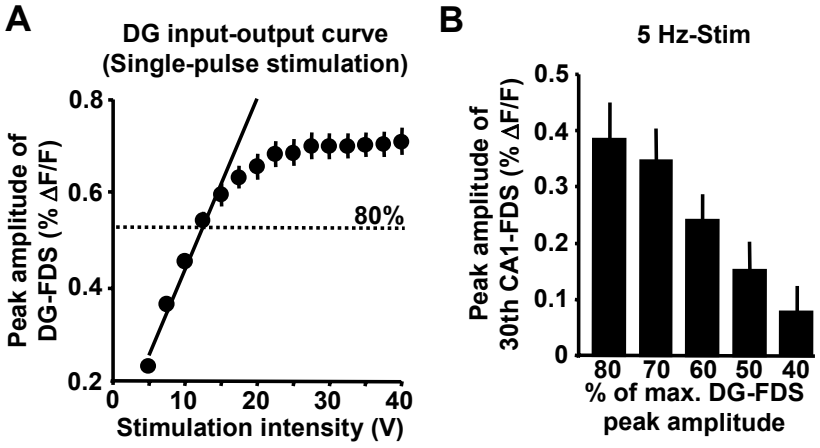

Fig. 4.11. HTC-waves in relation to the stimulation intensity. (A) *DG input/output curve obtained by single-pulse stimulations of EC/DG-input.* ***(B)*** *EC/DG-input below 80% of the maximal DG-FDS peak amplitude also induced HTC-waves (**A**, N = 8 slices/4 mice; **B**, N = 7 slices/5 mice) (**A,B**, adapted from Stepan et al., 2012).*

In detail, the induction of HTC-waves was preceded by single-pulse EC/DG-inputs to generate an input/output curve for every slice. Accordingly, the intensity of voltage during PP stimulations was adjusted in a manner to produce DG-FDSs with peak amplitudes of maximally 80% of the highest attainable value. The resultant FDSs ranged at the end of the linear upturn of the previously obtained input/output curve (Figure 4.11A). Hence, EC/DG-input may caused spiking of a substantial population of DG granule cells. Under *in vivo* conditions, however, recent experimental evidence suggests sparse firing of DG granule cells (Pernía-Andrade and Jonas, 2014; Henze et al., 2002;

Jung and McNaughton, 1993; Leutgeb et al., 2007). Therefore, it was examined whether polysynaptic activity flow within the HIP also occurs if only a small number of PP axons became activated. For this purpose, the stimulation intensity was decreased by significant steps (10 %) in a gradual manner down to 40 % of the highest achievable activity level in the DG. Providing substantial evidence for the sparse coding theory of DG granule cells, HTC-waves were also triggered with considerably lower activity states of the DG. Additionally, the resultant HTC-waves were characterized by a continuously decline in their strength, rather than by an abrupt drop off (Figure 4.11B).

4.1.2 HTC-waves depend on mossy fiber to CA3 synaptic transmission

The delayed and initially progressive appearance of HTC-waves (Figures 4.3, 4.4) indicates that the 5 Hz EC/DG-input somehow unlocked a frequency-dependent "gate" in the HTC for passages of neuronal activity. This comprises a two-dimensional process (unlocking/period) which may account for the amount of information flow. First, pronounced frequency facilitation of MF to CA3 synaptic transmission (Nicoll and Schmitz, 2005; Toth et al., 2000) may serve as the pivotal unlocking mechanism. A supporting factor for this scenario is the observation that frequency facilitation heavily took place during 5 Hz EC/DG-input, while neuronal activity in the DG decreased (Figures 4.3, 4.4).

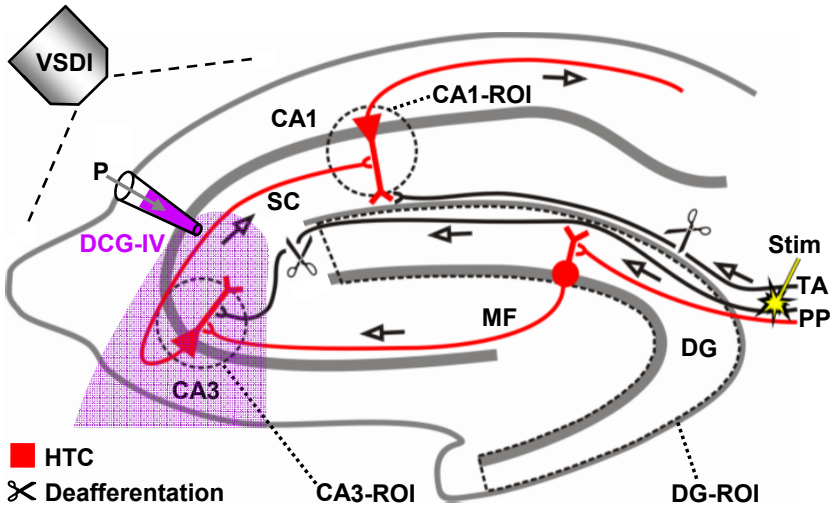

Fig. 4.12. Experimental setup used for spatially restricted administration of drugs to hippocampal subfields. *Arrangement used for investigations shown in Figures (4.13 - 4.15) (adapted from Stepan et al., 2012).*

Providing a direct proof that CA3 MF synaptic transmission is paramount in triggering HTC-waves, CA3-FDSs disappeared if glutamate release at CA3 MF terminals was selectively blocked by applying the mGluR2 agonist DCG-IV (Nicoll and Schmitz, 2005; Toth et al., 2000) specifically to area CA3 (Figures 4.12, 4.13A, 4.15). Frequency facilitation at MF synapses is a short-lasting form of synaptic plasticity (Nicoll and Schmitz, 2005). This characteristic may determine the timescale for opening of the "gate" and to exclude runaway excitation of the HTC. It is thus tempting to speculate that HTC-waves dissipate within a couple of seconds if 5 Hz EC/DG-input is followed by low-frequency (0.05

Hz) EC/DG-input (Toth et al., 2000). This was the case and reoccurring 5 Hz EC/DG-input again generated HTC-waves which displayed a delayed and initially progressive emergence (Figures 4.13B).

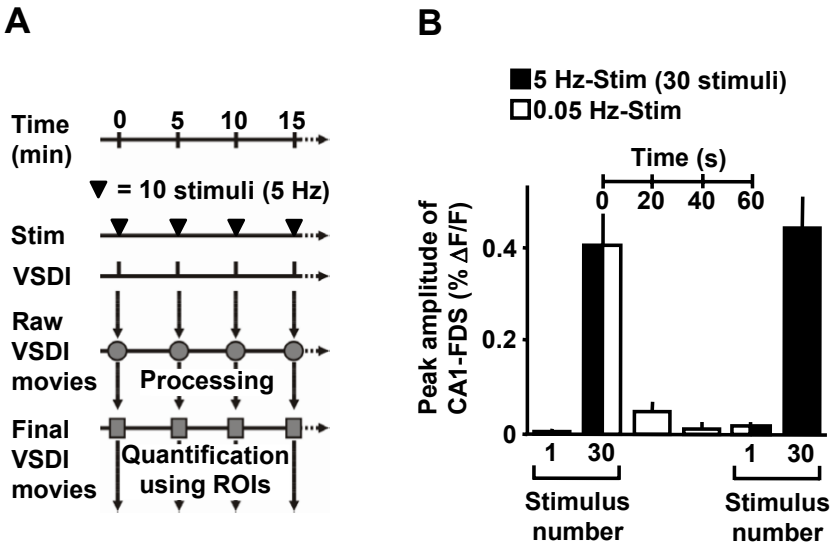

Fig. 4.13. Frequency-dependent gating of activity flow through the HIP. (A) *Experimental protocol used for investigations shown in (4.15).* ***(B)*** *During low frequency (0.05 Hz) EC/DG-input following 5 Hz EC/DG-input the HTC reverted to its locked state regarding passages of neuronal activity (**B**, N = 6 slices/3 mice) (**A,B**, adapted from Stepan et al., 2012).*

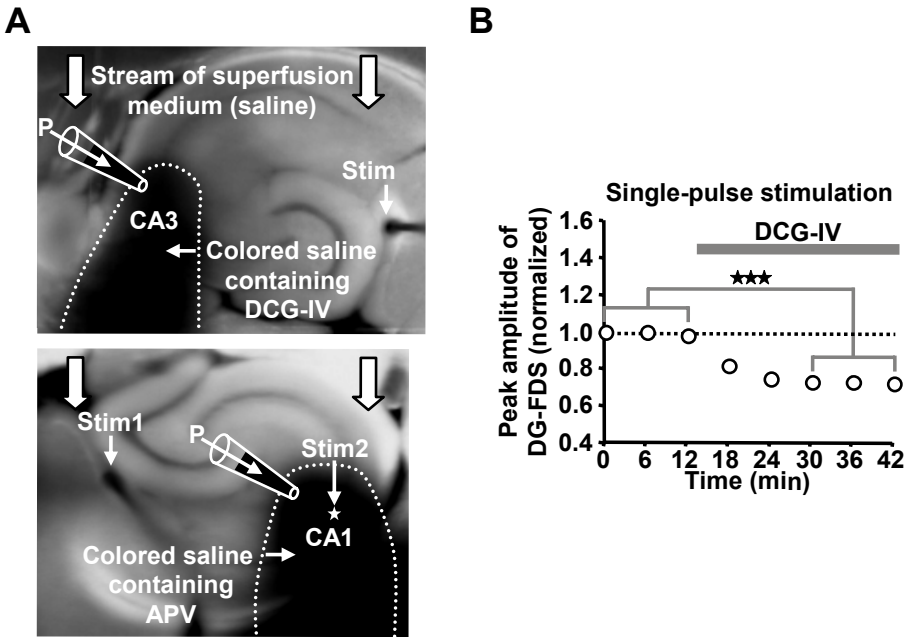

Fig. 4.14. Spatially restricted drug administration. ***(A)*** *Illustration of the locally restricted FLUO-guided administration of DGC-IV and D-APV to areas CA3 and CA1. For a better visualization of the spread of the pressure-ejected saline, Ponceau S was added instead of FLUO to the pipette solution.* ***(B)*** *Bath application of 1μM DCG-IV to brain slices markedly reduced neuronal activity in the DG (**B**, N = 6 slices/3mice).* ***(B)*** ****$p < 0.001$ (paired t-test) (**A,B**, adapted from Stepan et al., 2012).*

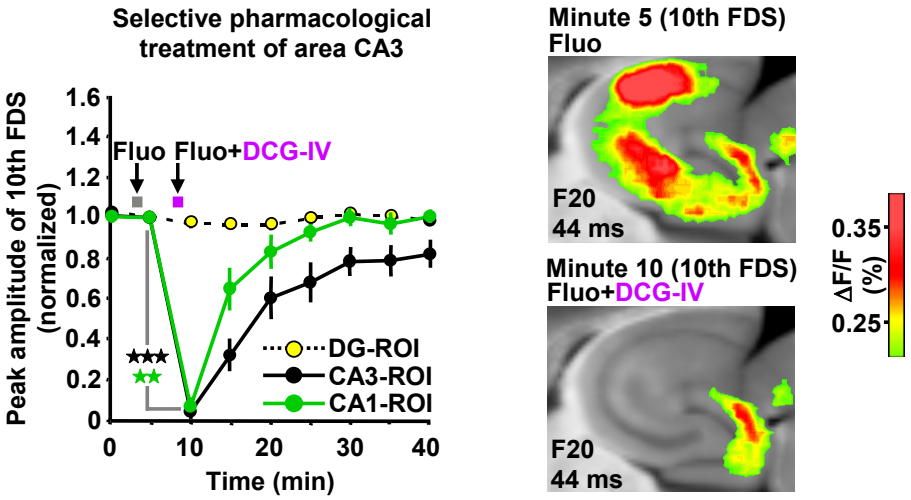

Fig. 4.15. Selective pharmacological treatment of area CA3. *A selective shutdown of MF synaptic transmission by a FLUO (10 μM)-guided administration of the mGluR2 agonist DCG-IV (30 μM; 1 min) specifically to area CA3 abolished HTC-waves without affecting DG activity (N = 8 slices/6 mice). $\star\star p < 0.01$ (paired t-test); $\star\star\star p < 0.001$ (paired t-test); (adapted from Stepan et al., 2012).*

4.1.3 Polysynaptic induction of CA1 LTP

Theta-burst stimulation of CA3 to CA1 projections is known to effectively induce CA1 LTP (Bliss and Collingridge, 1993), a cellular model of learning and memory in mammals. Here, 5 Hz EC/DG-input triggered high-frequency discharges of CA3 pyramidal neurons (Figure 4.7). This opens up the possibility that HTC-waves yield a kind of "theta-burst" activation of CA3 to CA1 synapses. Consequently, it was tested whether 5 Hz EC/DG-input can elicit CA1 LTP. To enable the imaging of the putative formation of CA1 LTP, the VSDI assay was refined. Beside 5 Hz electrical stimulation of PP axons, a second electrode was placed into the SC-commissural pathway to accurately gauge the strength of neurotransmission at CA3 to CA1 synapses. The amplitude of the CA1 (SR)-FDSs at imaging frame 13 (28.6 ms) after the stimulation pulse (FDS_{F13} amplitude) in response to repeated, low frequency stimulations of the SC-commissural pathway (Bliss and Collingridge, 1993; Figures 4.16 - 4.18) was used, to measure changes in the strength of neurotransmission at CA3 to CA1 synapses (Figure 4.18; "Materials and Methods"). Analysis of field potential recordings performed in CA1 stratum radiatum and VSDI data showed that 5 Hz EC/DG-input for 6 s was sufficient to evoke CA1 LTP (Figures 4.18, 4.19; "Materials and Methods"). This CA1 LTP was not saturated, because a second train of HTC-waves further increased its magnitude (Figure 4.20). Another set of experiments suggests the existence of an induction threshold for this neuroplastic phenomenon. This became evident by the observation that 10 stimuli were not sufficient for polysynaptic induction of CA1 LTP (Figure 4.21). Furthermore, the form of CA1 LTP obtained here critically depends on the activation of NMDA receptors (Bliss and Collingridge, 1993) as revealed by the administration of the NMDA receptor blocker D-APV specifically to area CA1 (Figure 4.22). 5 Hz EC/DG-input for 6 s also elicited CA1 LTP in the absence of BIM (Figure 4.23). In all LTP experiments, hippocampal activity resulting from EC/DG-input was monitored by means of VSDI (Figure 4.18 - Figure 4.23).

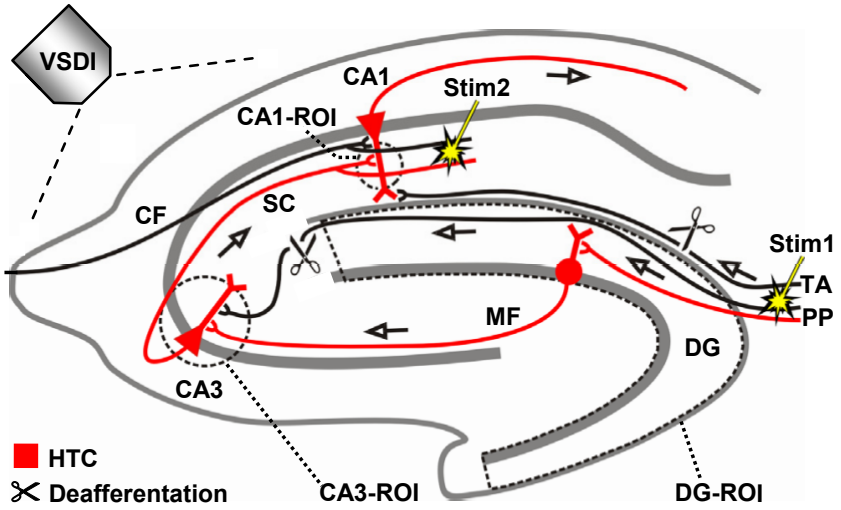

Fig. 4.16. Experimental arrangement used for LTP experiments. *Arrangement used for investigations shown in Figures (4.18 - 4.23). Abbreviation: CF, commissural fiber (adapted from Stepan et al., 2012).*

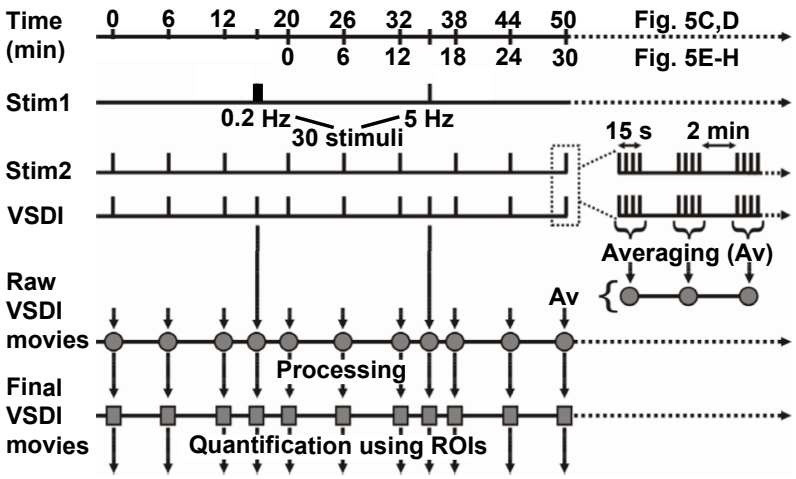

Fig. 4.17. Experimental protocol used for LTP experiments. *Protocol used for investigations shown in Figures (4.18 - 4.23) (adapted from Stepan et al., 2012).*

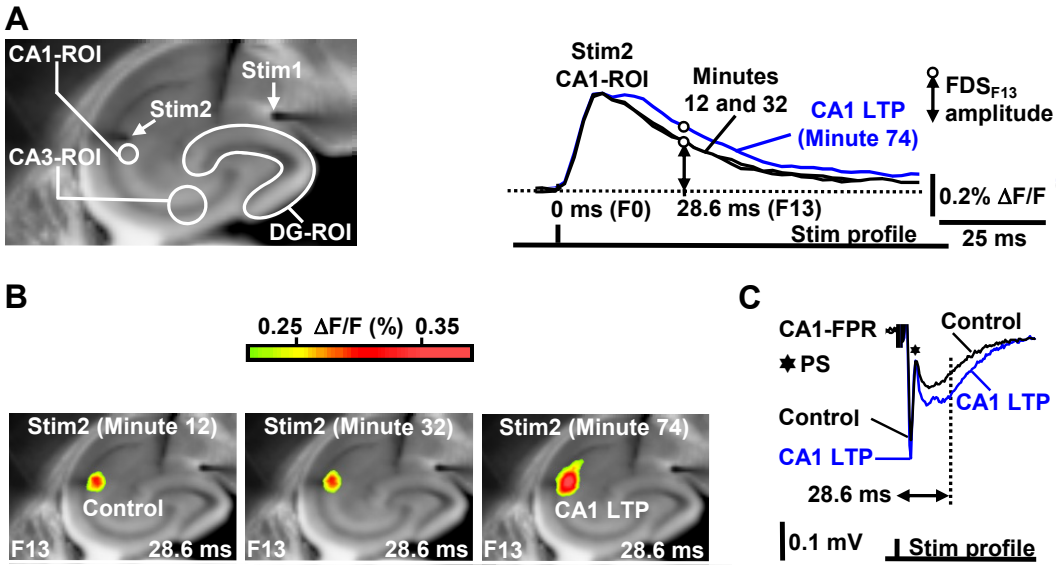

Fig. 4.18. Polysynaptic induction of CA1 LTP. (A,B) *Illustration and outcome of one representative experiment. The amplitude of CA1-FDSs at imaging Frame 13 (28.6 ms) after the stimulation pulse (*FDS_{F13} *amplitude) served as measure of synaptic strength.* ***(C)*** *5 Hz EC/DG-input for 6 s caused a long-lasting increase in the slope and the amplitude of CA1 (SR) fEPSPs 28 ms after the stimulation pulse, recorded 40 min after the 5 Hz stimulus train (**A-C**, adapted from Stepan et al., 2012).*

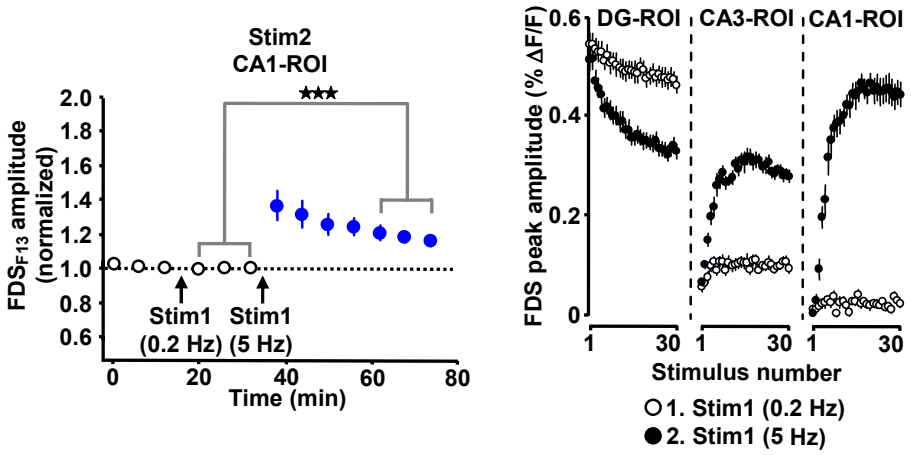

Fig. 4.19. EC/DG-input elicits CA1 LTP after a few seconds. *5 Hz EC/DG-input for 6 s elicited CA1 LTP (N = 13 slices/5 mice) ⋆⋆⋆$p < 0.001$ (paired t-test) (adapted from Stepan et al., 2012).*

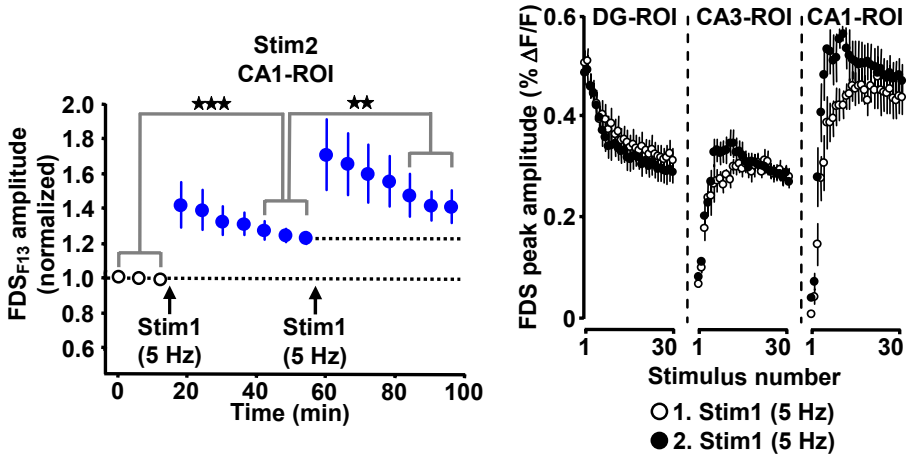

Fig. 4.20. CA1 LTP is not saturated after one 5 Hz stimulus train. *A second train of 5 Hz EC/DG-input for 6 s shows that CA1 LTP is not saturated (N = 8 slices/5 mice). ⋆⋆$p < 0.01$ (paired t-test); ⋆⋆⋆$p < 0.001$ (paired t-test) (adapted from Stepan et al., 2012).*

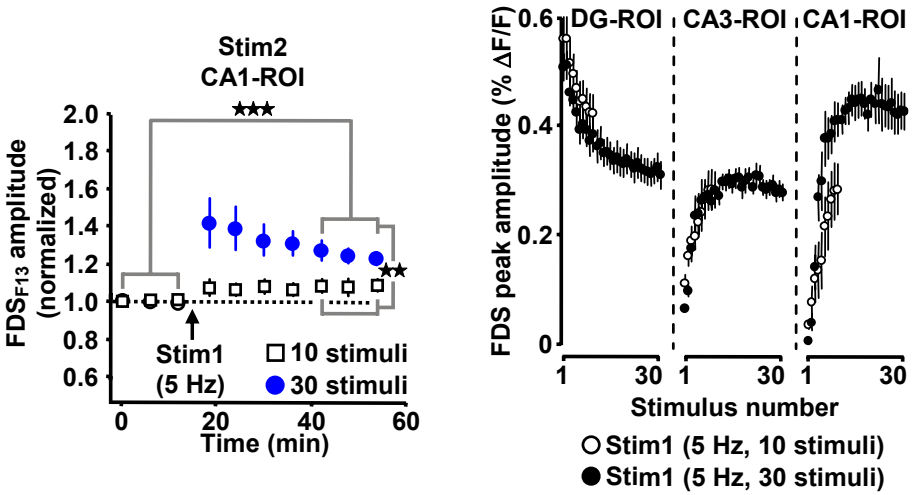

Fig. 4.21. Induction threshold of CA1 LTP. *5 Hz EC/DG-input for 2 s failed to evoke statistically significant CA1 LTP. Blue circles represent data shown in (Figure 4.20) (open squares; N = 7 slices/5 mice). ⋆⋆$p < 0.01$ (unpaired t-test); ⋆⋆⋆$p < 0.001$ (paired t-test) (adapted from Stepan et al., 2012).*

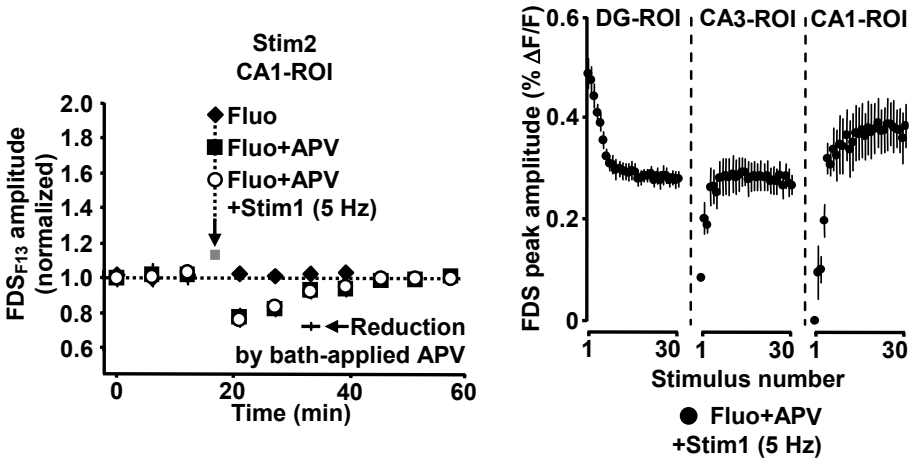

Fig. 4.22. Pharmacological blockade of CA1 LTP. *A blockade of NMDA receptors at CA3 to CA1 synapses by a FLUO (10 µM)-guided administration of D-APV (200 µM; 1 min) specifically to area CA1 prevented the formation of CA1 LTP (N = 6 slices/4 mice; N = 5 slices/4 mice for control experiments with FLUO; N = 6 slices/4 mice for control experiments with fluoxetine + D-APV and N = 5 slices/3 mice for control experiments with D-APV (50 µM) bath-applied to slices) (adapted from Stepan et al., 2012).*

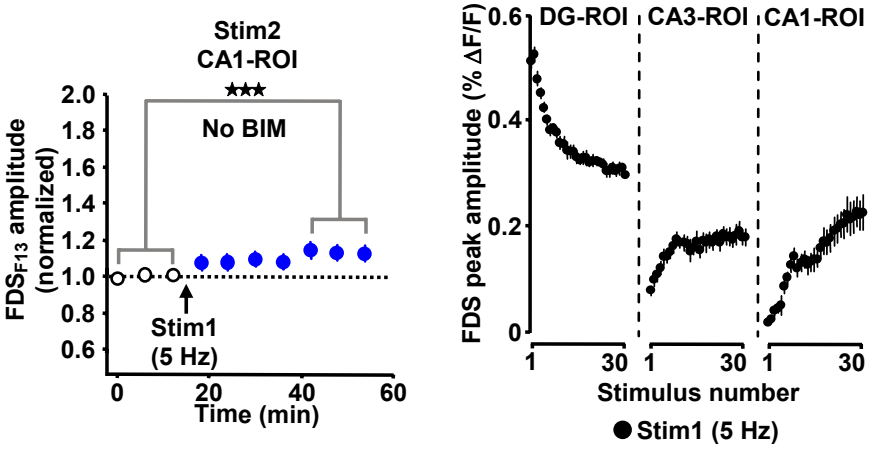

Fig. 4.23. CA1 LTP in the absence of BIM. *5 Hz EC/DG-input evoked CA1 LTP also in the absence of BIM (N = 10 slices/6 mice). ⋆⋆⋆$p < 0.001$ (paired t-test) (adapted from Stepan et al. (2012)).*

4.1.4 Pharmacological modulation of HTC-waves

HTC-waves might provide a valuable assay for studying drug effects on polysynaptic activity flow through the classical input/output circuit of the HIP. Because the HIP plays a fundamental role in cognitive processes, like memory formation (e.g., CA1 LTP; Whitlock et al., 2006), it seems reasonable to examine the impact of the cognitive enhancer caffeine (Nehlig, 2010) on HTC-waves. As already suggested by the DCG-IV and LTP experiments (Figures 4.15, 4.21), stimulation trains containing 10 stimuli (every 5 min), were suited to conduct stable baseline recordings of HTC-waves without inducing long-term synaptic changes (Figures 4.13, 4.24A). In these experiments, the FDS amplitude of the tenth stimulus served as measure of neuronal excitability. After stable baseline recordings over a period of 15 min, bath application of caffeine at a concentration found in the cerebrospinal fluid of humans after intake of 1-2 cups of coffee (5 μM; Fredholm et al., 1999), boosted HTC-waves (Figure 4.24A). Martín and Buño (2003) reported that caffeine mediates a presynaptic form of LTP at CA3 to CA1 synapses. To exclude that such LTP interferes with the caffeine-induced enhancement of HTC-waves, wash-out experiments were conducted. Contradicting the involvement of long-term synaptic changes, CA1-FDSs reverted to baseline strength if caffeine was removed from the superfusion medium (Figure 4.24B).

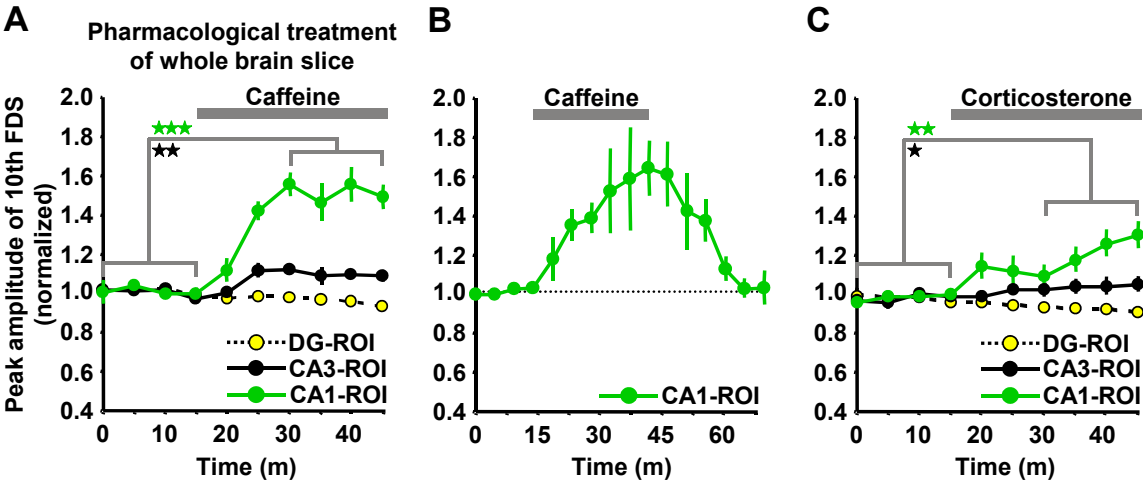

Fig. 4.24. Caffeine and CORT modulate HTC-waves. ***(A,B)*** *Caffeine rapidly boosted HTC-waves in a reversible manner.* ***(C)*** *CORT (100nm) quickly amplified HTC-waves (**A**, N = 8 slices/4 mice; **B**, N = 4 slices/3mice; **C** N = 7 slices/4mice).* ***(A,B,C)*** *$\star p < 0.05$ (paired t-test); $\star\star p < 0.01$ (paired t-test); $\star\star\star p < 0.001$ (paired t-test) (**A,B**, adapted from Stepan et al., 2012).*

Several neuromodulators are tightly linked to hippocampal physiology in health and disease. Especially CORT- and CRH receptors are densely expressed in the mouse HIP. Their activation has been implicated in HIP-dependent functions like memory formation and stress response, but experimental demonstrations how acute application affects polysynaptic activity flow in the HIP are lacking to date (Maras and Baram, 2012; McEwen, 1999). As observed previously for caffeine, CORT (100 nM) rapidly amplified HTC-waves (Figure 4.24C). Although 10 pulses at 5 Hz applied to the PP were not sufficient to induce CA1 LTP (Figure 4.21), it was attempted to further minimize the number

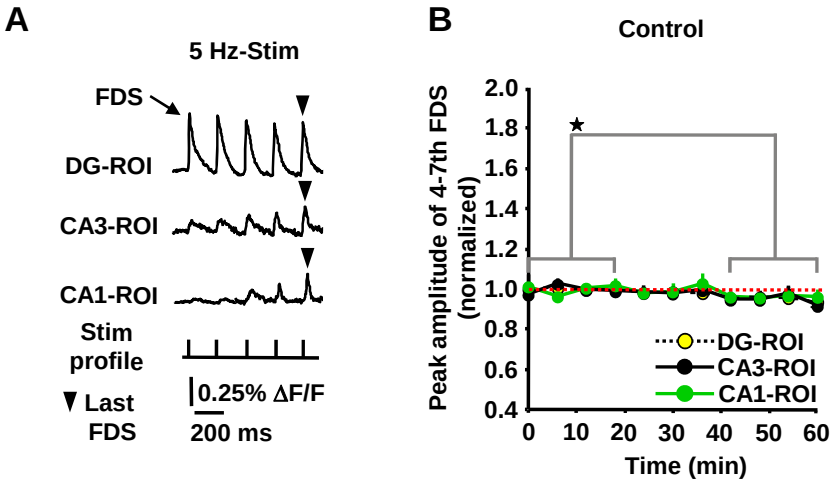

Fig. 4.25. Refined HTC-wave protocol for pharmacological experiments. ***(A)*** *Experimental protocol used for investigations shown in (Figure 4.26).* ***(B)*** *Recordings in the absence of drug revealed a slight decrease (significant in the DG and CA3) of FDSs in all hippocampal subregions. (**B**, N = 10 slices/5mice).* ***(B)*** $\star p < 0.05$ *(paired t-test);* $\star\star\star p < 0.001$ *(paired t-test) (**A**, modified from Stepan et al., 2012).*

of stimuli. Therefore, pilot experiments were carried out, testing stable baseline recordings with a reduced number of pulses (4 to 7) at a shorter time interval (2min; Figure 4.25A). The number of stimuli was held constant within an experiment. As a final measure of DG, CA3, and CA1 activity levels, the mean of the last FDS out of three consecutive acquisitions was used and paired t-tests were employed to determine the distinct concentration(s) with significant change of FDSs at minutes 0 to 18 vs. minutes 42 to 60. Electrical stimulation intensity was set (15-35 V) in order to obtain CA1-FDS ranging within 0.1 to 0.3 % $\triangle$F/F. Applying these settings, control experiments in the absence of any drug revealed a slight decrease (significant in DG and CA3) of FDS amplitudes in all hippocampal subregions (Figure 4.25B). To avoid under-/overestimation of drug effects the corresponding percentage of decrease (DG, 4.4 $\pm$ 1 %; CA3, 4.4 $\pm$ 2 %; CA1, 3.5 $\pm$ 2 %), was subtracted in subsequent experiments. Additionally, this refined experimental protocol facilitated baseline recordings. If not stated otherwise, the adapted protocol and the correction factor were applied in all experiments, starting with bath application of CRH. CRH (5 and 50 nM), subsequently probed by means of this refined protocol, also rapidly amplified HTC-waves at considerably low concentrations (Figure 4.26A,B).

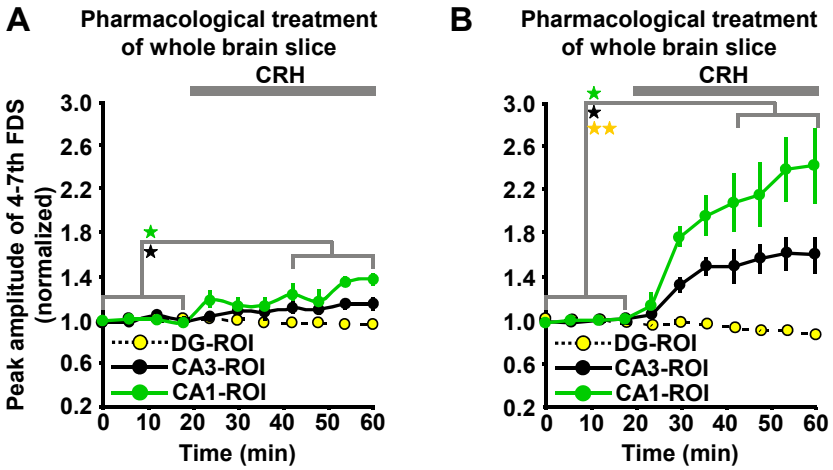

Fig. 4.26. CRH modulates HTC-waves. ***(A,B)*** *Bath application of CRH (5 nM/50 nM) rapidly amplified HTC-waves (**A**, N = 7 slices/4mice; **B**, N = 6 slices/3 mice).* ***(A,B)*** $\star p < 0.05$ *(paired t-test);* $\star\star p < 0.01$ *(paired t-test).*

4.2 HTC-waves in an animal model of chronic stress

Beside pharmacological investigations, the HTC-wave assay appears suited to uncover alterations in hippocampal network dynamics in animal models of disease. A constant EC/DG-input is an important prerequisite to reliably compare output patterns (activity in areas CA3 and CA1) across slices. In order to meet this objective (see Material and Methods, 3.5.1), single pulse EC/DG-input was used to obtain FDSs within a specific DG-ROI (DGS-ROI) with fixed values ("default DGS-FDS", low intensity = 0.35, middle intensity = 0.45, high intensity = 0.55 % $\triangle$F/F). Subsequently, 15 pulses at 5 Hz were applied at each intensity level (separated by 3 min) to induce HTC-waves (Figure 4.27A,B). Experiments in wild-type C57BL/6N mice revealed a substantial match between the default DGS-FDS and the 1st DGS-FDS of a subsequent 15 pulse train at 5 Hz at all three intensity levels (Figure 4.28A). Most importantly, CA3- and CA1-FDS amplitudes were found to increase linearly within the stimulus range and reliably across slices (Figure 4.28B).

It is well established that sustained exposure of rodents to elevated stress levels results in severe hippocampal damage, accompanied by an impairment of HIP-dependent cognitive abilities (Kim and Diamond, 2002; McEwen, 2007). How this disturbed brain homeostasis affects polysynaptic signal propagation within the HIP is unknown to date (Pavlides et al., 2002). To elucidate the impact of chronic stress on HTC-waves, the efficacy of evoked EC/DG-input was examined in acute brain slices from chronic social defeat stress (CSDS) and control (CTRL) mice (see Material and Methods, 3.1.1). For this purpose, animals were tested after two weeks of defeat in a random manner and blinded to the experimentalist on six consecutive days.

According to the initial experiments, the 1st DGS-FDS was precisely set in CTRL and CSDS mice and no differences in DGS activity levels were detected (Figures 4.28A, 4.29, 4.31). Furthermore, CA3- and CA1-FDSs also increased linearly in the stimulus range (Figures 4.30A), indicating a reproducible EC/DG-input across slices. In striking contrast

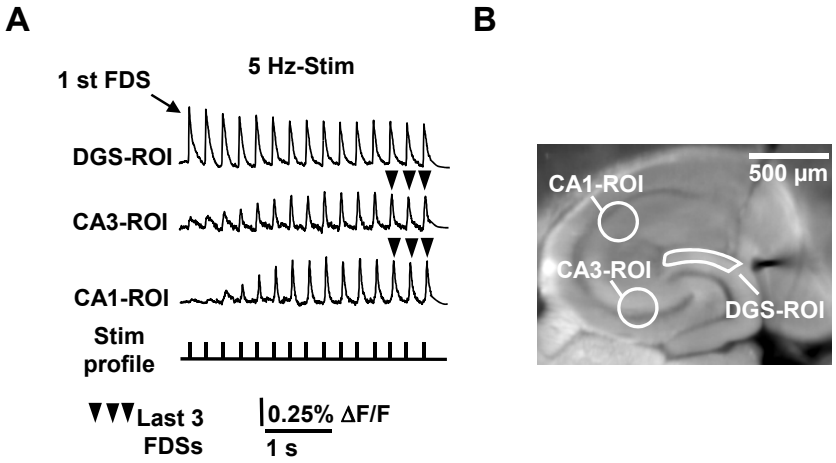

Fig. 4.27. Refined HTC-wave assay for group comparisons. (A) *Experimental protocol used for investigations shown in Figures (4.28 - 4.33). The first DGS-FDS and the mean of the last three CA1-FDSs were used for statistical analysis.* ***(B)*** *Anatomical positions of the DGS-, CA3-, and CA1-ROI (**A**, modified from Stepan et al., 2012).*

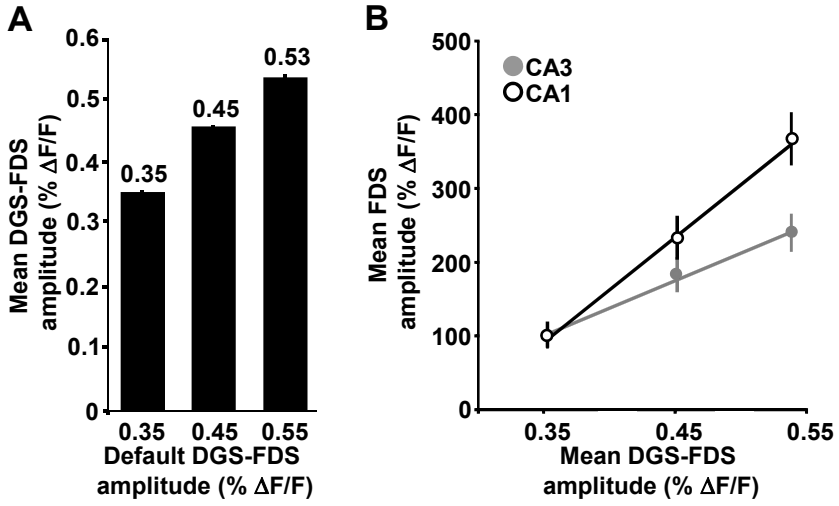

Fig. 4.28. Characteristics of HTC-waves in response to constant EC/DG-input. (A) *Nearly complete match of the first DGS-FDS in response to single pulse stimulation and 5 Hz EC/DG-input.* ***(B)*** *CA3- and CA1-FDSs linearly increased within the stimulus range.* ***A,B****; N = 13 slices/6 mice.* ***(B)*** *One-way repeated-measures ANOVA: $p< 0.001$ for CA3; $p< 0.001$ for CA1; followed by Student-Newman-Keuls post hoc tests, DGS-FDS (% △F/F) 0.35 vs 0.45: $p< 0.001$ for CA3; $p< 0.001$ for CA1; DGS-FDS (% △F/F) 0.35 vs 0.55: $p< 0.001$ for CA3; $p< 0.001$ for CA1; DGS-FDS (% △F/F) 0.45 vs 0.55: $p< 0.01$ for CA3; $p< 0.001$ for CA1.*

to DG-FDSs, CA3- and CA1-FDSs were markedly weaker in brain slices obtained from CSDS mice (Figures 4.31, 4.32). The only exception are signals in area CA3 at the lowest intensity level (Figure 4.32). It has previously been shown that DG function is modified by chronic stress and stress associated adjustments (Ikrar et al., 2013; Karst and Joëls, 2003). Therefore, stimulation intensities that were capable of inducing the default activity levels in the DGS-ROI were analyzed and found to be markedly decreased in CSDS mice (Figure 4.30B), indicating enhanced DG activity in stressed mice.

All animals were tested during the third week of CSDS on six consecutive days. Previous work indicates that mice exhibit a constant phenotype and stable patterns of molecular, cellular and morphological changes in the HIP after 2 weeks of defeat (Berton and

Nestler, 2006; Sousa et al., 2000). Nevertheless, to exclude the possibility that further changes in the hippocampal network became apparent over time, the effect of testing day on activity levels within the HTC was examined. This analysis revealed no relationship between day of data acquisition and neuronal activity levels in areas CA3 and CA1 (Figure 4.33).

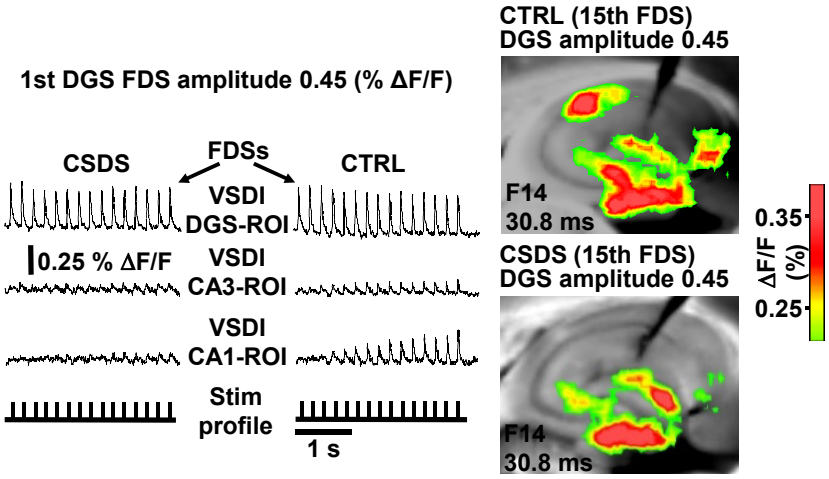

Fig. 4.29. Illustration and outcome of a representative experiment in CTRL vs. CSDS mice. *VSDI recordings in CTRL and CSDS mice with analogous 1st DGS-FDS amplitudes (0.45 % △F/F) revealed markedly decreased CA3- and CA1-FDSs in CSDS mice.*

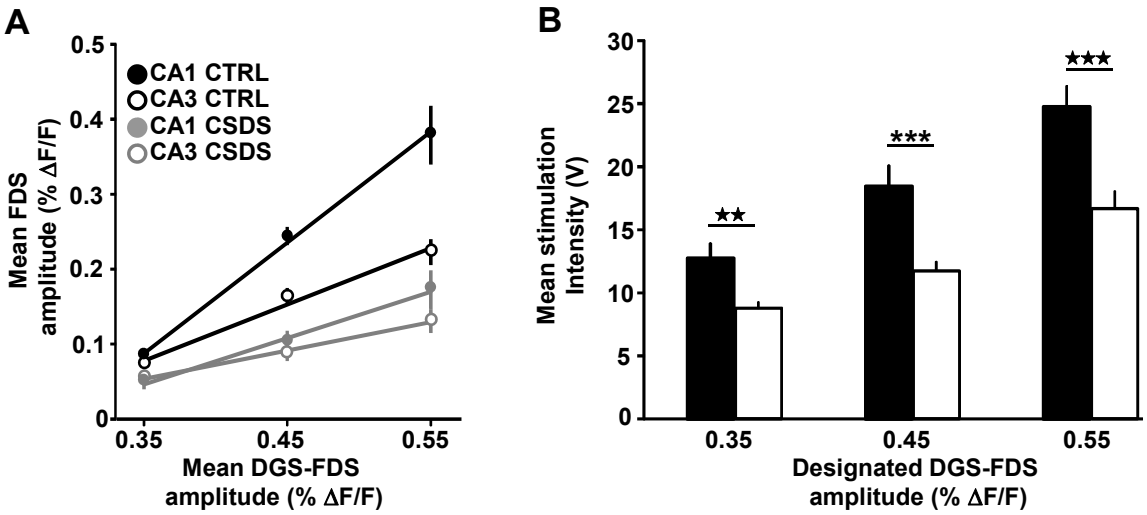

Fig. 4.30. Characteristics of HTC-waves in CSDS mice and stimulation intensities used to induce the default DGS-FDSs. in CTRL vs. CSDS mice. (A) *CA3- and CA1-FDSs linearly increased with increasing DGS-input in CTRL and CSDS mice.* ***(B)*** *Required voltage intensities to evoke analogous DGS-FDSs in CTRL and CSDS mice (**A,B**, CTRL: N = 6 mice; CSDS: N = 7 mice).* ***(A)*** *One-way repeated-measures ANOVA: $p< 0.001$ for CA3 in CTRL mice; $p< 0.001$ for CA1 in CTRL mice; $p< 0.001$ for CA3 in CSDS mice; $p< 0.001$ for CA1 in CSDS mice followed by Student-Newman-Keuls post hoc tests, CTRL mice: DGS-FDS (% △F/F) 0.35 vs 0.45: $p< 0.001$ for CA3; $p< 0.001$ for CA1; DGS-FDS (% △F/F) 0.35 vs 0.55: $p< 0.001$ for CA3; $p< 0.001$ for CA1; DGS-FDS (% △F/F) 0.45 vs 0.55: $p< 0.01$ for CA3; $p< 0.01$ for CA1; CSDS mice: DGS-FDS (% △F/F) 0.35 vs 0.45: $p< 0.05$ for CA3; $p< 0.05$ for CA1; DGS-FDS (% △F/F) 0.35 vs 0.55: $p< 0.001$ for CA3; $p< 0.001$ for CA1; DGS-FDS (% △F/F) 0.45 vs 0.55: $p = 0.01$ for CA3; $p< 0.01$ for CA1;* ***(B)*** *$\star\star p < 0.01$ (unpaired t-test); $\star\star\star p < 0.001$ (unpaired t-test); $***p < 0.001$ (Mann-Whitney test on ranks).*

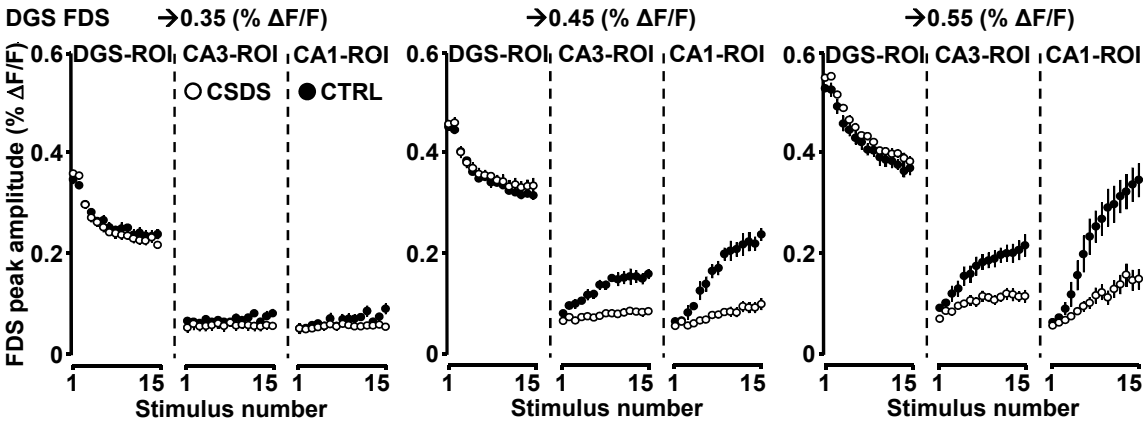

Fig. 4.31. Quantification of neuronal activities in hippocampal subregions. *CA3- and CA1-FDSs are markedly decreased in CSDS mice (CTRL: N = 6 mice; CSDS: N = 7 mice).*

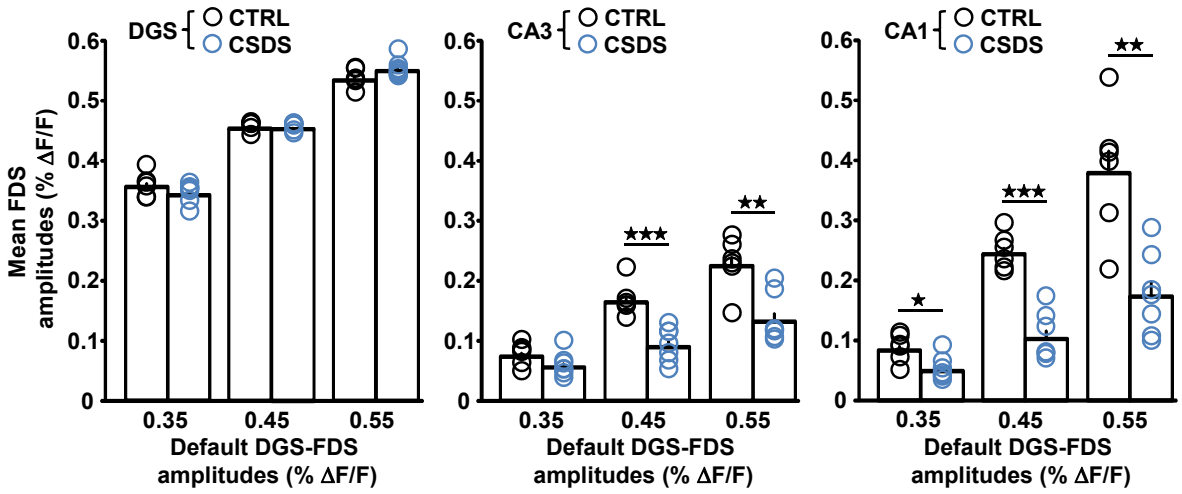

Fig. 4.32. HTC-waves are markedly decreased in CSDS mice. *CTRL and CSDS mice exhibit no difference in 1st DGS-FDS, while CA3- and CA1-FDSs are markedly decreased in CSDS mice, except for CA3 FDSs at the lowest intensity level (CTRL: N = 6 mice; CSDS: N = 7 mice); ⋆p < 0.05 (unpaired t-test); ⋆⋆p < 0.01 (unpaired t-test); ⋆⋆⋆p < 0.001 (unpaired t-test).*

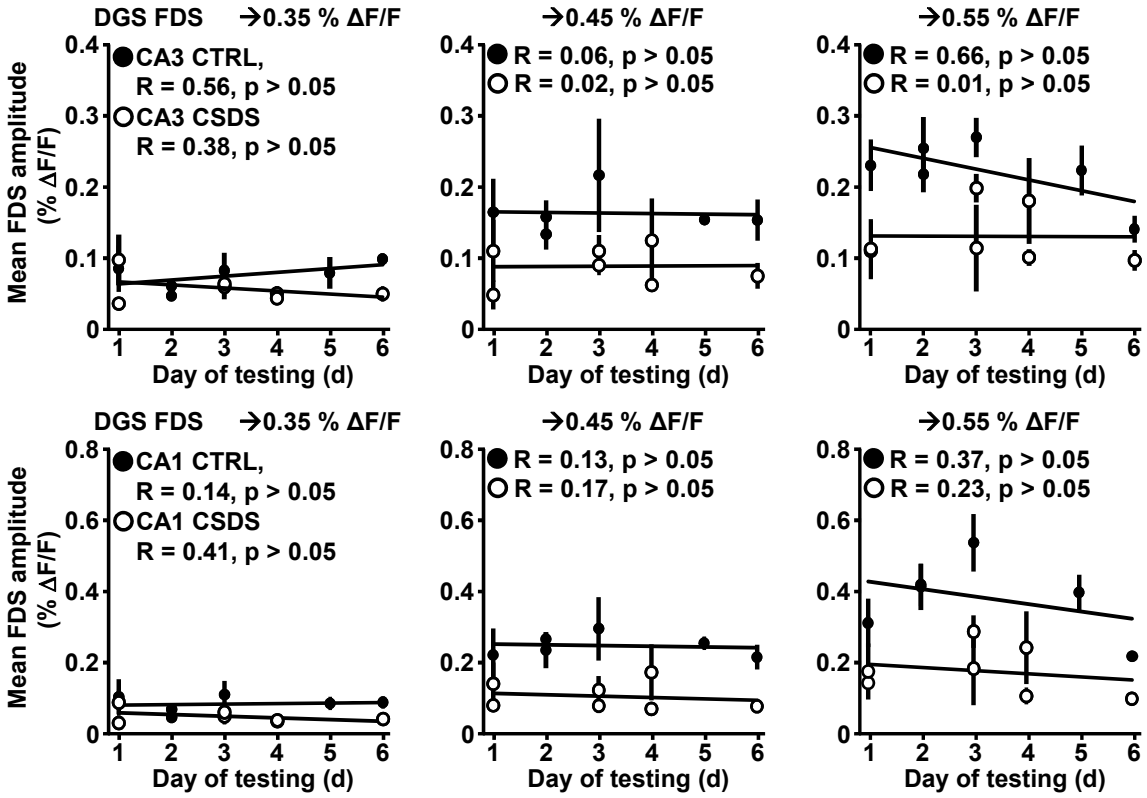

Fig. 4.33. Relationship between day of data acquisition and activity levels in areas CA3 and CA1. *No relationship between day of testing and activity levels in areas CA3 and CA1 in CTRL vs. CSDS mice was found. (CTRL: N = 6 mice; CSDS: N = 7 mice).*

4.3 Circuit-level mechanism of antidepressant drug action

4.3.1 Antidepressants enhance HTC-waves at low micromolar concentrations

Considering that chronic stress markedly impaired activity percolations through the HTC (Figure 4.29), it was tested whether and how ADs, the first line treatment for SRPDs, modulate hippocampal network activity. Using the HTC-wave assay for pharmacological investigations (Figure 4.25A,B), the acute effect(s) of various ADs (the tricyclic ADs amitryptyline and clomipramine, the selective serotonine reuptake inhibitors (SSRIs) fluoxetine, citalopram and fluvoxamine, the selective serotonine/norepinephrine reuptake inhibitor (SSNRI) venlafaxine, the selective serotonin reuptake enhancer (SSRE) tianeptine and the monoamino-oxidase A and B inhibitor (MAOI) tranylcypromine were tested in nearly 450 brain slices.

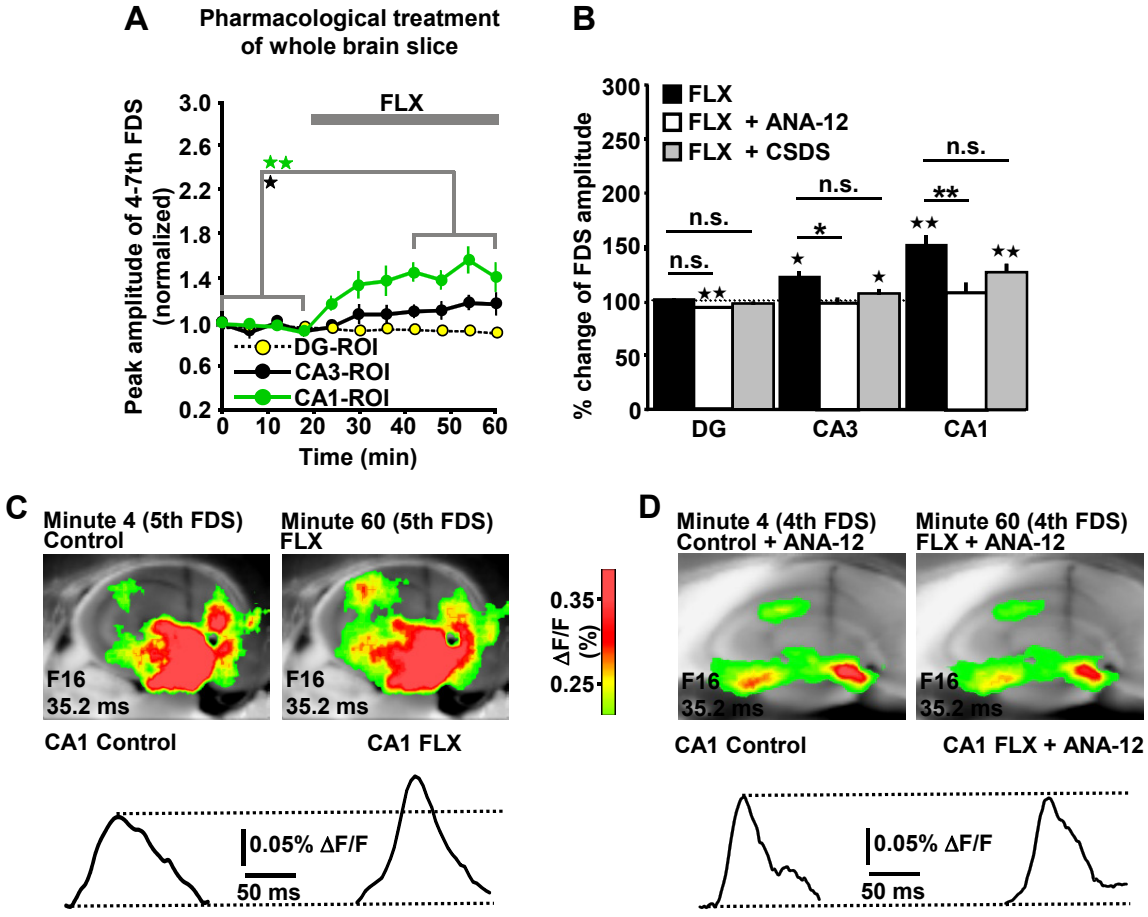

Fig. 4.34. Fluoxetine enhance HTC-waves in a TrkB-dependent manner but independent from CSDS ***(A)*** *Bath applied fluoxetine (10 µM) strongly enhanced CA3- and CA1 FDSs.* ***(B)*** *This effect is abolished in the presence of the TrkB ligand ANA-12, but preserved in CSDS mice* ***(C)*** *Illustration and outcome of one representative experiment showing the effect of bath-applied fluoxetine (10 µM) on HTC-waves.* ***(D)*** *Illustration and outcome of one representative experiment showing the effect of bath-applied fluoxetine (10 µM) and ANA-12 (10 µM) on HTC-waves. (**A**, N = 7 slices/4 mice; **B**, fluoxetine + ANA-12: N = 11 slices/4 mice; CSDS: N = 8 slices/4 mice).* ***(A,B)*** *$\star p < 0.05$ (paired t-test); $\star\star p < 0.01$ (paired t-test); $*p < 0.05$ (unpaired t-test); $**p < 0.01$ (unpaired t-test). Abbreviations: FLX, fluoxetine.*

ADs are known to effectively elevate brain serotonin and/or norepinephrine levels (caused by inhibition of the corresponding reuptake transporters or monoamine oxidases) at

low nanomolar concentrations (Boldenwatson and Richelson, 1993; Tatsumi et al., 1997). However, recent evidence suggests that they also modulate several other targets (e.g., neurotrophin receptors, ion channels) at high nanomolar/low micromolar concentrations (Jang et al., 2009; Méndez et al., 2012; Rammes and Rupprecht, 2007). Therefore, ADs at different concentrations (0.1, 0.5, 1, 5, 10, and except for tianeptine also at 15 and 20 μM) were bath-applied. To check the data for concentration-dependent effects, one-way ANOVAs were applied to the data for every hippocampal subregion (DG, CA3, and CA1) and drug. When the criteria of normal distribution and equal variance were not met, a Kruskal-Wallis ANOVA on ranks was used (Figures 4.35A,B; 4.36A-C; 4.37A-C). If the corresponding ANOVA reported statistical differences, t-tests were used to determine the different concentration(s) with significant change in FDSs at minutes 0 to 18 vs. minutes 42 to 60 (Figure 4.25B).

All ADs tested (with the exception of 0.5 and 10 μM fluvoxamine and 1 and 10 μM venlafaxine), did not affect DG-FDSs (Figures 4.34A; 4.35A,B; 4.36A-C; 4.37A-C; left panels with bars in grey and white). In contrast, all ADs exerted enhancing effects on CA1-FDSs in the same experiments (Figures 4.34A,D; 4.35A,B; 4.36A-C; 4.37A-C; right panels with bars in black). Interestingly, the concentration dependence of this pharmacological effect in CA1 is not uniform across drugs. Amitriptyline, clomipramine, and tranylcypromine enhanced CA1-FDSs at one particular substance-specific concentration. Citalopram and venlafaxine elevated neuronal network activity in CA1 at several concentrations and only data sets obtained for fluoxetine and tianeptine are reconcilable with a classical dose-response relationship. Furthermore, only tranylcypromine weakened CA1-FDSs at 0.1 μM (Figures ; 4.35A,B; 4.36A-C; 4.37A-C; right panels with bars in black and white). As exemplarily tested for fluoxetine at a concentration of 10 μM, enhancing effects on HTC-waves are preserved in CSDS mice (Figure 4.34B).

Direct axonal projections from EC to areas CA3 and CA1 are functionally inactivated in the HTC-wave assay (Figure 3.1A,B). Therefore, CA1 activity is solely driven by action potential firing of CA3 pyramidal neurons. Effects of ADs may therefore not be restricted to area CA1, but also take place in area CA3. Supporting this scenario, fluoxetine, venlafaxine, and tianeptine also exerted enhancing effects (except for tranylcypromine in area CA3; Figure 4.37C) on CA3-FDSs, with the same concentration dependency as observed for CA1-FDSs (Figures 4.36A; 4.37A,B; middle panels with bars in black).

Neurotrophins and their receptors (Trk and p75NTR) have repeatedly been implicated in the pathophysiology of SRPDs and as a key mediator of the therapeutic response to ADs. Independent of their chemical structure and primary mechanism of action, all ADs and lithium are known to rapidly activate TrkB receptors (Castrén et al., 2007). Accordingly, it was tested if fluoxetine enhanced CA3- and CA1 FDSs in a TrkB receptor-dependent manner (Castrén et al., 2007; Duman and Aghajanian, 2012). Therefore, the low-molecular weight TrkB ligand ANA-12 was used in one set of pharmacological experiments (minimum time of incubation, 1h). ANA-12 has been shown to selectively prevent phosphorylation of TrkB receptors by BDNF highly effectively and potent at submicromolar concentrations (Cazorla et al., 2011; Longo and Massa, 2013). In slices pretreated with

ANA-12 enhancing effects of fluoxetine (10 μM) on CA3- and CA1-FDSs were abolished (Figure 4.34A-D).

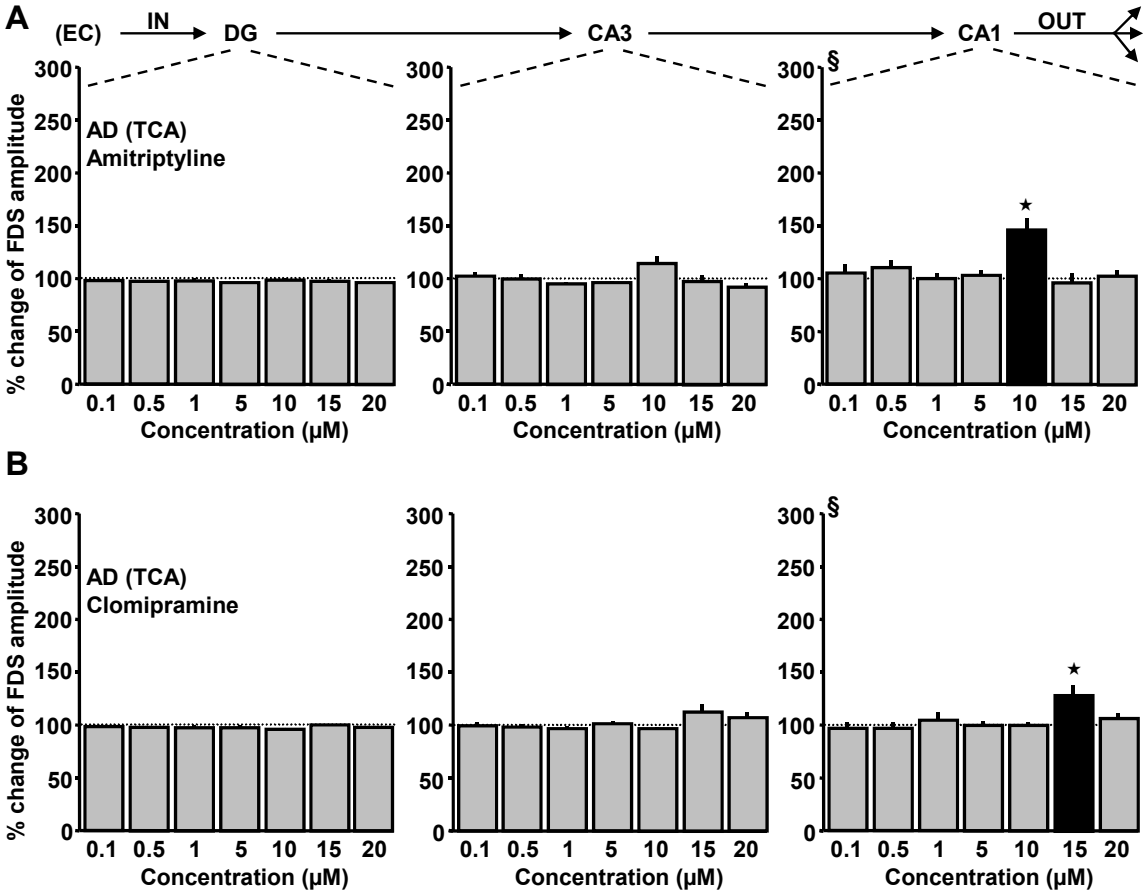

Fig. 4.35. Tricyclic ADs enhance HTC-waves. ***(A,B)*** *Effects of the tricyclic ADs amitriptyline and clomipramine on DG-, CA3-, and CA1 FDSs (**A**, 0.1 μM = 8 slices/4 mice; 0,5 μM = 8 slices/4 mice; 1 μM = 8 slices/4 mice; 5 μM = 7 slices/4 mice; 10 μM = 7 slices/3 mice; 15 μM = 7 slices/4 mice; 20 μM = 8 slices/5 mice; **B**, 0.1 μM = 9 slices/5 mice; 0.5 μM = 12 slices/7 mice; 1 μM = 10 slices/6 mice; 5 μM = 10 slices/5 mice; 10 μM = 8 slices/5 mice; 15 μM = 9 slices/3 mice; 20 μM = 8 slices/4 mice).* ***(A,B)*** *§, one-way ANOVAs: $p = 0.002$ for amitriptyline in CA1 and $p = 0.02$ for clomipramine in CA1; followed by paired t-tests: $\star p < 0.05$.*

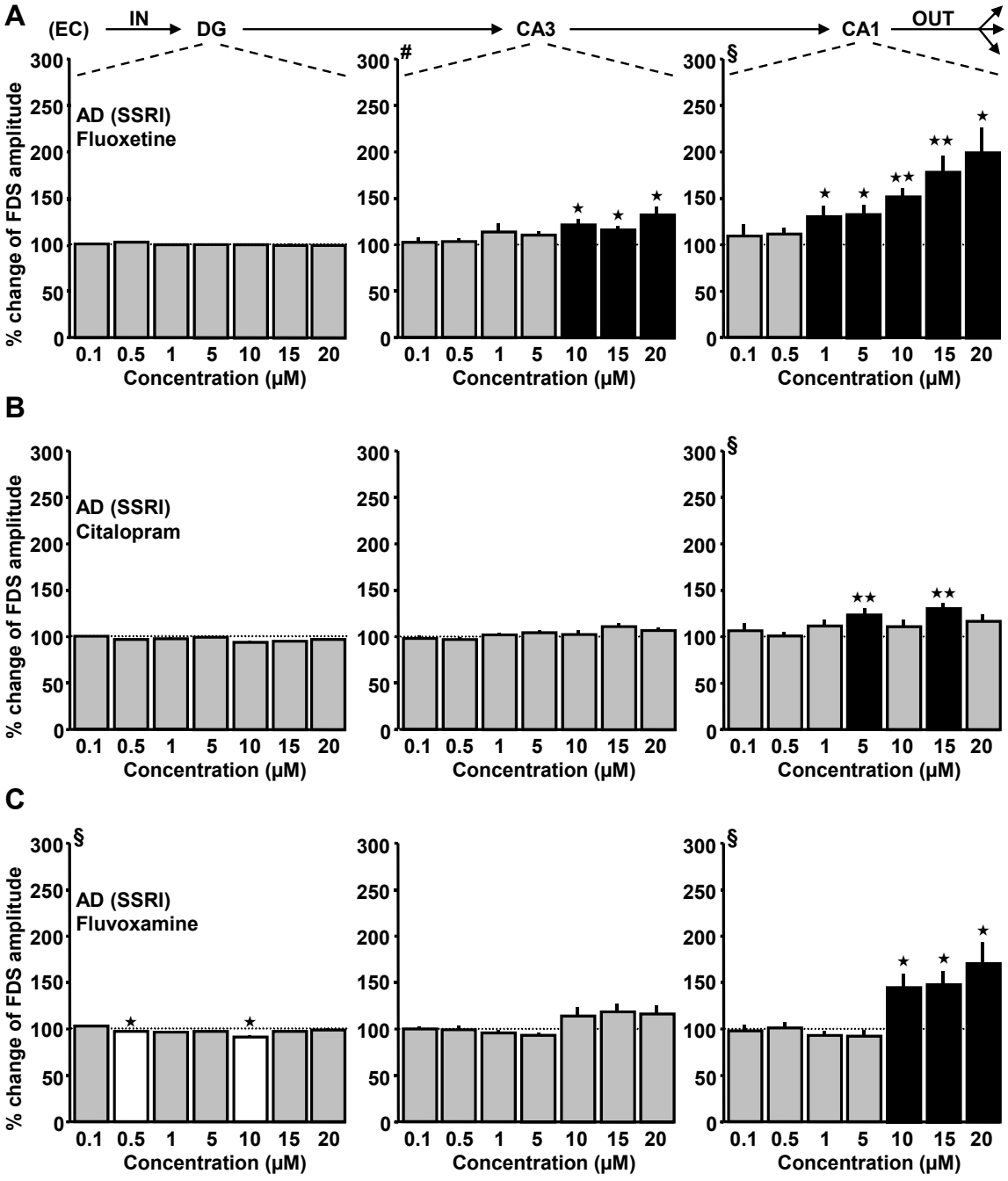

Fig. 4.36. ***SSRIs enhance HTC-waves.*** ***(A-C)*** *Effects of the SSRIs fluoxetine, citalopram, and fluvoxamine on DG-, CA3- and CA1 FDSs (**A**, 0.1 μM = 8 slices/4 mice; 0.5 μM = 8 slices/4 mice; 1 μM = 8 slices/4 mice; 5 μM = 8 slices/4 mice; 10 μM = 7 slices/5 mice; 15 μM = 7 slices/4 mice; 20 μM = 7 slices/3 mice; **B**, 0.1 μM = 7 slices/4 mice; 0,5 μM = 9 slices/5 mice; 1 μM = 8 slices/4 mice; 5 μM = 10 slices/5 mice; 10 μM = 8 slices/5 mice; 15 μM = 8 slices/4 mice; 20 μM = 7 slices/3 mice; **C**, 0.1 μM = 8 slices/3 mice; 0,5 μM = 8 slices/5 mice; 1 μM = 8 slices/4 mice; 5 μM = 8 slices/4 mice; 10 μM = 8 slices/3 mice; 15 μM = 8 slices/3 mice; 20 μM = 9 slices/4 mice).* ***(A-C)*** *#, Kruskal-Wallis ANOVA on ranks: $p = 0.033$ for fluoxetine in CA3; §, one-way ANOVAs: $p < 0.001$ for fluoxetine in CA1; $p = 0.049$ for citalopram in CA1; $p = 0.002$ for fluvoxamine in DG; $p < 0.001$ for fluvoxamine in CA1; followed by paired t-tests: ⋆ $p < 0.05$; ⋆⋆ $p < 0.01$.*

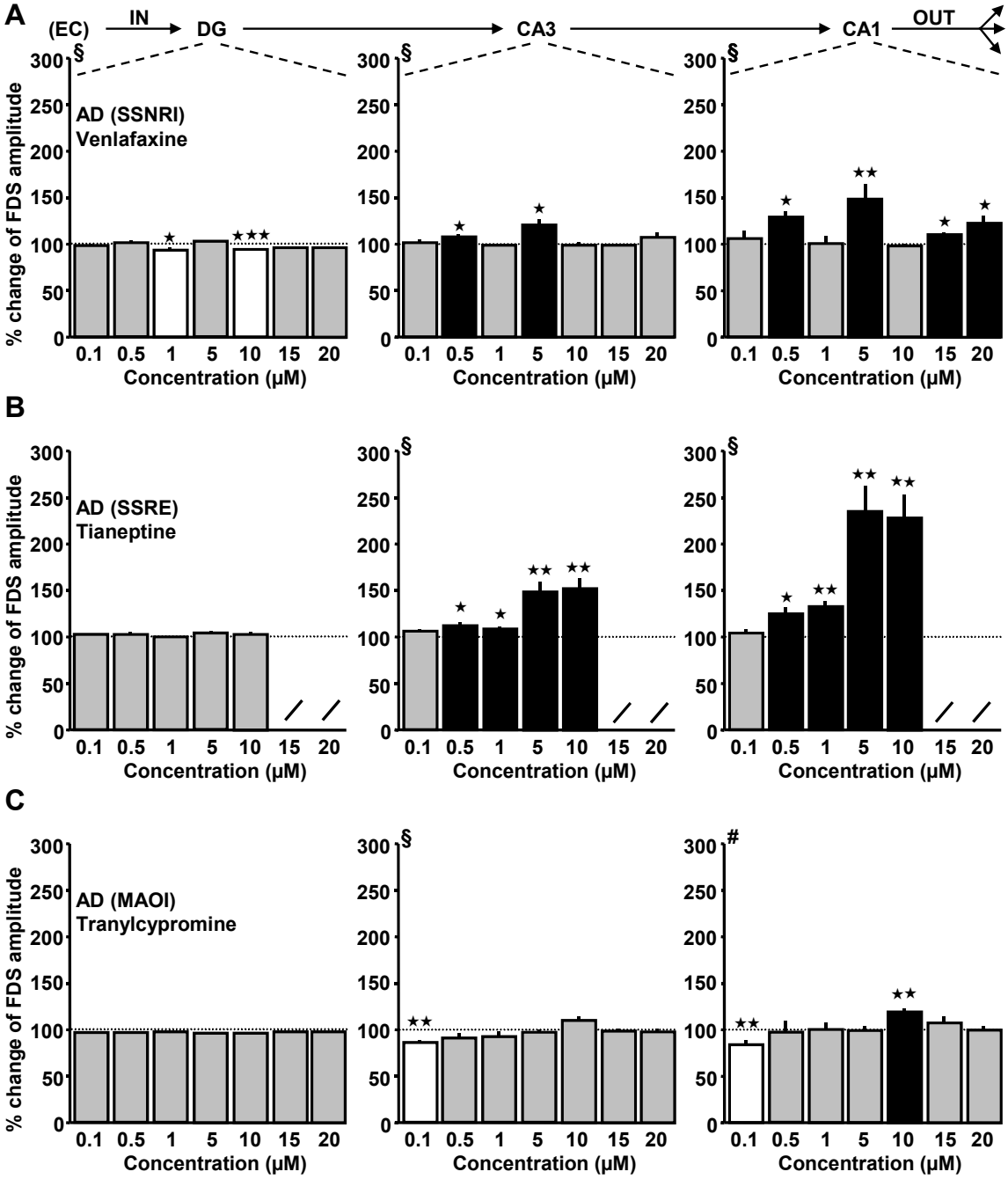

Fig. 4.37. Venlafaxine, tianeptine, and tranylcypromine enhance HTC-waves. (A-C) *Effects of venlafaxine (SSNRI), tianeptine (SSRE), and tranylcypromine (MAOI) on DG-, CA3-, and CA1 FDSs (**A**, 0.1 μM = 8 slices/4 mice; 0.5 μM = 10 slices/6 mice; 1 μM = 9 slices/4 mice; 5 μM = 8 slices/5 mice; 10 μM = 9 slices/5 mice; 15 μM = 8 slices/4 mice; 20 μM = 7 slices/5 mice; **B**, 0.1 μM = 7 slices/4 mice; 0,5 μM = 7 slices/4 mice; 1 μM = 7 slices/4 mice; 5 μM = 7 slices/4 mice; 10 μM = 7 slices/4 mice; **C**, 0.1 μM = 8 slices/4 mice; 0.5 μM = 10 slices/5 mice; 1 μM = 8 slices/4 mice; 5 μM = 8 slices/4 mice; 10 μM = 8 slices/4 mice; 15 μM = 13 slices/8 mice; 20 μM = 8 slices/4 mice).* ***(A-C)*** *#, Kruskal-Wallis ANOVA on ranks: $p = 0.005$ for tranylcypromine in CA1; §, one-way ANOVAs: $p = 0.021$ for venlafaxine in DG; $p = 0.002$ for venlafaxine in CA3; $p < 0.001$ for venlafaxine in CA1; $p < 0.001$ for tianeptine in CA3; $p < 0.001$ for tianeptine in CA1; $p = 0.004$ for tranylcypromine in CA3; followed by paired t-tests: $\star p < 0.05$; $\star\star p < 0.01$.*

4.3.2 Lithium, BDNF, and ketamine amplify HTC-waves

The HIP is severely damaged by stress (Kim and Diamond, 2002), accompanied by a pronounced impairment of activity flow through the HTC (Figure 4.29). Recent evidence suggests that failed function of distinct neuronal networks underlie SRPDs (Castrén, 2005). Thus, the AD drug-induced enhancement of activity flow through the HTC (Figures 4.35A,B; 4.36A-C; 4.37A-C; middle and right panels with bars in black) suggests a common, circuit-level mechanism for compounds with AD potential, that counteracts the detrimental effects of chronic stress. To potentially provide further evidence for this scenario, the mood stabilizer lithium and the neurotrophin brain-derived neurotrophic factor (BDNF) were tested using the HTC-wave assay. Both substances exert AD activity in animal models and/or humans (Cipriani et al., 2009; Nixon et al., 1994; Shirayama et al., 2002; Worrall et al., 1979). Lithium, bath-applied at clinically relevant concentrations (0.5 mM, 1 mM; Smith et al., 2011), readily enhanced CA1-FDSs while having no effect on DG- and CA3-FDSs (Figure 4.38A). BDNF (0.4 nM; Kang and Schuman, 1995) enhanced CA3- and CA1-FDSs, while leaving DG-FDSs unaffected (Figure 4.38B). A growing body of preclinical and clinical data demonstrates that single subanesthetic doses of ketamine (NMDA receptor antagonist) rapidly (within hours) alleviate symptoms of SRPDs in animals and humans (Autry et al., 2011; Berman et al., 2000). This is of particular interest since traditional ADs need chronic administration to become clinically effective (Duman and Aghajanian, 2012). To check whether "slow" and "fast" acting ADs share a common network level mechanism in the HIP, ketamine (20 μM, Autry et al., 2011) was added to the superfusion medium in the recording chamber. Replicating the findings from ADs, ketamine strongly enhanced CA3- and CA1-FDSs (Figure 4.38C).

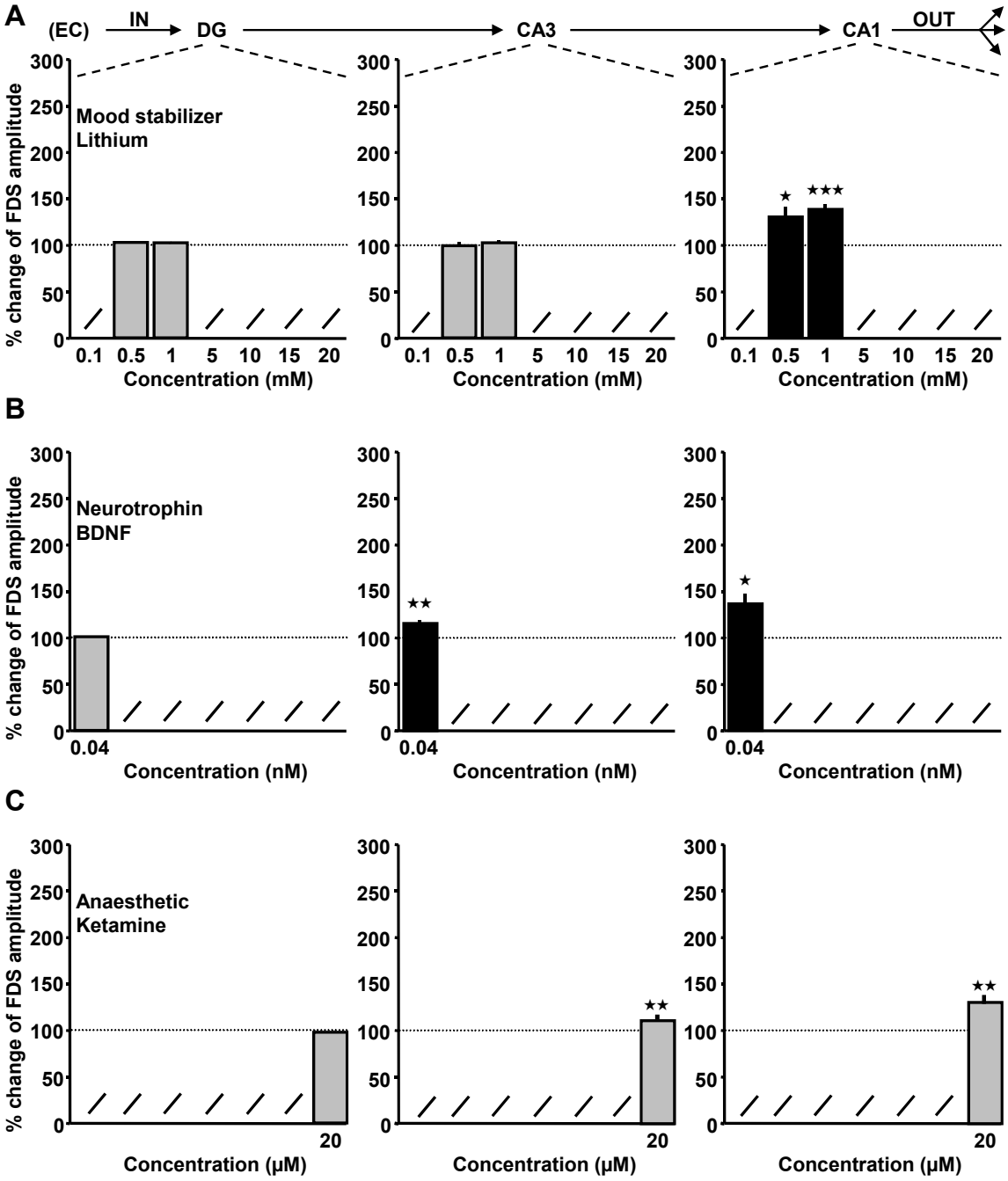

Fig. 4.38. Lithium, BDNF, and ketamine enhance HTC-waves. ***(A,B,C)*** *Effects of lithium, BDNF and ketamine on DG-, CA3-, and CA1 FDSs (**A**, 0,5 mM = 7 slices/3 mice; 1 mM = 7 slices/5 mice; **B**, 0.4 nM = 8 slices/4 mice; **C**, 20 µM = 8 slices/5 mice.* ***(A,B,C)****; ⋆ $p < 0.05$ (paired t-test); ⋆⋆ $p < 0.01$ (paired t-test); ⋆⋆⋆ $p < 0.001$ (paired t-test).*

4.3.3 Haloperidol and diazepam weaken HTC-waves

All substances previously tested (ADs, lithium,BDNF, and ketamine), share two important characteristics: They have AD effects in animal models and/or humans (Cipriani et al., 2009; Shirayama et al., 2002; Worrall et al., 1979), and they enhance HTC-waves (Figures 4.35A,B; 4.36A-C; 4.37A-C). To additionally investigate the pharmacology of drugs

with no obvious AD potential (Airan et al., 2007; Rygula et al., 2008), the impact of the antipsychotic haloperidol and the anxiolytic diazepam (allosteric modulator of $GABA_A$ receptor) on HTC-waves was examined. In contrast to ADs, lithium, BDNF, and ketamine, haloperdiol and diazepam weakened DG-, CA3-, and CA1-FDSs at low micromolar concentration (Kornhuber et al., 1999; Rupprecht et al., 2009), in a manner reminiscent of a classical dose-dependent relationship (Figure 4.39A,B; left, middle and right panels with bars in white).

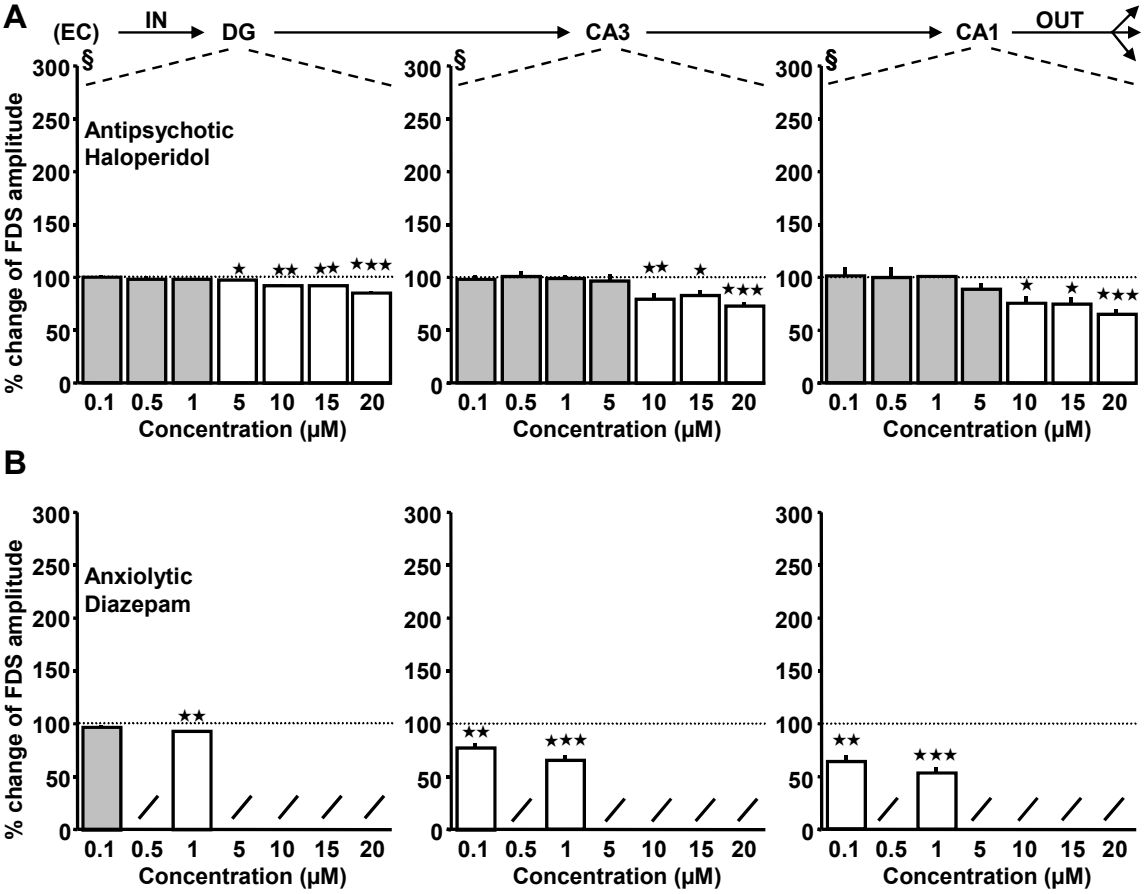

Fig. 4.39. Haloperidol and Diazepam weaken HTC-waves. (A,B) *Effects of haloperidol and diazepam on DG-, CA3-, and CA1 FDSs (**A**, 0.1 μM = 8 slices/5 mice; 0,5 μM = 8 slices/5 mice; 1 μM = 6 slices/4 mice; 5 μM = 8 slices/5 mice; 10 μM = 8 slices/5 mice; 15 μM = 6 slices/4 mice; 20 μM = 6 slices/3 mice; **B**, 0.5 μM = 7 slices/4 mice; 1 μM = 6 slices/3 mice).* ***(A)*** *§, one-way ANOVAs: $p < 0.001$ in the DG; $p = 0.002$ in CA3; $p = 0.005$ in CA1; followed by paired t-tests: ⋆ $p < 0.05$; ⋆⋆ $p < 0.01$; ⋆⋆⋆ $p < 0.001$;* ***(B)*** *⋆⋆ $p < 0.01$ (paired t-test); ⋆⋆⋆ $p < 0.001$ (paired t-test).*

4.3.4 Fluoxetine modulates LTP of HTC-waves

ADs acutely enhance activity flow through the HIP, but may also modulate HTC-wave efficacy on longer time scales and thus, persistently counteract SRPD associated cognitive dysfunction (Sapolsky et al., 1986). Therefore, the impact of ADs on neuronal plasticity was examined in the experimental setting used for pharmacological investigations (see 4.1.4 and Figure 4.25A). To reliably compare neuronal activities across slices, the last CA1-FDS was set within narrow limits (0.15-0.18% $\Delta F/F$) and six pulses at 5 Hz were applied during control stimulations in all experiments (Figures 4.19). Again, the mean of the last

FDSs out of three consecutive acquisitions was used as a final measure of DG, CA3, and CA1 activity levels, and paired t-tests were employed to determine the intervention(s) with significant changes in FDSs at minutes 0 to 18 (baseline) vs. the last 18 minutes after LTP induction or drug application. Following an initial period of stable HTC-wave recordings, stimulation was stopped to apply a 6 second EC/DG-input train (5 Hz), generating network patterns which are capable of inducing LTP of synaptic transmission in the HIP (Figures 4.20, 4.40A). Once stimulation with six control pulses at 5 Hz was resumed, a potentiation of CA3- and CA1-FDSs was detected, which quickly returned to baseline levels after a few minutes (Figure 4.40B). In a second set of experiments plasticity induction was preceded by bath application of fluoxetine (5 μM) which strongly amplified CA3- and CA1-FDSs, replicating previous findings (Figure 4.36A). If the 6 second EC/DG-input at 5 Hz was applied after stable fluoxetine-mediated amplification of HTC-waves, a significant LTP of HTC-waves above baseline levels was detected (Figure 4.40C). To investigate whether this observation depends on enhanced HTC-waves or the sole presence of the drug, brain slices were preincubated with fluoxetine (5 μM) for approx. 18 minutes, resulting in equal exposition times to fluoxetine in both sets of experiments. In contrast to drug free experiments, the 6 second EC/DG-input at 5 Hz also induced LTP of HTC-waves (Figures 4.40D). Importantly, DG-, CA3-, and CA1-FDSs show equal activity levels during LTP induction across groups (Figure 4.40A). The DG did not exhibit LTP and DG-FDSs significantly declined in all three experimental settings (Figure 4.40A,B,C,D).

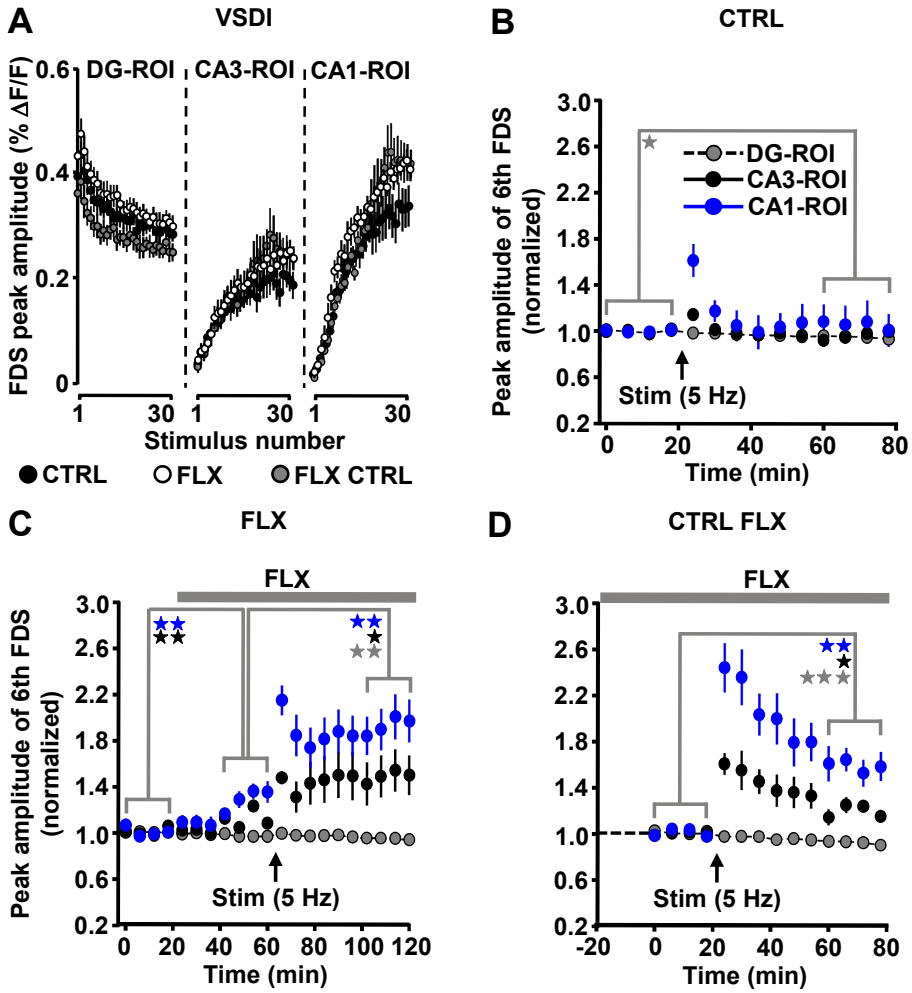

Fig. 4.40. Fluoxetine modulates LTP of HTC-waves. ***(A)*** *Quantification of neuronal activities in hippocampal subregions in response to 5 Hz EC/DG-input (6 s.).* ***(B)*** *5 Hz EC/DG-input (6 s.) failed to induce LTP of HTC-waves.* ***(C)*** *Replicating results described above, 5 µM fluoxetine strongly enhanced HTC-waves (Figure 4.36A). Subsequent 5 Hz EC/DG-input (6 s) induced LTP of HTC-waves.* ***(D)*** *After preincubation of slices with fluoxetine (5 µM, 18 min), 5 Hz EC/DG-input (6 s) likewise induced LTP of HTC-waves. (**CTRL**, N = 6 slices/6 mice; **FLX**, N = 8 slices/8 mice; **FLX CTRL**, N = 6 slices/4 mice).* ***(C,D)*** *$\star p < 0.05$ (paired t-test); $\star\star p < 0.01$ (paired t-test); $\star\star\star p < 0.001$ (paired t-test). Abbreviations: CTRL, control; FLX, fluoxetine.*

Chapter 5

Discussion

5.1 Polysynaptic activity flow in the hippocampus

In accordance with the aims of the present thesis, it was first tested whether evoked synaptic input from the entorhinal cortex to the dentate gyrus (EC/DG-input) triggers hippocampal network dynamics, allowing the investigation of several aspects of polysynaptic activity flow within this limbic brain structure. For this purpose, VSDI was applied to mouse brain slices, enabling the direct investigation of neuronal activity on a millisecond time scale, with a micrometer-range spatial resolution and a scope spanning the entire HIP (Airan et al., 2007; von Wolff et al., 2011). In contrast to single pulse stimulation of the PP, synchronous 5 Hz spike trains highly effectively induce neuronal activity waves, which percolate through the entire trisynaptic circuit of the HIP. These so-called "HTC-waves" precisely follow the rhythm of the EC/DG-input, drive high-frequency firing (>100 Hz) of CA3 pyramidal neurons, and induce NMDA receptor-dependent CA1 LTP within a few seconds. Moreover, the "HTC-wave assay" emerged as a valuable tool to investigate drug effects on hippocampal network dynamics. Bath application of neuromodulators (CORT, CRH) and the cognitive enhancer caffeine rapidly boosts HTC-waves.

5.1.1 5 Hz EC/DG-input induce polysynaptic activity flow through the hippocampus

The effective induction of HTC-waves using 5 Hz EC/DG-input, is in line with the hypothesis that such coordinated activity across neuronal cell ensembles represents a fundamental property of the entorhinal-hippocampal complex (Buzsàki, 2002). In the intact brain, theta oscillations are thought to facilitate information transfer within neuronal networks, leading to the formation and correct recall of explicit memories, and previous research links their disturbance to the pathophysiology of SRPDs (Pernía-Andrade and Jonas, 2014; Buzsàki, 2002; Linkenkaer-Hansen et al., 2005; Lega et al., 2012; Rutishauser et al., 2010; Winson, 1978). It is assumed that the EC is fed with polymodal sensory information (Watson et al., 2011) and, indeed, recently published *in vivo* data suggests that the EC layer II stellate cell population activity is characterized by strong spike phase-locking

to the local theta field potential during spatial navigation (Burgalossi et al., 2011; Fernandez et al., 2013; Mizuseki et al., 2009; Quilichini et al., 2010). Moreover, several inherent properties of the DG-CA3 network favors excitation of principle neurons over their inhibition via GABAergic interneurons in a theta-frequency-dependent manner (Pernía-Andrade and Jonas, 2014; Mizuseki et al., 2009; Scharfman et al., 1990; Thompson and Gähwiler, 1989). *In vivo* recordings suggest that EC theta oscillations are tightly associated with theta-frequency discharges in DG granule cells (Jung and McNaughton, 1993; Mizuseki et al., 2009; Skaggs et al., 1996). This hypothesis was recently validated by means of recordings from intracellulary labeled granule cells (Pernía-Andrade and Jonas, 2014). Thereunto, in contrast to single action potentials, theta frequency trains in presynaptic MFs increase the discharge probability of CA3 pyramidal neurons (Henze et al., 2002; Hsu, 2007; Mott and Lewis, 1992; Scharfman et al., 1990; Thompson and Gähwiler, 1989). Different mechanisms within the CA3 principal neuron-interneuron circuitry have been reported to mediate such an "activity-dependent disinhibition" (Scharfman et al., 1990; Mott and Lewis, 1992). These studies suggest that a decrease of inhibitory postsynaptic currents in CA3 pyramidal neurons after repetitive stimulations results from an increase of the intracellular Cl^- concentration, accompanied by a shift in its reversal potential which leads to a decrease in driving force for chloride-mediated GABAergic inhibition. Previous research also found a $GABA_B$ receptor-mediated reduction of presynaptic GABA release probability (Hsu, 2007; Mott and Lewis, 1992; Thompson and Gähwiler, 1989). Although, DG granule cells provide the main input onto GABAergic interneurons situated in CA3 SL and thereby conferring net inhibition of the hippocampal CA3 network after activation of the MF pathway (Henze et al., 2000; Mori et al., 2004). This suggests a switch to net excitation in a (theta)frequency-dependent manner. Together with simultaneously occurring frequency depression at MF synapses onto CA3 inhibitory interneurons, suprathreshold EPSPs in CA3 pyramidal neurons are likely to occur (Toth et al., 2000).

Here, the strong facilitation of MF onto CA3 pyramidal transmission likely took advantage of these network characteristics and is presumably such strongly pronounced that even unitary EPSPs are able to fire CA3 pyramidal neurons (Henze et al., 2002; Jonas et al., 1993; Toth et al., 2000). The recently reported involvement of membrane derived lipids as retrograde messengers in facilitation of MF synaptic transmission (Carta et al., 2014) is unlikely to occur during the induction of HTC-waves, since the HTC reverted to its locked state after approx. 60 seconds, whereas MF to CA3 potentiation observed by Carta et al. (2014) lasts several minutes. The pivotal role of the MF to CA3 synapse is in line with the observation that a selective shutdown of neurotransmission at these synapses is associated with the disappearance of HTC-waves. Supporting evidence comes from recordings in anesthetized mice (Stepan et al., 2012). 5 Hz PP stimulation triggers pop spikes in CA1 with the same delayed and initially progressive appearance and with comparable latencies to onset ($\sim$ 18 ms) as the CA1 neuronal responses in the *in vitro* experiments. Moreover, HTC-waves are never observed if the PP is stimulated

with 0.2 Hz and the occurrence and strength of activity propagations through the HTC critically depends on the frequency and persistency of EC/DG-input (Figures 4.4, 4.4). This previous research on this brain area, links neuronal network dynamics in the DG with a gate or basic filter mechanism at the entrance to the HIP, modulating or filtering incoming information from the EC (Andersen et al., 1966; Ewell and Jones, 2010; Hsu, 2007; Iijima et al., 1996; Scharfman et al., 1990). These considerations are supported by the observation that DG-FDSs increasingly decline in their magnitude during 0.2, 1, 5, and 20 Hz EC/DG-input, respectively (Figure 4.4). Similarly, Andersen et al. (1966), who placed intracellular- and extracellular recording electrodes into the DG of rabbits to study its activation after PP stimulation, also found induction EPSPs after a few seconds of repetitive stimulation, with the highest degree of facilitation around theta and nearly abolished signals at frequencies above 10 Hz (Andersen et al., 1966). Using VSDI, Iijima et al. (1996) showed that only repetitive stimulation at 1 Hz or several reverberations of bicuculline-induced excitation in the EC resulted in invasion of activity into area CA3, even if their pharmacologically induced excitation is reminiscent of epileptic-like activity sometimes observed in the present study (Figure, 4.9, Figure 4.10A). However, comparable to the situation in the CA3 network, the switch from inhibition to excitation is likely mediated by disinhibition of granule cells in response to repeated activation (Scharfman et al., 1990; Thompson and Gähwiler, 1989). In combination with the fact that facilitation at MF synapses develops stronger with higher frequencies (Toth et al., 2000), it is tempting to speculate that the DG-CA3 complex acts as a "low-order band-pass filter," in which the DG circuitry serves as the "low-pass unit" and the CA3 MF system as the "high-pass device." All this might explain, why the DG network is effectively passed by simultaneously and repetitive incoming information encoded in the theta-frequency range. Hence, an important physiological function of theta-rhythmical spiking of EC stellate cells might be to drive sensory information through the whole entorhinal-hippocampal loop, but only information presented for sufficient time and carried at certain frequencies might pass. Moreover, the strengthening of HTC-waves by caffeine suggests that the amount of information flow is modifiable by attention enhancing drugs (Nehlig, 2010).

5.1.2 HTC-waves induce CA1 LTP

Beside effective gating of HTC-waves, the pronounced frequency facilitation at the MF to CA3 synapse may promote action potential firing in CA3 pyramidal neurons and, thus, is very likely responsible for the subsequent formation of CA1 LTP. Here, the occurrence of multiple pop spikes in CA3 SL in response to 5 Hz EC/DG-input is in line with reports from intracellular recordings demonstrating that CA3 pyramidal neurons typically respond with burst spiking (100-300 Hz) to suprathreshold depolarizations (Andersen et al., 2006; de la Prida et al., 2006). Previous research support the finding that burst activity of CA3 pyramidal neurons triggers the formation of CA1 LTP (Bliss and Collingridge, 1993; Buzsàki et al., 1987; Larson and Lynch, 1986). Buzsàki et al. (1987) induced high frequency spiking of CA3 pyramidal neurons through local application

of bicuculline, whereas other studies demonstrated that CA1 LTP is evoked most effectively by theta-burst stimulation of CA3 to CA1 projections (Bliss and Collingridge, 1993; Larson and Lynch, 1986).
Several lines of evidence suggest that DG granule cells are characterized by a sparse firing (Pernía-Andrade and Jonas, 2014; Leutgeb et al., 2007; Schmidt et al., 2012), which is in contrast to the widespread activation of all hippocampal subfields in response to theta-rhythmical EC/DG-input. However, the inherent properties of the entorhinal-hippocampal network, in particular the gradual decrease of HTC-wave amplitude in response to a stepwise reduction of EC/DG-input and the results from recordings of individual cell pairs (Mori et al., 2004), suggest that activity percolations through the HTC and the concomitant induction of CA1 LTP also naturally take place at the level of a sparsely active hippocampal network (Jung and McNaughton, 1993; Leutgeb et al., 2007; Whitlock et al., 2006). The critical role of the HTC in learning and memory is supported by a recent study providing evidence that some forms of HIP-dependent learning require the integrity of the full HTC (Daumas et al., 2009; Nakashiba et al., 2008). In the first study, a transgenic mouse line that permits selective shutdown of CA3 output displayed deficits in contextual and spacial learning tasks (Nakashiba et al., 2008). Pharmacological suppression of MF to CA3 synaptic transmission likewise impairs HIP-dependent learning tasks (Daumas et al., 2009). However, these findings do not exclude contributions of other afferent inputs. (e.g., direct EC input to area CA3 (Tsukamoto et al., 2003) and CA1 (Remondes and Schuman, 2004) to CA1 LTP formation , but ascribe a major role to the HTC.
It was also shown that activity propagations through the HTC occur during 1 and 20 Hz EC/DG-input. Although these frequencies were not tested with regard to their potential to induce synaptic plasticity, it is likely that such EC/DG-input can also elicit CA1 LTP. However, the present data and a previous study (Capocchi et al., 1992) suggest a more effective induction of CA1 LTP in response to theta-rhythmical EC/DG-input. Theta frequency EC/DG-input elicits a markedly higher strength of HTC-waves than any other stimulation pattern (Figure 4.4). Second, the observations that 10 HTC-waves caused no formation of CA1 LTP (Figure 4.4) and 30 stimuli were inefficient to evoke LTP of HTC-waves in the absence of fluoxetine (Figure 4.40B,D), suggests an induction threshold for long-term synaptic plasticity in the HIP, that might be merely reached through inappropriate activation of the HTC. Finally, Capocchi et al. (1992) show that theta-burst stimulation of CA3-CA1 projections leads to considerably stronger CA1 LTP than 1 and 20 Hz burst stimulation.
The present study confirms previous research (Buzsàki, 1988; Nakagami et al., 1997) on "polysynaptic induction of LTP" in the CA1 subfield of the HIP, but provides more direct evidence for this phenomenon. There are significant differences between the present work and the studies from Buzsàki and Nakagami et al.. In particular, there are some methodological caveats, which question the validity of previous results. Buzsàki reported a long-lasting enhancement of CA1 population spikes in response to several high-frequency (400 Hz) trains of stimuli delivered to the angular bundle. With regard to the proposed function of the DG as a low-pass filter and the literature showing that high

frequency input cause prominent inhibition of DG granule cells (Andersen et al., 1966; Mott and Lewis, 1992; Scharfman, 1991) it is questionable whether any activity enters the CA subfields via the trisynaptic pathway. Indeed, Buzsàki recognized that hippocampal neurons are not able to follow high-frequency PP activity and that therefore the HTC as a main route of information flow through the HIP (Andersen et al., 2006; Nicoll and Schmitz, 2005; Neves et al., 2008) is effectively shut down. For this reason, he states that direct EC-inputs to areas CA3 and CA1, which were functionally inactivated in this study, most likely played an essential role in the induction of the population spike LTP in area CA1. Moreover, it is questionable if 400 Hz spiking represents an physiological activity pattern of any EC neuron that sends projections via the PP to the HIP (Andersen et al., 2006; Pernía-Andrade and Jonas, 2014; Burgalossi et al., 2011; Mizuseki et al., 2009; Quilichini et al., 2010).
In the second study, Nakagami et al. (1997) used voltage-sensitive dyes to monitor neuronal activity in rat brain slices and report that a 1-s-long high-frequency (100 Hz) train of pulses delivered to the dendritic field (ML) of the DG caused "trisynaptic LTP induction." However, it is again questionable how effectively such a stimulation pattern induces spiking of DG granule cells, in consideration of the effective blocking of high frequency excitation from the EC (Andersen et al., 1966; Mott and Lewis, 1992). Furthermore, the probable contribution of changed neurotransmission at direct PP-input to CA3 pyramidal neurons and non-synaptic excitation of DG granule cells remains elusive. Additionally, the authors provide no clear evidence of LTP at CA3 to CA1 synapses. In the present study, this methodological problem was circumvented by showing an increase of CA1 responses through direct stimulation of the SC-commissural pathway and by inhibiting CA1 LTP formation via a locally restricted blockade of NMDA receptors in area CA1 (Figure 4.22).

5.1.3 Pharmacological modulation of HTC-waves

Beside their capacity to induce CA1 LTP, HTC-waves might be a valuable tool for studying drug effects on polysynaptic activity flow through the HIP. Strong experimental evidence suggest that caffeine exerts memory enhancing effects in animals and humans (Borota et al., 2014; Kopf et al., 1999; Nehlig, 2010). Kopf et al. (1999) reported facilitation of memory consolidation in rats when caffeine was administered after performing a passive avoidance task. Similar results come from a recent study, demonstrating that caffeine specifically enhanced memory consolidation in humans, when given within a time-frame of 24 h after a behavioral discrimination task (Borota et al., 2014). For this reason, the cognitive enhancer caffeine was added to the superfusion medium at a concentration found in the cerebrospinal fluid of humans after intake of 1-2 cups of coffee (5 μM Fredholm et al., 1999). The alkaloid rapidly boosted HTC-waves, which might partly underlie its beneficial action on cognitive processes, although it is not known whether HTC-waves also occur during memory consolidation (Borota et al., 2014; Kopf et al., 1999; Nehlig, 2010). The mechanisms by which caffeine enhanced HTC-waves remains to be determined. However, the antagonistic action of caffeine on adenosine A_1 receptors is a

strong candidate (Kukley et al., 2004). Pharmacological blockade of these receptors exerts caffeine like effects on memory consolidation in behaving rats (Kopf et al., 1999) and was reported to strengthen neurotransmission at MF to CA3 and SC to CA2-synapses (Kukley et al., 2004; Simons et al., 2012). In addition, previous studies suggest the contribution of a caffeine-induced form of CA1 LTP (Martín and Buño, 2003). However, the disappearance of the caffeine-mediated effect on HTC-waves within approximately 15 min after removing the substance from the bath solution does not support the involvement of long-term synaptic changes. This discrepancy might be related to the high caffeine concentration (10 mM) used by Martín and Buño.

Furthermore, it was demonstrated that the stress hormones CORT (100 nM) and CRH (5 and 50 nM) also quickly amplified HTC-waves. As already suggested for caffeine, this effect might contribute to enhanced cognitive functions in response to acutely elevated stress hormone levels, i.e. in stressful situations (Blank et al., 2002; de Kloet et al., 1999). Previous research demonstrates various acute effects of CRH on neuronal function in the HIP (Blank et al., 2002; Hollrigel et al., 1998; Kratzer et al., 2013), but the underlying mechanisms are poorly understood. Complicating the picture, contrasting effects on neuronal excitability were reported (Blank et al., 2002; Sheng et al., 2008). In recent years, $CRHR_1$ emerged as a crucial mediator of CRH effects on hippocampal physiology (Kratzer et al., 2013; Refojo et al., 2011; von Wolff et al., 2011). The rapid effect of CRH (50 nM) on HTC-waves corroborates the results from a recent VSDI study (von Wolff et al., 2011). von Wolff et al. (2011) demonstrate that the modulatory effect of CRH is abolished in $CRHR_1$ receptor knockout mice (von Wolff et al., 2011). Although von Wolff et al. evoked activity percolations through the HIP non-synaptically by direct stimulation of the DG granule cell layer, the similar activation pattern in downstream regions suggests that HTC-wave amplification likewise requires intact $CRHR_1$ receptor function (von Wolff et al., 2011). This is of specific interest since $CRHR_1$ deficient mice are impaired in spatial recognition memory (Contarino et al., 1999). Strikingly, a considerably lower concentration (5 nM) of CRH than usually used *in vitro* (Kratzer et al., 2013; Refojo et al., 2011; von Wolff et al., 2011) was still sufficient to modulate HTC-waves. This finding suggests the HTC-wave assay to be highly sensitive to pharmacological modifications.

Several lines of evidence indicate that CORT facilitates hippocampal excitability via genomic (GRs) and non-genomic (MRs) mechanisms (de Kloet et al., 1999), although opposing actions were also reported, e.g., non-genomic GR-mediated modification of inhibitory networks in the HIP, that cause an increase in inhibitory postsynaptic currents in CA1 pyramidal neurons (Hu et al., 2010). However, previous work indicates that the rapid effects of CORT cannot be explained by genomic effects (Groeneweg et al., 2011; Karst et al., 2005). First evidence for such a scenario came from Karst et al. (2005), demonstrating enhanced miniature excitatory postsynaptic current (mEPSC)s in area CA1 after bath application of 100 nM CORT in wild-type mice, an effect that was preserved in brain specific GR knockout's, but not in animals without MR receptors (Karst et al., 2005). Furthermore, pharmacological activation of GRs did not increase mEPSC frequency, whereas the MR agonist aldosterone (higher affinity for MR receptors) has pronounced effects

(Karst et al., 2005). The present data gives support for such a rapid, non-genomic CORT-mediated modulation of the hippocampal network (Karst et al., 2005).
Yet, independent from the underlying mechanism, the present findings suggest that CRH and CORT are able to rapidly increase hippocampal output (Groeneweg et al., 2011). From this it is tempting to speculate that both stress hormones positively modulate the fast, inhibitory feedback onto the HPA axis (Radley, 2012).
An issue not addressed in this study was whether LTP formation plays a causal role in the CRH and CORT-induced enhancement of HTC-waves (Blank et al., 2002; Wiegert et al., 2006) However, the fast facilitation under moderate PP stimulation (Figures 4.24C, 4.26) is an argument against the contribution of a long-term plasticity-dependent change in glutamatergic neurotransmission, but rather a $CRHR_1$-mediated enhancement of neuronal excitability and a non-genomic mineralocorticoid receptor-mediated increase in glutamate release probability, respectively (Groeneweg et al., 2011; Karst et al., 2005; von Wolff et al., 2011).
It is important to note that the acute application of all drugs tested here, shares one important similarity. They shape neuronal function via diverse cellular mechanisms (Nehlig, 2010; Joëls, 2006; Maras and Baram, 2012), thus rendering the prediction of their impact on the neuronal network level practically impossible. In contrast, the HTC-wave assay integrates all cellular adjustments in response to pharmacological intervention and reports the "net" outcome.

Taken together, the present results describe for the first time that theta-rhythmical stimulation of PP fibers is sufficient to induce polysynaptic activity flow within the HIP. This activity likely reflects synchronous spiking of EC stellate cells (including grid cells (Burgalossi et al., 2011; Hafting et al., 2008) and the resultant HTC-waves trigger CA1 LTP within a few seconds. Moreover, this approach proved to be a valuable tool for studying drug effects on neuronal network dynamics. On that account, HTC-waves might be useful to examine polysynaptic activity flow through the HIP in animal models of disease.

5.2 HTC-waves and stress

After the development and validation of the HTC-wave assay, it was found that chronic stress impairs polysynaptic activity flow through the HIP. To compare VSDI signals, the HTC-wave assay was refined by normalizing the EC/DG-input strength, using a specific ROI in the DG (DGS-ROI; Figure 4.27). Initial studies revealed a linear relationship between DGS-, CA3-, and CA1-FDSs in a given stimulus range. Although, DGS-FDSs were nearly identical in CTRL vs. CSDS animals, stimulation intensities to evoke predefined DGS-FDSs were significantly higher in CSDS mice. The most obvious finding to emerge from these experiments was that CA3- and CA1-FDSs were markedly decreased in CSDS mice. In addition, these differences were stable over the entire time of experimentation (6 days with ongoing defeat for prospective animals), suggesting a stable pattern of hippocampal adjustments after two weeks of CSDS.

5.2.1 CA3- and CA1-FDSs increase linearly with increasing DGS-FDSs

Analogous activation pattern at the input region of the HTC turned out to be vital to reliably detect downstream stress effects in CSDS mice (Airan et al., 2007; Kim et al., 2012). However, the occurrence of HTC-waves is very likely not uniform across slices. Previous research has documented adverse modifications of EC principle cells in response to chronic stress, which could possibly lead to structural adjustments, including axonal arborizations (Lucassen et al., 2001; Cooper et al., 2009). Such alterations might bias electrical stimulation of the PP. Differences in the electrode position and, thus, the number of recruited fibers and/or deviations of neuronal connectivity and the extend of cut fibers of distinct neuronal populations in brain slices may also increase the variability across experiments (Amaral and Witter, 1989; Andersen et al., 2006; Jackson and Scharfman, 1996). Thus, it seems obvious that fixed voltage intensities or percentage shares are not suited to generate equal activation patterns in all experiments. This point is particularly relevant since voltage intensities which were capable of evoking distinct FDSs in the DG, markedly differed between CTRL and CSDS mice. Initial studies revealed normalization of neuronal activity in the DGS-ROI suited to fulfill the requirement of equal input into the HTC. This was done using single pulse EC/DG-input to evoke specific DGS-FDSs. In a wide stimulus range, FDSs within this particular ROI were found to be linear with subsequent CA3- and CA1-FDSs in response to 15 pulses at 5 Hz (Figure 4.28B), a finding that was preserved in CSDS mice (Figure 4.30A).
The exact explanation for this observation remains to be determined. In this context, it is important to note that anatomy and function is not homogenous along the transverse axis of the DG. As mentioned above, the DG is divided into a suprapyramidal and infrapyramidal blade (Andersen et al., 2006; Witter, 2007) and several anatomical differences between granule cells in both regions have been reported (Andersen et al., 2006; Scharfman et al., 2002; Witter, 2007). For example, interaction between granule cells and CA3 pyramidal neurons via the MF pathway depends on their position along the transverse axis of the DG and HIP, respectively. Proximal CA3 cells are preferentially innervated by neurons in the infrapyramidal blade, whereas granule cells in the suprapyramidal blade innervate CA3 pyramidal neurons along the entire transverse axis (Witter, 2007). Furthermore, inputs originating from different parts of DG also exert differential influence along the dendritic tree of individual CA3 pyramidal neurons (Witter, 2007). These anatomical findings are of specific interest because several studies found functional differences along the transverse axis of the DG (Choi et al., 2003; Jaarsma et al., 1992; Schmidt et al., 2012; Scharfman et al., 2002). For instance, Schmidt et al. (2012) investigated the expression of immediate early genes in rats after a spatial exploration task and found that granule cells in the suprapyramidal blade were more active than in the infrapyramidal blade. In another study, Scharfman et al. (2002) reported effects of epileptic seizures on molecular and electrophysiological parameters in the two blades. Using VSDI, they found a stronger spread of activity into the infrapyramidal blade, an observation that they associated with a more important role of the infrapyramidal blade in activating hippocampal neurons. Despite the heterogeneity of these findings, they might

account for the strong correlation of neuronal activity between the suprapyramidal blade and areas CA3 and CA1.

5.2.2 Reduced activity flow through the hippocampus

Using the refined HTC-wave assay, the current study found that CSDS markedly reduced the strength of polysynaptic activity flow through the HIP. This was very likely an effect of the well documented adverse physical changes in the HIP in response to persistently elevated stress hormone levels (Magariños and McEwen, 1995; Sapolsky et al., 1986; Sousa et al., 2000; Vyas et al., 2002). In this context, the HPA axis is most often recognized (Magariños and McEwen, 1995; Nestler and Hyman, 2010; Sousa et al., 2000; Vyas et al., 2002) since chronic stress paradigms consistently demonstrate elevated blood levels of stress hormones, most frequently CORT and CRH (Herman et al., 1995; Makino et al., 1995; Sousa et al., 2000; Wagner et al., 2011). Other issues are that the HIP seems to be a major target of GCs, since its GC receptor expression is enriched (McEwen et al., 1968), exogenous GC administration mimics adverse effects of chronic stress on hippocampal structure and function (McEwen, 2001), and hippocampal efferents are thought to inhibit emotional stress-induced HPA axis activation, via GC receptor-mediated negative feedback (McEwen and Gianaros, 2011; Jacobson and Sapolsky, 1991; Sapolsky et al., 1984a). Supporting evidence comes from human studies, showing abnormal activity of the HPA axis (hypercortisolism or hypocortisolism) and HPA axis insensitivity to GC receptor agonist treatment (i.e., dexamethasone supression test) is observed in approximately one half of depressed individuals (Carroll et al., 1976; Holsboer, 1983; Krishnan and Nestler, 2008). Accordingly, the CSDS paradigm has been shown to robustly induce chronic stress parameters associated with HPA axis dysregulation, including increased adrenal glands weight, reduced thymus weight, and increased basal plasma levels of CORT (Hartmann et al., 2012; Wagner et al., 2011). The association of these adjustments with human SRPDs corresponds well with evidence from behavioral experiments in rodents. A minimum of 10 days CSDS (Berton and Nestler, 2006) results in a high anxiety phenotype, a reduction in exploratory behavior, an increased emotionality and a decreased grooming behavior (indicated by reduced fur quality), which are supposed to represent depression-like symptoms (Berton and Nestler, 2006; Hartmann et al., 2012; Wagner et al., 2011).

No differences between groups were found in CA3-FDSs at the lowest stimulation intensity. A possible explanation is that FDSs were such less pronounced that differences did not come into effect. However, the trend towards higher activity levels in area CA1 is in line with results obtained from stronger stimulation intensities.

In agreement with CSDS used here, various other animal models of chronic stress (e.g., chronic immobilization stress (CIS), chronic unpredictable stress (CUS), chronic mild stress (CMS), chronic variable stress (CVS); Airan et al., 2007; Berton and Nestler, 2006; Fuchs and Flúgge, 2003; Herman et al., 1995; Ulrich-Lai et al., 2006; Wagner et al., 2011) applied to different species (mice, rats, tree shrews; Airan et al., 2007; Berton and Nestler, 2006; Fuchs and Flúgge, 2003; Wagner et al., 2011) have identified many of signaling

molecules and receptors likely involved in neuronal response to prolonged stress exposure (e.g., neuromodulators, neurotransmitters, neurotrophic factors; Duric and Duman, 2013). Furthermore, there are multiple forms of adjustments involved, ranging from changes on the molecular level (Wagner et al., 2011) to cellular adaptions (Snyder et al., 2011) to remodeling of principle neurons (Magariños and McEwen, 1995; Figure 1.3). Likewise, stress-induced modification in the structure of the HIP may also play a causal role in humans, since alterations in neurotrophin signaling (Dwivedi et al., 2005; Knable et al., 2004), neuronal morphology (Kempton et al., 2011) and volume (Neumeister et al., 2005; Sheline et al., 2003) were observed in individuals suffering from SRPDs.
However, significant bias might be associated with the utilization of different animal models (Nestler and Hyman, 2010). For example, Vyas et al. (2002) demonstrated that two different animal models exhibit distinct chronic stress effects in the HIP. In their study, only CIS caused the typical morphological adjustments in CA3 pyramidal neurons, which was not detectable after CUS. This is in contrast to the observations made by Sousa et al. (2000) and Magariños and McEwen (1995) who reported significant alterations in CA3 pyramidal neurons also in response to CUS. Similar inconsistencies across animal models were also reported for adjustments of basal CORT levels and adrenal glands weight (Herman et al., 1995; Magariños and McEwen, 1995; Wagner et al., 2011). Hence, more circuit-centered approaches might be better suited to integrate the diverse physical changes in response to chronic stress (Airan et al., 2007; Karayiorgou et al., 2012). In line with this suggestion, CSDS shares critical stress indices with other animal models. For instance, prominent indicators of chronic stress are baseline hypersecretion of CORT and adrenal hypertrophy. Both were demonstrated after exposure to CSDS, CUS and CVS (Herman et al., 1995; Magariños and McEwen, 1995; Sapolsky et al., 1984b; Wagner et al., 2011; Watanabe et al., 1992). These paradigms but also chronically administered CORT, have been shown to promote a reversible shortening and debranching of apical and basal dendrites of CA3 pyramidal neurons (Magariños and McEwen, 1995; Watanabe et al., 1992; Vyas et al., 2002). In a recent study Numakawa et al. (2009) demonstrated that chronic exposure to dexamethasone and CORT reduced TrkB-GR interaction, BDNF-stimulated PLC-γ and BDNF-triggered glutamate release. In line with the study of Numakawa et al. (2009), stress-induced glutamatergic dysfunction might be an underlying cause of hippocampal adjustments (Kallarackal et al., 2013; Moghaddam et al., 1994; Lowy et al., 1993; Popoli et al., 2012). Numakawa et al.'s study might also explain reduced neurotrophic factors (e.g., BDNF mRNA) in chronically stressed rodents (Murakami et al., 2005). BDNF in turn maintains neuronal survival and morphology of hippocampal neurons (Chao, 2003; Smith et al., 1995; Saarelainen et al., 2003) and is critically involved in synaptic plasticity in *vitro* (Kovalchuk et al., 2002) and *in vivo* (Ying et al., 2002).
Furthermore, downregulation of GR mRNA in the HIP is also observed in response to CSDS, CVS, and CUS likely attenuates the GC negative feedback, thereby exacerbating CORT-induced adverse effects on neuronal morphology (Herman et al., 1995; Holsboer, 1983; Makino et al., 1995; Sapolsky et al., 1984b; Wagner et al., 2011).

Finally, CSDS and CVS trigger CRH mRNA expression in the PVN (Herman et al., 1995; Hartmann et al., 2012), which is associated with morphological changes of hippocampal neurons, similar to those observed after prolonged exposure to high levels of CORT (Chen et al., 2004; Duric and Duman, 2013).
From all this, it is possible to hypothesize that chronic stress-induced changes in hippocampal physiology result in a circuit-level phenotype, independent from a common etiology or mechanism (Airan et al., 2007; von Wolff et al., 2011).
Another important finding was that FDSs were severely reduced in both CA regions under investigation. In this regard it is important to note that the approach presented here aimed to explore circuit-level mechanisms of chronic stress in the HIP. VSDI together with the methodology to induce polysynaptic activity flow within the HIP offers the advantage to directly measure neuronal activity in large-scale neuronal networks and compute input/output relationships (Airan et al., 2007; Avrabos et al., 2013; Ikrar et al., 2013; Refojo et al., 2011; von Wolff et al., 2011). Although this approach can thereby support data from indirect brain imaging techniques (e.g., fMRI), it was not deployed to detect alterations on the cellular level and, consequently, it is not suited to quantify the contribution of adverse stress effects in distinct neuronal subpopulations of the HIP. Maladaptions in response to chronic stress are not restricted to area CA3 (Magariños and McEwen, 1995; Watanabe et al., 1992) and, although its effects on neurons in area CA1 are less well characterized (Kallarackal et al., 2013; Sousa et al., 2000), it is very likely that adverse effects in both regions contribute to reduced HTC-waves in stressed mice.
As far as known, only two other studies employed VSDI in the HIP to gain evidence for a network-level neurophysiological endophenotype in animal models (Airan et al., 2007; Kim et al., 2012), but none of these studies investigated polysynaptic activity flow. Kim et al. (2012) showed that knockdown of hyperpolarization-activated cyclic nucleotide-gated 1 channels (HCN1) in the dorsal CA1 region resulted in antidepressant behavior in the forced swim test (FST) and was associated with a widespread increase of VSDI signals in response to afferent stimulation of SC. The results of this research support the idea that decreased hippocampal activity is associated with depression-like behavior (Kim et al., 2012; Sheline et al., 2003).
However, Kim et al.'s and the present investigation differ from Airan et al.'s observation of enhanced neuronal activity in area CA1 in response to chronic stress (Airan et al., 2007). Kim et al. (2012) hypothesized that this discrepancy might be related to the brain region under study (ventral vs. dorsal, see discussion below), or the position of stimulus electrode (SC vs. PCL; Kim et al., 2012). Here, this discrepancy most likely results from a different experimental setup. In contrast to the HTC-wave assay, Airan et al. (2007) evoked neuronal activity in stratum pyramidale of CA1. Since CA1 neuronal activity predominantly depends on excitatory drive from CA3 pyramidal neurons, it seems impossible to predict the "net" outcome in CA1 without considering CA3. Similarly their observation of reduced activity in the DG in the same experiments, rises the question how reduced output from upstream DG could result in enhanced activity in downstream CA1 (Airan et al., 2007). Moreover, there is a wealth of evidence showing that chronic

stress has manifold detrimental effects in the HIP causing impairment in spatial navigation (Langston et al., 2010), memory formation (Whitlock et al., 2006), and HPA axis regulation (Radley, 2012), which is difficult to bring into conformity with enhanced output from CA1 pyramidal cells or a generally enhanced neuronal activity in the CA1 network (Kim et al., 2012). Support for Airan et al.'s findings comes from Kallarackal et al. (2013), demonstrating no decrease of AMPA receptor-mediated excitation at SC to CA1 synapses in chronically stressed rats. However, since multifarious adjustments result from chronic stress (Smith et al., 1995; Sousa et al., 2000), a lack of association with AMPA-receptor-mediated excitation does not exclude that other adverse changes in area CA1 contribute to an overall diminished network activity. Direct axonal projections from EC to areas CA3 and CA1 are functionally inactivated in the HTC-wave assay. Stimulation of direct CA1-inputs by Airan et al. might explain the contradicting results. However, this is in contrast to another finding from Kallarackal et al.'s study. They showed that chronic stress reduced AMPA receptor-mediated excitation at PP to CA1 synapses, but again, this does not exclude the implication of other, more pronounced effects which change the "net" outcome.

Next to adjustments in the CA regions, it is important to consider alterations in the DG, a significant factor associated with detrimental stress effects on HTC-waves. Although the input normalization for group comparisons avert detection of chronic stress effects by means of neuronal activity in the DG, the pronounced differences in stimulation intensities between groups indicates an maladaptive hyperexcitability of the DG network. Although it may be counterintuitive that hyperexcitability at the first tier of the HTC reduces activity flow through the HIP, these results are in line with a recent report, in which the authors used VSDI in an animal model of enhanced or reduced neurogenesis (Ikrar et al., 2013). In recent years, neurogenesis has been increasingly recognized as an possible mediator of stress-induced adverse changes in the HIP (Duric and Duman, 2013; Gould and Tanapat, 1999; Santarelli et al., 2003; Snyder et al., 2011). Stress-induced decreases in proliferation of new neurons in the DG subgranular zone is well established, supported by a number of different rodent and primate studies using various types of stress models (Malberg and Duman, 2003; Snyder et al., 2011). Ikrar et al. (2013) demonstrated a modestly increased excitability of the DG in mice in which adult neurogenesis was ablated, likely compatible with the situation observed after chronic stress exposure (Ikrar et al., 2013; Gould and Tanapat, 1999). However, this finding is again in striking contrast to Airan et al. (2007) results, who found that VSDI signals in the DG were reduced after 3 weeks of CMS. Enhanced excitability of DG granule cells is thought to be mediated by compensatory local circuit mechanisms such as reduced excitatory drive onto inhibitory interneurons (Ikrar et al., 2013; Singer et al., 2011). Although, the manipulations of hippocampal neurogenesis did not change the output from granule cells to CA3 pyramidal neurons (Ikrar et al., 2013), it may have important implications for reduced activity flow through the HTC. Since granule cells predominantly exert inhibitory influence onto CA3 pyramidal neurons (di-synaptic feed forward inhibition via SL interneurons) a changed number of granule cells could greatly influence activation patterns

of the CA3 network and subsequent activation of neurons in area CA1 (Ikrar et al., 2013; Mori et al., 2004).

5.2.3 Functional implications of impaired HTC-waves

Impaired HTC-waves support previous research on the HIP, linking detrimental modifications after chronic stress with disturbed hippocampal function (Kim and Diamond, 2002; McEwen, 2001). Elevated stress-hormone levels, induced by chronic stress or exogenously administered CORT, cause suppression of LTP in the HIP *in vitro* and *in vivo* (Alfarez et al., 2003; Bodnoff et al., 1995; Foy et al., 1987; Kim et al., 1996; Pavlides et al., 2002; Xu et al., 1997). Whereas LTP is compromised, the induction of LTD is facilitated both, *in vitro* and *in vivo* (Kim et al., 1996; Xu et al., 1997). Consistently, chronically stressed animals display deficits in HIP-dependent learning paradigms (Diamond et al., 1996). This is in line with a impaired performance of humans in HIP-dependent memory tasks observed after the administration of high doses of CORT (Newcomer et al., 1999) and in depressed individuals (Burt et al., 1995).
Reduced activity flow through the HTC and the related decreased output from area CA1 in response to CSDS has not only important implications for cognitive processes, it might also have negative consequences for termination of the neuroendocrine stress response (Radley, 2012). A wealth of research links chronic stress and elevated GCs in the HIP to disruption of the negative feedback control of the HPA axis, likely promoting a vicious circle and further exacerbation of neuronal damage by excessive production of stress hormones (see 1.3.1.1; Radley and Sawchenko, 2011; Radley, 2012; Jacobson and Sapolsky, 1991). However, several other limbic brain regions integrate stress responses by feedback control of HPA axis activity as indicated by the observation that inhibitory influence is not fully abolished in rodents with a lesioned ventral SUB (Radley, 2012).
Within this framework, a limitation of this study is that the experiments were conducted in dorsal or intermediate parts of the HIP. Although pyramidal neurons in area CA1 are heavily connected to neurons in the subiculum (Amaral et al., 1991), the only relevant extrinsic projections to the PVN arise from ventral parts of the HIP, in particular from the ventral subiculum (Amaral et al., 1991; Andersen et al., 2006). This is consistent with the proposed functions of the ventral (stress and emotional reactions) and dorsal (learning and memory, spatial navigation) HIP (Fanselow and Dong, 2010; Moser and Moser, 1998). However, recent evidence supports the hypothesis that detrimental alterations in response to chronic stress also take place in the ventral zone. Hawley and Leasure (2012) investigated the effects of CUS in the ventral and dorsal HIP. They found that adverse effects on hippocampal physiology (e.g., neurogenesis) were even more severe in ventral parts. Furthermore, several lines of evidence suggest that the three parts of the HIP are not completely isolated from each other, rather they can interact via several routes (Fanselow and Dong, 2010). One important connection is the dorsal zone's projections to the medial septal complex and supramammillary nucleus, because both of these structures send projections back to the ventral HIP. In this way,

pyramidal neurons situated in dorsal parts of area CA1 might gain access to the hypothalamic network and, thus, HPA axis regulation (Fanselow and Dong, 2010). Finally, using fMRI, Campbell and Macqueen (2004) showed reduced posterior hippocampal volume in depressed humans (dorsal HIP in rodents), suggesting that the posterior HIP might be involved in stress associated functions.

5.2.4 Stress effect on HTC-waves is independent from the day of testing

Although CSDS was not stopped after 2 weeks (see 3.1.1), the reduction of FDSs in areas CA3 and CA1 were stable over the entire time of experimentation (6 days). This indicates that detrimental changes in the HIP were present after 14 days of defeat, but this does not exclude the occurrence of additional or more severe alterations of HTC-waves in response to longer periods of stress.
This finding corroborates previous research showing that CSDS robustly increased stress parameters in the HIP after 10 days (Berton and Nestler, 2006; Hartmann et al., 2012; Wagner et al., 2011). However, it is important to note and demonstrated in this study (Figures 4.24C, 4.26, 4.31) that the effects of stress and its mediators are highly variable along a continuum of temporal domains, with frequently opposing modifications in relation to the period of stress exposure (de Kloet et al., 2005; Karst et al., 2005; Magariños and McEwen, 1995).

In summary, refinement of the HTC-wave assay proposes a high-speed imaging approach to compare polysynaptic activity flow through the HIP in animal models of disease. While it was speculated that adverse changes of hippocampal structure and function induced by chronic stress resets input/output relationship (Pavlides et al., 2002), a direct demonstration was missing until now. Moreover, these data suggest impaired activity flow through the HTC, a common circuit-level phenotype of stress-related adjustments in the HIP. This stress-induced dysfunctional hippocampal network may in turn impair the acquisition of new information and negative feedback on HPA axis activity and, thus, lead to cognitive deficits and elevated stress hormone levels that are common in SRPDs. This circuit-centered approach might help, to bridge the gap between molecular, cellular, and morphological changes to behavioral alterations.

5.3 Antidepressant drug action in the hippocampus

The data of the last section points to a shared, circuit-level mechanism of AD drugs in the HIP that works in the opposite direction of chronic stress. The HTC-wave assay in combination with bath application of diverse classes of ADs at low micromolar and high nanomolar concentrations shows that all of them acutely increase the strength of HTC-waves in wild-type and, as exemplary tested for fluoxetine, also in chronic social defeat stress (CSDS) mice. Notably, this effect is not present at 100 nM and in most cases also not at 500 nM, suggesting an monoaminergic system-independent effect. Moreover, the

mood stabilizer lithium, the neurotrophin BDNF and the anesthetic ketamine exert similar modifications, whereas the antipsychotic haloperidol and the anxioloytic diazepam weaken activity percolations through the HIP. Fluoxetine not only enhances HTC-waves rapidly, but is also capable of facilitating LTP of activity percolations through the HIP. Finally, the TrkB receptor ligand ANA-12 blocks the fluoxetine-induced modifications of HTC-waves.

5.3.1 Antidepressants enhance HTC-waves

The present results show that tricyclic ADs (amitriptyline, clomipramine), SSRIs (citalopram, fluoxetine, fluvoxamine), SSNRI (venlafaxine), MAOI (tranylcypromine), and SSRE (tianeptine) acutely enhance neuronal activity waves on the way from the classical hippocampal input region (DG) to an important output region of the HIP (CA1) at therapeutically relevant concentrations (Bolo et al., 2000; Couet et al., 1990; Strauss et al., 1997), irrespective of their pharmacological classification (Richelson, 2001). Together with the finding that fluoxetine is able to facilitate LTP of HTC-waves, this supports the hypothesis that drugs with AD potential cause a rapid and sustained elevation of hippocampal output, linking AD action to a common circuit-level phenotype that counteracts the chronic stress-induced hippocampal impairment (Airan et al., 2007; Kim et al., 2012; Maya Vetencourt et al., 2008; Sapolsky et al., 1986; von Wolff et al., 2011). As already discussed in the previous section, experiments were conducted in dorsal or intermediate parts of the HIP, whereas ventral parts are thought to be primarily involved in brain function associated with emotion and stress (Fanselow and Dong, 2010) and some potent candidate mechanisms (e.g., neurogenesis) for "network" actions of ADs were attributed to this hippocampal segment (Airan et al., 2007; Banasr et al., 2006; Fanselow and Dong, 2010). However, the acute amplification and LTP of HTC-waves by ADs is very unlikely to be mediated by the addition of new cells in the DG, because newly generated granule cells are not considered to contribute to hippocampal physiology before 4 weeks of age (Snyder et al., 2009). Two scenarios might explain the observed effects of ADs on HTC-waves with respect to a functional differentiation of the HIP along its septotemporal axis. First, the same repeating lamellar organization, together with the same serial trisynaptic connectivity throughout the entire HIP, suggests that ADs may have similar effects in brain slices from ventral parts of the HIP (Andersen et al., 2006) or, in contrast, ADs produce inverse effects with respect to different memory functions (e.g., ventral = emotional memory vs. dorsal = spatial memory) that should also be inversely modulated during pharmacological treatment (Fanselow and Dong, 2010). Unfortunately, this hypothesis is difficult to prove since HTC-waves are most reliably generated in slices from the dorsal HIP and very limited data on effects of ADs in the dorsal vs. the ventral zone of the HIP is currently available. Second, emerging evidence suggests dorsal parts of the HIP to be involved in the pathophysiology of SRPDs and to serve as an important site of action for ADs, thereby inhibiting pathological hypoactivity (see 5.2.3; Campbell and Macqueen, 2004; Gould et al., 2007;

Kim et al., 2012). In line with this, genetic modulation of ion channel function in the dorsal HIP has been associated with AD action in animal models (Kim et al., 2012). By using VSDI, Kim et al. show that enhancement of dorsal hippocampal activity by knockdown of HCN1 channels leads to AD-like behaviors in mice (Kim et al., 2012). Interestingly, this was associated with a upregulation of BDNF (see discussion below).

A core symptom of many SRPDs and corresponding animal models is reduced cognitive performance including an impairment of HIP-dependent memories (e.g., spatial and explicit memory; Campbell and Macqueen, 2004; Gould et al., 2007; Pittenger and Duman, 2008; Song et al., 2006), which is strongly associated with dorsal hippocampal function (Krishnan and Nestler, 2008; Morris et al., 1986; Tsien et al., 1996). Consistently, animal models of SRPDs exhibit facilitated LTD and blocked LTP in area CA1, both in *in vitro* and *in vivo* (Foy et al., 1987; Kim et al., 1996; Shors et al., 1989; Xu et al., 1997). Studies investigating the acute effects and chronic administration of ADs on HIP-dependent cognitive functions in patients (respectively animal models of SRPDs) and healthy volunteers (respectively wild type animals) have produced contradicting results (Harmer et al., 2009; Holderbach et al., 2007; Keith et al., 2007; Mowla et al., 2007; Shakesby et al., 2002; Stäubli and Xu, 1995; Vouimba et al., 2006; Vythilingam et al., 2004). For instance, acute application of tianeptine and fluoxetine *in vivo* were found to inversely modulate CA1 LTP (Shakesby et al., 2002). Only tianeptine was able to reverse stress-induced impairment of CA1 LTP, whereas fluoxetine blocked this effect, a finding that is attributed to a differential modulation of monoaminergic signaling by these drugs (Shakesby et al., 2002; see discussion below). At least for animal experiments, these controversial results might be related to methodological issues, since no previous study incorporated the entire hippocampal network instead of isolated subregions or synapses (Holderbach et al., 2007; Von Frijtag et al., 2001; Keith et al., 2007; Shakesby et al., 2002). Since fluoxetine exerts strong effects on CA3 activity (Figure 4.36; Kobayashi et al., 2008), it would also be interesting to investigate fluoxetine effects on MF to CA3 synaptic transmission in Shakesby et al.'s study. However, these mixed results are not supported by the present data, rather they suggest a circuit-level effect of ADs facilitating LTP in the HIP. Together with the observation that acute effects are also present in CSDS mice, this suggests that ADs may counteract SRPDs-related malfunction of cognitive abilities via enhanced neuronal activity flow in the HIP, but also improve cognition in healthy subjects (Mowla et al., 2007). In contrast to hampered activity percolations in response to CSDS, enhanced hippocampal activity after AD treatment may positively influence the activity of the amygdala, prefrontal cortex, hypothalamus, and other brain structures associated with the pathophysiology of SRPDs and, thus, restore normal activity patterns in disease-related brain networks, including the HPA axis (Castrén, 2005; Radley, 2012; Snyder et al., 2011).

Beside classical ADs, several other compounds are known to have AD potential. The neurotrophin BDNF seems to be particularly relevant, since previous data suggests its involvement in both the development of SRPDs (Castrén, 2005) and the action of ADs (Saarelainen et al., 2003). Consistently, BDNF rapidly reduces depression-like behavior

in animal models of depression (Gould et al., 2008; Shirayama et al., 2002). The mood-stabilizer lithium exerts AD effects in animal models and humans and is widely used to treat SRPDs (Smith et al., 2011; Holsboer et al., 2012; Worrall et al., 1979). These findings might explain why BDNF and lithium exert similar adjustments on HTC-waves, when compared to classical ADs. Furthermore, the observation that the antipsychotic haloperidol and the anxiolytic diazepam, two substances with no AD potential (Airan et al., 2007; Holsboer et al., 2012) weakened HTC-waves, suggests that the enhancement of HTC-waves is a characteristic feature of ADs and further support the hypothesis of a common, circuit-level mechanism of ADs in the HIP.

This "net" outcome of acute pharmacological intervention in the HIP is most likely driven by diverse molecular and cellular modifications that operate in a drug-specific manner (Berton and Nestler, 2006; Castrén, 2005; McEwen et al., 2010; Luscher et al., 2011). Several studies have examined acute effects of ADs *in vitro*, but none of these used circuit-centered approaches, like VSDI and varying results were obtained depending on drug type and hippocampal subfield under study (Cai et al., 2013; Kobayashi et al., 2008; Otmakhova et al., 2005). Population responses in area CA1 of the HIP were found to be unchanged or even depressed after application of low micromolar concentrations of ADs or the monoamines serotonin, norepinephrine, and dopamine (Cai et al., 2013; Otmakhova et al., 2005), while fluoxetine at comparable concentrations facilitated serotonine-induced amplification of fEPSPs in area CA3 (Kobayashi et al., 2008). Thus, it is not surprising that a closer inspection of the present data, revealed differences between ADs regarding the position of neuronal activity adjustments in the HTC and their effects as a function of concentration. At least one concentration of all ADs exerted enhancing effects on neuronal activity in area CA1. The only exception is tranylcypromine which weakened activity levels at a concentration of 100 nM. Moreover, only fluoxetine, fluvoxamine, tianeptine, and lithium effects were reminiscent of a classical dose-dependent relationship. All other drugs modified CA1 FDS either at several distinct concentrations (citalopram, venlafaxine) or at a single concentration (TCAs, tranylcypromine, BDNF). In area CA3, only fluoxetine, venlafaxine, tianeptine, and BDNF enhanced FDSs, although not all concentrations were effective when compared to CA1 data, whereas tranylcypromine weakened FDSs at the lowest drug concentration. This analysis further indicates that enhanced activity in area CA3 is always associated with enhanced activity in area CA1, which seems obvious, since activity in CA1 neurons is solely driven by action potential firing of CA3 pyramidal neurons (Figure 3.1A,B). However, enhanced activity in area CA1 is not necessarily associated with enhanced drive from area CA3, pointing to isolated (enhancing) effects of ADs on CA1 neurons, although concentrations that displayed an increase in CA1 only, always exhibited a trend to higher activity levels in area CA3. Thus, drug-induced modifications seem to occur in both, area CA3 and area CA1, which is in agreement with recent research (Cai et al., 2013; Kobayashi et al., 2008; Kole et al., 2002) and the effects of CSDS. Additionally, DG circuitry seems to be largely resistant to AD treatment, except for fluvoxamine at 10 μM and venlafaxine at 1 and 10 μM. These findings are in line with previous reports, predominantly demonstrating

unchanged or depressed neuronal activity in the DG in response to acute AD drug application (Birnstiel and Haas, 1991; Watanabe et al., 1993). The relative insensitivity of DG-FDSs might also be related to the tightly regulated inhibitory network in the DG and the known habituation of granule cells in response to repeated stimuli (Scharfman et al., 1990; Teyler and Alger, 1976). Together, these observations and previous research seem to be quite heterogeneous, what is not surprising, if considering the numerous distinct, region specific and substance specific effects of acute AD drug administration in the HIP (Boldenwatson and Richelson, 1993; Bouron and Chatton, 1999; Cai et al., 2013; Jang et al., 2009; Kobayashi et al., 2008; Kole et al., 2002; Lenkey et al., 2006; Marchetti et al., 2010; Méndez et al., 2012; Otmakhova et al., 2005; Rammes and Rupprecht, 2007; Rantamäki et al., 2007; Rantamäki et al., 2011). Although studies conducted at the molecular or cellular level (Berton and Nestler, 2006), together with previous research using VSDI in hippocampal subregions (Airan et al., 2007), yielded essential insights how ADs may modulate neuronal function via diverse physiological adaptions, receptors, and appendant intracellular signaling cascades, they do not warrant a reliable prediction of a circuit-level mechanism of AD drug action. In turn, the present data is nearly perfectly homogeneous from a network point of view, which further emphasizes the significance of high-speed imaging approaches to dissect complex neuronal network dynamics in response to pharmacological intervention (Airan et al., 2007; Avrabos et al., 2013; Kim et al., 2012; von Wolff et al., 2011). Independent from common cellular mechanisms of AD drugs or region specific changes, at least one concentration increased "net" HTC output. It is important to note that for direct cortical input the same is true compared to what was discussed in previous sections. It has been shown that ADs modulate direct cortical inputs (Cai et al., 2013; Otmakhova et al., 2005), but the prominent effects in the HTC shown here, suggest a major role of the indirect pathway in mediating acute effects of AD drugs.

As mentioned above, nearly all ADs rapidly and effectively elevate the extracellular concentrations of monoamines serotonin or norepinephrine either by blocking their uptake or by blocking their degradation and the classical model of AD action ("monoamine-hypothesis") assumes that SRPDs are characterized by a lack of monoamine neurotransmitters and/or an impaired monoamine function in the brain and that AD treatment reverse this deficit (Berton and Nestler, 2006; Krishnan and Nestler, 2008; Richelson, 2001). Thus, the circuit-level effect induced by ADs might be mediated through acute modulation of monoamine neurotransmission or downstream targets of the associated GPCRs (Richelson, 2001). This seem critical since all ADs tested exert no effect at a concentration of 100 nM, which is clearly above or close to the K_i for noradrenaline/serotonin reuptake inhibition of all drugs tested (Boldenwatson and Richelson, 1993; Tatsumi et al., 1997). Additionally, most of them also exert no effect at a concentration of 500 nM. This might also explain, why the atypical AD tianeptine (a selective serotonine reuptake enhancer; McEwen et al., 2010), which is thought to exert its AD effect via modulation of glutamatergic signaling (Kole et al., 2002; Pillai et al., 2012), enhanced HTC-waves in a comparable manner. Since hippocampal neurons do not produce monoamines and monoaminergic innervation of the HIP is cut during the slicing procedure (Andersen et al., 2006) low

ambient monoamine levels are likely present in brain slices that are constantly superfused with physiological saline (Méndez et al., 2012). This does not exclude contributions from the monoamine system on a longer timescale involving transcriptional and translational changes that initiate neuroplastic processes (Krishnan and Nestler, 2008; Castrén, 2005), but ascribes a major role to monoaminergic-independent mechanisms mediating acute effects of ADs on HTC-waves. In turn, corroborating evidence suggests that ADs modulate various other targets at concentrations markedly higher than those required for norepinephrine/serotonine reuptake inhibition (Cai et al., 2013; Kobayashi et al., 2008; Méndez et al., 2012; Yang and Kuo, 2002). As one example, ADs interact with GABAergic interneurons, which mediate perisomatic inhibition onto CA1 pyramidal neurons (Méndez et al., 2012). This seems relevant since interneurons are indispensable for normal information processing in neuronal networks and their malfunction is related to the pathophysiology of SRPDs (Luscher et al., 2011). Méndez et al. (2012) showed that ADs reduce the amplitude of inhibitory synaptic responses in CA1 pyramidal cells by a reduction of presynaptic GABA release from fast spiking interneurons, a process that might favor excitation in the hippocampal network. Most importantly, these effects occurred after chronic treatment of mice but also after acute administration of imipramine and fluoxetine (10 to 20 μM) to brain slices and the effects were still present after pharmacological occlusion of amine transporters or receptors, whereas lower concentrations of ADs did not effect GABA release (Méndez et al., 2012).

Acute effects of ADs are of particular interest because they conflict a long standing dogma in psychiatric research and take up a major drawback of current pharmacological therapies for SRPDs. ADs rapidly modulate several disease-related brain targets, but it takes weeks to months until they become clinically effective (Krishnan and Nestler, 2008; Méndez et al., 2012; Saarelainen et al., 2003). However, some authors argue that the putative delay bases on "ad hoc-propter hoc evidence" from clinical trials that is still uncritically incorporated into the literature (Katz et al., 2010) and several lines of evidence suggest that ADs act more rapidly (Katz et al., 2010; Novotný and Faltus, 2003; Stassen et al., 1997). The most compelling evidence for faster acting compounds comes from the observation that the anesthetic ketamine produces rapid (minutes to hours) AD responses in patients suffering from MD and in animal models (of disease) (Berman et al., 2000; Autry et al., 2011). Accordingly, ketamine amplifies HTC-waves in the same manner as ADs. In line with this, various acute AD treatment, including all drugs used here, efficaciously reduce the time of immobility in the FST, an animal model which is predictive of AD activity and widely used in psychiatric research for screening of (novel) AD drugs (Autry et al., 2011; Slattery and Cryan, 2012). But how might acute amplification and LTP of HTC-waves by ADs be related to clinical efficacy? In agreement with Méndez et al.'s study, drug effects were only seen with low micromolar concentrations of ADs in acute experiments, suggesting them to be independent from monoaminergic signaling. Consistently, spectroscopic measurements in animals and humans revealed that such concentrations are reached after approximately 4 weeks of drug administration, matching the time point at which ADs therapy usually start to be effective (Bolo et al., 2000;

Strauss et al., 1997; Sugita et al., 1989). This suggests that chronic treatment does not necessarily imply effects to be chronic as well. It still remains elusive, how hippocampal physiology is affected by the various pharmacological intervention in humans and animals (per os, intravenous, intraperitoneal, intracerebral, intraventricular) and how distinct brain concentrations develop over time and influence receptor systems and intracellular signaling cascades (Bolo et al., 2000; Strauss et al., 1997). From all this, it is tempting to speculate that the lengthy treatment with ADs is necessary because ADs fail to become effective until a certain brain concentration threshold is reached, thus possibly leading to acute-like effects after appropriate time of AD drug administration (Méndez et al., 2012).

5.3.2 ANA-12 blocks acute fluoxetine effects

The present work demonstrates that the effects of 10 μM fluoxetine are abolished after TrkB receptor blockade by ANA-12. Recent evidence suggests a crucial role of neurotrophins and their receptors in mediating the molecular and behavioral actions of ADs and chronic stress (Duman and Aghajanian, 2012; Krishnan and Nestler, 2008). This data show that ADs rapidly increase TrkB signaling in the rodent brain *in vitro* and *in vivo*, but the exact mechanism remains elusive (Jang et al., 2009; Koponen et al., 2005; Rantamäki et al., 2007; Rantamäki et al., 2011; Saarelainen et al., 2003). Some studies indicate that ADs directly bind to TrkB receptors (Jang et al., 2009), while other reports suggest that ADs transactivate TrkB receptors via an unknown mechanism and independent from BDNF (Rantamäki et al., 2011). Interestingly, Jang et al. (2009) and Rantamäki et al. (2011) also reported that monoamines are not involved in TrkB activation, which further supports monoaminergic-independent mechanism of AD drug action. However, TrkB receptor activation by BDNF or ADs produce acute AD-like responses in rodents (Saarelainen et al., 2003; Shirayama et al., 2002), while mice with inhibited TrkB signaling or reduced BDNF expression do not respond to ADs in behavioral tests (Saarelainen et al., 2003). These data suggest that activation of TrkB receptors induced by ADs contributes to their effect in rodents. More indirect evidence also points to reduced BDNF levels in brains from patients diagnosed with MD and additionally, carriers of a polymorphism in the BDNF gene have a decreased hippocampal volume, cognitive impairment, and are more vulnerable to suffer from SRPDs (Duman and Aghajanian, 2012; Knable et al., 2004). This might explain, why fluoxetine-mediated amplification of HTC-waves was abolished under TrkB receptor blockade. Although acute AD treatment does not increase synthesis of the main ligand of TrkBs, BDNF (Saarelainen et al., 2003), previous research indicates that acute AD treatment modulates several TrkB-related signaling cascades including phosphorylation of CREB, an important upstream regulator of BDNF synthesis (Rantamäki et al., 2011; Saarelainen et al., 2003). The TrkB-mediated effect of fluoxetine is of particular interest since all AD tested, including lithium and ketamine, have been shown to modulate the TrkB receptor - BDNF system (Autry et al., 2011; Jang et al., 2009; McEwen et al., 2010; Nibuya et al., 1995; Rantamäki et al., 2007; Rantamäki et al., 2011;

Saarelainen et al., 2003). Whether modulation of neurotrophin signaling might be a common mechanism underlying the circuit-level effects of drugs with AD potential remains to determined.

5.3.3 Antidepressants counteract detrimental effects of stress

Stress decreases the strength of HTC-waves and, inversely, ADs increase neuronal activity percolations through the HTC. This suggest a circuit-level mechanism of AD treatment and chronic stress, that bidirectionally modulate hippocampal activity patterns (Cai et al., 2013; Malberg and Duman, 2003). This is broadly consistent with a recent hypothesis in psychiatric research, suggesting that dysregulation of information processing in neuronal networks represents a common final pathway of SRPDs. In turn, ADs are thought to restore the brains capacity to adequately adapt to ongoing environmental changes (Castrén, 2005; Duman and Aghajanian, 2012; Leistedt and Linkowski, 2013). A key assumption of this theory is that new information in the brain is stored within complex neuronal networks and neurotransmitters are necessary to shape these networks in a activity-dependent manner (Castrén, 2013). Corroborating evidence comes from studies showing similar bidirectional effects of chronic stress and ADs in neuronal networks (Castrén, 2005; Malberg and Duman, 2003; Santarelli et al., 2003; Snyder et al., 2011). Within this framework, the modulation of HTC-waves may represent a critical first step that rapidly improves activity patterns in the hippocampal network. One candidate mechanism through which chronic stress and AD might influence network function on longer timescales is TrkB activation and subsequent alteration of BDNF signaling, which have been implicated in both, the adverse changes in response to chronic stress and AD treatment (Duman and Aghajanian, 2012; Saarelainen et al., 2003). The network hypothesis of SRPDs also constitutes a framework for the high comorbidity among SRPDs and their highly overlapping symptom criteria, which is in line with the fact that ADs are effectively used to treat a variety of brain-related diseases (Duman and Aghajanian, 2012; Porsteinsson et al., 2014; Ressler and Mayberg, 2007). However, the observation that many patients relapse to disease even after years of AD treatment argues that pharmacological intervention necessarily triggers other, slower processes such as neurotrophic factor expression and structural plasticity (Duman and Aghajanian, 2012; Krishnan and Nestler, 2008).

In conclusion, this data strongly suggests that AD drug-induced enhancement of HTC-waves is independent from a common cellular mechanism, including monoaminergic signaling. Instead, it is conceivable that these widely used therapeutics mediate their acute effects via a circuit-level effect in the HIP, a novel pharmacological trajectory for their AD properties. These findings underscore the necessity to consider more circuit-centered approaches in psychiatric research to find novel therapeutic approaches for the treatment of SRPDs.

Chapter 6

Future perspective

With the development and characterization of the HTC-wave assay, this dissertation has given an account of and the reasons for the use of circuit-centered approaches as powerful tools to uncover physiologically meaningful neuronal network patterns in the HIP. The empirical findings in this study provide a new understanding how hippocampal neurons selectively respond to entorhinal activity in a frequency and duration-dependent manner. Obviously, they can distinguish relevant and, thus, potentially recollection-worth input from irrelevant one, permitting only significant information presented for a sufficient period to be gated through the HTC for subsequent long-term storage.

There are plenty possible approaches where to go next and how to increase the predictive significance of HTC-waves. It would be of great interest to optogenetically manipulate small sets of entorhinal or DG neurons, or to directly test the existence of HTC-waves on the level of sparse numbers. The light-induced activation of excitatory or inhibitory neurons throughout the HF just as the manipulation of selective neurotransmitter system in a polysynaptic setting may also greatly facilitate the understanding of hippocampal signal processing. Direct innervation of areas CA3 and CA1 was functionally inactivated in the present study. Including these pathways by selective and temporally precise activation or inhibition, either electrically or optogenetically, may also provide further knowledge of their contribution in a comprehensive, hence circuit-centered manner (Suh et al., 2011).

ADs and chronic stress likely affect the HIP via a multitude of molecular, cellular and structural modifications (Duric and Duman, 2013). The present data provides a circuit-level mechanism how these alterations are integrated in a neuronal network, providing interesting applications for future research. The HTC-wave assay might be a valuable tool for screening novel AD drugs, regarding their efficacy to modulate activity flow in the HIP or to directly counteract stress-induced hippocampal impairment in animal models. Although the study has successfully demonstrated that ADs enhance HTC-waves at low micromolar concentrations, it has certain limitations in terms of restricted availability of research investigating therapeutically relevant brain concentrations of these drugs (Bolo et al., 2000; Strauss et al., 1997). Further work needs to be done to establish how brain concentrations of ADs develop over time an how they are associated with clinical efficacy and modulation of specific brain targets.

Beside pharmacological intervention, HTC-waves provide a potent assay to observe neuronal network dynamics in genetically modified animals. For instance, manipulation of neurogenesis in the HIP seems worthwhile, since this mechanism has repeatedly recognized to be involved in AD drug action (Eisch and Petrik, 2012; Santarelli et al., 2003). Furthermore, comparable network approaches are applicable to other brain regions, including the amygdala and the prefrontal cortex, which may help to elucidate the impact of ADs and chronic stress on a broader neurocircuitry that is likely involved in the pathophysiology of SRPDs (Avrabos et al., 2013; Radley, 2012).

Chapter 7

Bibliography

Airan RD, Meltzer LA, Roy M, Gong Y, Chen H, Deisseroth K (2007) High-speed imaging reveals neurophysiological links to behavior in an animal model of depression. *Science* 317:819–23.

Alfarez DN, Joëls M, Krugers HJ (2003) Chronic unpredictable stress impairs long-term potentiation in rat hippocampal CA1 area and dentate gyrus in vitro. *Eur J Neurosci* 17:1928–34.

Alonso A, Llinás RR (1989) Subthreshold Na^+-dependent theta-like rhythmicity in stellate cells of entorhinal cortex layer II. *Nature* 342:175–7.

Amaral DG (1993) Emerging principles of intrinsic hippocampal organization. *Curr Opin Neurobiol* 3:225–9.

Amaral DG, Dolorfo C, Alvarez-Royo P (1991) Organization of CA1 projections to the subiculum: A PHA-L analysis in the rat. *Hippocampus* 1:415–35.

Amaral DG, Scharfman HE, Lavenex P (2007) The dentate gyrus: fundamental neuroanatomical organization (dentate gyrus for dummies). *Dentate Gyrus: A Comphrehensive Guide to Structure, Function, and Clinical Implications* 163:3–22.

Amaral DG, Witter MP (1989) The three-dimensional organization of the hippocampal formation: A review of anatomical data. *Neuroscience* 31:571–91.

Andersen P, Holmqvist B, Voorhoeve PE (1966) Entorhinal activation of dentate granule cells. *Acta Physiol Scand* 66:448–60.

Andersen P, Morris R, Amaral D, Bliss T, O'Keefe J (2006) *The Hippocampus Book*. New York, NY: Oxford University Press.

Anderson IM (2000) Selective serotonin reuptake inhibitors versus tricyclic antidepressants: A meta-analysis of efficacy and tolerability. *J Affect Disord* 58:19–36.

Autry AE, Adachi M, Nosyreva E, Na ES, Los MF, Cheng PF, Kavalali ET, Monteggia LM (2011) NMDA receptor blockade at rest triggers rapid behavioural antidepressant responses. *Nature* 475:91–5.

Avrabos C, Sotnikov SV, Dine J, Markt PO, Holsboer F, Landgraf R, Eder M (2013) Real-time imaging of amygdalar network dynamics in vitro reveals a neurophysiological link to behavior in a mouse model of extremes in trait anxiety. *J Neurosci* 33:16262–7.

Axmacher N, Mormann F, Fernández G, Elger CE, Fell J (2006) Memory formation by neuronal synchronization. *Brain Res Rev* 52:170–82.

Banasr M, Soumier A, Hery M, Mocaër E, Daszuta A (2006) Agomelatine, a new antidepressant, induces regional changes in hippocampal neurogenesis. *Biol Psychiatry* 59:1087–96.

Bauer M, Bschor T, Pfennig A, Whybrow PC, Angst J, Versiani M, Möller HJ, WFSBP (2007) World Federation of Societies of Biological Psychiatry (WFSBP) Guidelines for biological treatment of unipolar depressive disorders in primary care. *World J Biol Psychiatry* 8:67–104.

Berman RM, Cappiello A, Anand A, Oren DA, Heninger GR, Charney DS, Krystal JH (2000) Antidepressant effects of ketamine in depressed patients. *Biol Psychiatry* 47:351–4.

Berry SD, Thompson RF (1978) Prediction of learning rate from the hippocampal electroencephalogram. *Science* 200:1298–300.

Berton O, McClung CA, Dileone RJ, Krishnan V, Renthal W, Russo SJ, Graham D, Tsankova NM, Bolanos CA, Rios M, Monteggia LM, Self DW, Nestler EJ (2006) Essential role of BDNF in the mesolimbic dopamine pathway in social defeat stress. *Science* 311:864–8.

Berton O, Nestler EJ (2006) New approaches to antidepressant drug discovery: Beyond monoamines. *Nat Rev Neurosci* 7:137–51.

Binder EB, Salyakina D, Lichtner P, Wochnik GM, Ising M, Pütz B, Papiol S, Seaman S, Lucae S, Kohli MA, Nickel T, Künzel HE, Fuchs B, Majer M, Pfennig A, Kern N, Brunner J, Modell S, Baghai T, Deiml T, Zill P, Bondy B, Rupprecht R, Messer T, Köhnlein O, Dabitz H, Brückl T, Müller N, Pfister H, Lieb R, Mueller JC, Lõhmussaar E, Strom TM, Bettecken T, Meitinger T, Uhr M, Rein T, Holsboer F, Müller-Myhsok B (2004) Polymorphisms in FKBP5 are associated with increased recurrence of depressive episodes and rapid response to antidepressant treatment. *Nat Genet* 36:1319–25.

Birnstiel S, Haas HL (1991) Acute Eeffects of antidepressant drugs on long-term potentiation (LTP) in rat hippocampal slices. *Naunyn-Schmiedebergs Archives of Pharmacology* 344:79–83.

Bischofberger J, Engel D, Li L, Geiger JR, Jonas P (2006) Patch-clamp recording from mossy fiber terminals in hippocampal slices. *Nature Protocols* 1:2075–81.

Blank T, Nijholt I, Eckart K, Spiess J (2002) Priming of long-term potentiation in mouse hippocampus by corticotropin-releasing factor and acute stress: Implications for hippocampus-dependent learning. *J Neurosci* 22:3788–94.

Bliss TV, Collingridge GL (1993) A synaptic model of memory: Long-term potentiation in the hippocampus. *Nature* 361:31–9.

Bliss TV, Lømo T (1973) Long-lasting potentiation of synaptic transmission in the dentate area of the anaesthetized rabbit following stimulation of the perforant path. *J Physiol* 232:331–56.

Bodnoff SR, Humphreys AG, Lehman JC, Diamond DM, Rose GM, Meaney MJ (1995) Enduring effects of chronic corticosterone treatment on spatial learning,

synaptic plasticity, and hippocampal neuropathology in young and mid-aged rats. *J Neurosci* 15:61–9.

Boeijinga PH, Van Groen T (1984) Inputs from the olfactory bulb and olfactory cortex to the entorhinal cortex in the cat. II. Physiological studies. *Exp Brain Res* 57:40–8.

Boldenwatson C, Richelson E (1993) Blockade by newly-developed antidepressants of biogenic-amine uptake into rat-brain synaptosomes. *Life Sciences* 52:1023–1029.

Bolo NR, Hodé Y, Nédélec JF, Lainé E, Wagner G, Macher JP (2000) Brain pharmacokinetics and tissue distribution in vivo of fluvoxamine and fluoxetine by fluorine magnetic resonance spectroscopy. *Neuropsychopharmacology* 23:428–38.

Borota D, Murray E, Keceli G, Chang A, Watabe JM, Ly M, Toscano JP, Yassa MA (2014) Post-study caffeine administration enhances memory consolidation in humans. *Nat Neurosci* 17:201–3.

Bouron A, Chatton JY (1999) Acute application of the tricyclic antidepressant desipramine presynaptically stimulates the exocytosis of glutamate in the hippocampus. *Neuroscience* 90:729–36.

Burgalossi A, Herfst L, von Heimendahl M, Förste H, Haskic K, Schmidt M, Brecht M (2011) Microcircuits of functionally identified neurons in the rat medial entorhinal cortex. *Neuron* 70:773–86.

Burgess N, Maguire EA, O'Keefe J (2002) The human hippocampus and spatial and episodic memory. *Neuron* 35:625–41.

Burt DB, Zembar MJ, Niederehe G (1995) Depression and memory impairment: A meta-analysis of the association, its pattern, and specificity. *Psychol Bull* 117:285–305.

Buzsàki G (1988) Polysynaptic long-term potentiation: A physiological role of the perforant path-CA3/CA1 pyramidal cell synapse. *Brain Res* 455:192–5.

Buzsàki G (2002) Theta oscillations in the hippocampus. *Neuron* 33:325–40.

Buzsàki G, Haas HL, Anderson EG (1987) Long-term potentiation induced by physiologically relevant stimulus patterns. *Brain Res* 435:331–3.

Bylund DB (2007) Selecting selectivities and the neuropharmacology of antidepressant drug action: A commentary. *FASEB J* 21:3417–8.

Byrne J, Menzel R, Roediger III H, Eichenbaum H, Sweatt J (2008) *Learning and memory: a comprehensive reference.* San Diego, CA: Academic Press.

Cai X, Kallarackal AJ, Kvarta MD, Goluskin S, Gaylor K, Bailey AM, Lee HK, Huganir RL, Thompson SM (2013) Local potentiation of excitatory synapses by serotonin and its alteration in rodent models of depression. *Nat Neurosci* 16:464–72.

Campbell S, Macqueen G (2004) The role of the hippocampus in the pathophysiology of major depression. *J Psychiatry Neurosci* 29:417–26.

Canepari M, Zecevic D (2010) *Membrane potential imaging in the nervous system: Methods and applications.* New York, NY: Springer.

Capocchi G, Zampolini M, Larson J (1992) Theta burst stimulation is optimal for induction of LTP at both apical and basal

dendritic synapses on hippocampal CA1 neurons. *Brain Res* 591:332–6.

Carlson GC, Coulter DA (2008) In vitro functional imaging in brain slices using fast voltage-sensitive dye imaging combined with whole-cell patch recording. *Nature Protocols* 3:249–55.

Carroll, Curtis GC, Mendels J (1976) Neuroendocrine regulation in depression. I. Limbic system-adrenocortical dysfunction. *Arch Gen Psychiatry* 33:1039–44.

Carta M, Lanore F, Rebola N, Szabo Z, Da Silva SV, Lourenço J, Verraes A, Nadler A, Schultz C, Blanchet C, Mulle C (2014) Membrane lipids tune synaptic transmission by direct modulation of presynaptic potassium channels. *Neuron* 81:787–99.

Castrén E (2005) Opinion - Is mood chemistry? *Nature Reviews Neuroscience* 6:241–246.

Castrén E (2013) Neuronal network plasticity and recovery from depression. *JAMA Psychiatry* 70:983–9.

Castrén E, Voikãr V, Rantamäki T (2007) Role of neurotrophic factors in depression. *Curr Opin Pharmacol* 7:18–21.

Cazorla M, Prámont J, Mann A, Girard N, Kellendonk C, Rognan D (2011) Identification of a low-molecular weight TrkB antagonist with anxiolytic and antidepressant activity in mice. *J Clin Invest* 121:1846–57.

Chao MV (2003) Neurotrophins and their receptors: A convergence point for many signalling pathways. *Nat Rev Neurosci* 4:299–309.

Chemla S, Chavane F (2010) Voltage-sensitive dye imaging: Technique review and models. *J Physiol Paris* 104:40–50.

Chen Y, Bender RA, Brunson KL, Pomper JK, Grigoriadis DE, Wurst W, Baram TZ (2004) Modulation of dendritic differentiation by corticotropin-releasing factor in the developing hippocampus. *Proc Natl Acad Sci U S A* 101:15782–7.

Choi YS, Lee MY, Sung KW, Jeong SW, Choi JS, Park HJ, Kim ON, Lee SB, Kim SY (2003) Regional differences in enhanced neurogenesis in the dentate gyrus of adult rats after transient forebrain ischemia. *Mol Cells* 16:232–8.

Chrousos GP (2009) Stress and disorders of the stress system. *Nat Rev Endocrinol* 5:374–81.

Chrousos GP, Gold PW (1992) The concepts of stress and stress system disorders. Overview of physical and behavioral homeostasis. *JAMA* 267:1244–52.

Cipriani A, Furukawa TA, Salanti G, Geddes JR, Higgins JP, Churchill R, Watanabe N, Nakagawa A, Omori IM, McGuire H, Tansella M, Barbui C (2009) Comparative efficacy and acceptability of 12 new-generation antidepressants: A multiple-treatments meta-analysis. *Lancet* 373:746–58.

Claiborne BJ, Amaral DG, Cowan WM (1986) A light and electron microscopic analysis of the mossy fibers of the rat dentate gyrus. *J Comp Neurol* 246:435–58.

Contarino A, Dellu F, Koob GF, Smith GW, Lee KF, Vale W, Gold LH (1999) Reduced anxiety-like and cognitive performance in mice lacking the corticotropin-releasing factor receptor 1. *Brain Res* 835:1–9.

Cooper B, Fuchs E, Flügge G (2009) Expression of the axonal membrane glycoprotein M6a is regulated by chronic stress. *PLoS One* 4:e3659.

Couet W, Girault J, Latrille F, Salvadori C, Fourtillan JB (1990) Kinetic profiles of tianeptine and its MC5 metabolite in plasma, blood and brain after single and chronic intraperitoneal administration in the rat. *Eur J Drug Metab Pharmacokinet* 15:69–74.

Cryan JF, Markou A, Lucki I (2002) Assessing antidepressant activity in rodents: Recent developments and future needs. *Trends Pharmacol Sci* 23:238–45.

Daumas S, Ceccom J, Halley H, Francés B, Lassalle JM (2009) Activation of metabotropic glutamate receptor type 2/3 supports the involvement of the hippocampal mossy fiber pathway on contextual fear memory consolidation. *Learn Mem* 16:504–7.

de Kloet ER, Joëls M, Holsboer F (2005) Stress and the brain: From adaptation to disease. *Nat Rev Neurosci* 6:463–75.

de Kloet ER, Karst H, Joëls M (2008) Corticosteroid hormones in the central stress response: Quick-and-slow. *Front Neuroendocrinol* 29:268–72.

de Kloet ER, Oitzl MS, Joëls M (1999) Stress and cognition: Are corticosteroids good or bad guys? *Trends Neurosci* 22:422–6.

de la Prida LM, Huberfeld G, Cohen I, Miles R (2006) Threshold behavior in the initiation of hippocampal population bursts. *Neuron* 49:131–42.

Diamond DM, Bennett MC, Fleshner M, Rose GM (1992) Inverted-U relationship between the level of peripheral corticosterone and the magnitude of hippocampal primed burst potentiation. *Hippocampus* 2:421–30.

Diamond DM, Fleshner M, Ingersoll N, Rose GM (1996) Psychological stress impairs spatial working memory: Relevance to electrophysiological studies of hippocampal function. *Behav Neurosci* 110:661–72.

Duman RS, Aghajanian GK (2012) Synaptic dysfunction in depression: potential therapeutic targets. *Science* 338:68–72.

Duric V, Duman RS (2013) Depression and treatment response: Dynamic interplay of signaling pathways and altered neural processes. *Cell Mol Life Sci* 70:39–53.

Dwivedi Y, Mondal AC, Rizavi HS, Conley RR (2005) Suicide brain is associated with decreased expression of neurotrophins. *Biol Psychiatry* 58:315–24.

Eder M, Becker K, Rammes G, Schierloh A, Azad SC, Zieglgänsberger W, Dodt HU (2003) Distribution and properties of functional postsynaptic kainate receptors on neocortical layer V pyramidal neurons. *J Neurosci* 23:6660–70.

Eisch AJ, Petrik D (2012) Depression and hippocampal neurogenesis: A road to remission? *Science* 338:72–5.

Ewell LA, Jones MV (2010) Frequency-tuned distribution of inhibition in the dentate gyrus. *J Neurosci* 30:12597–607.

Fanselow MS, Dong HW (2010) Are the dorsal and ventral hippocampus functionally distinct structures? *Neuron* 65:7–19.

Fernandez FR, Malerba P, Bressloff PC, White JA (2013) Entorhinal stellate cells show preferred spike phase-locking to

theta inputs that is enhanced by correlations in synaptic activity. *J Neurosci* 33:6027–40.

Fluhler E, Burnham VG, Loew LM (1985) Spectra, membrane binding, and potentiometric responses of new charge shift probes. *Biochemistry* 24:5749–55.

Foord SM, Bonner TI, Neubig RR, Rosser EM, Pin JP, Davenport AP, Spedding M, Harmar AJ (2005) International Union of Pharmacology. XLVI. G protein-coupled receptor list. *Pharmacol Rev* 57:279–88.

Foy MR, Stanton ME, Levine S, Thompson RF (1987) Behavioral stress impairs long-term potentiation in rodent hippocampus. *Behav Neural Biol* 48:138–49.

Fredholm BB, Bättig K, Holmén J, Nehlig A, Zvartau EE (1999) Actions of caffeine in the brain with special reference to factors that contribute to its widespread use. *Pharmacol Rev* 51:83–133.

Fuchs E, Flúgge G (2003) Chronic social stress: Effects on limbic brain structures. *Physiol Behav* 79:417–27.

Fyhn M, Hafting T, Witter MP, Moser EI, Moser MB (2008) Grid cells in mice. *Hippocampus* 18:1230–8.

Gartlehner G, Hansen RA, Morgan LC, Thaler K, Lux L, Van Noord M, Mager U, Thieda P, Gaynes BN, Wilkins T, Strobelberger M, Lloyd S, Reichenpfader U, Lohr KN (2011) Comparative benefits and harms of second-generation antidepressants for treating major depressive disorder: An updated meta-analysis. *Ann Intern Med* 155:772–85.

Gould E, Tanapat P (1999) Stress and hippocampal neurogenesis. *Biol Psychiatry* 46:1472–9.

Gould NF, Holmes MK, Fantie BD, Luckenbaugh DA, Pine DS, Gould TD, Burgess N, Manji HK, Zarate CA J (2007) Performance on a virtual reality spatial memory navigation task in depressed patients. *Am J Psychiatry* 164:516–9.

Gould TD, O'Donnell KC, Dow ER, Du J, Chen G, Manji HK (2008) Involvement of AMPA receptors in the antidepressant-like effects of lithium in the mouse tail suspension test and forced swim test. *Neuropharmacology* 54:577–587.

Goutagny R, Jackson J, Williams S (2009) Self-generated theta oscillations in the hippocampus. *Nat Neurosci* 12:1491–3.

Groeneweg FL, Karst H, de Kloet ER, Joëls M (2011) Rapid non-genomic effects of corticosteroids and their role in the central stress response. *J Endocrinol* 209:153–67.

Gruart A, Muñoz MD, Delgado-García JM (2006) Involvement of the CA3-CA1 synapse in the acquisition of associative learning in behaving mice. *J Neurosci* 26:1077–87.

Hafting T, Fyhn M, Bonnevie T, Moser MB, Moser EI (2008) Hippocampus-independent phase precession in entorhinal grid cells. *Nature* 453:1248–52.

Hafting T, Fyhn M, Molden S, Moser MB, Moser EI (2005) Microstructure of a spatial map in the entorhinal cortex. *Nature* 436:801–6.

Hammen C (2005) Stress and depression. *Annu Rev Clin Psychol* 1:293–319.

Harmer CJ, O'Sullivan U, Favaron E, Massey-Chase R, Ayres R, Reinecke A, Goodwin GM, Cowen PJ (2009) Effect of acute antidepressant administration on

negative affective bias in depressed patients. *Am J Psychiatry* 166:1178–84.

Hartmann J, Wagner KV, Liebl C, Scharf SH, Wang XD, Wolf M, Hausch F, Rein T, Schmidt U, Touma C, Cheung-Flynn J, Cox MB, Smith DF, Holsboer F, Muller MB, Schmidt MV (2012) The involvement of FK506-binding protein 51 (FKBP5) in the behavioral and neuroendocrine effects of chronic social defeat stress. *Neuropharmacology* 62:332–9.

Hasselmo ME (2005) What is the function of hippocampal theta rhythm?-Linking behavioral data to phasic properties of field potential and unit recording data. *Hippocampus* 15:936–49.

Hawley DF, Leasure JL (2012) Region-specific response of the hippocampus to chronic unpredictable stress. *Hippocampus* 22:1338–49.

Hebb D (2002) *The Organization of Behavior: A Neuropsychological Theory.* Oxford, Ox: Psychology Press.

Henze DA, Urban NN, Barrionuevo G (2000) The multifarious hippocampal mossy fiber pathway: A review. *Neuroscience* 98:407–27.

Henze DA, Wittner L, Buzsáki G (2002) Single granule cells reliably discharge targets in the hippocampal CA3 network in vivo. *Nat Neurosci* 5:790–5.

Herman JP, Adams D, Prewitt C (1995) Regulatory changes in neuroendocrine stress-integrative circuitry produced by a variable stress paradigm. *Neuroendocrinology* 61:180–90.

Herman JP, Mueller NK (2006) Role of the ventral subiculum in stress integration. *Behav Brain Res* 174:215–24.

Ho VM, Lee JA, Martin KC (2011) The cell biology of synaptic plasticity. *Science* 334:623–8.

Holderbach R, Clark K, Moreau JL, Bischofberger J, Normann C (2007) Enhanced long-term synaptic depression in an animal model of depression. *Biol Psychiatry* 62:92–100.

Hollrigel GS, Chen K, Baram TZ, Soltesz I (1998) The pro-convulsant actions of corticotropin-releasing hormone in the hippocampus of infant rats. *Neuroscience* 84:71–9.

Holsboer F (1983) The dexamethasone suppression test in depressed patients: Clinical and biochemical aspects. *J Steroid Biochem* 19:251–7.

Holsboer F (2000) The corticosteroid receptor hypothesis of depression. *Neuropsychopharmacology* 23:477–501.

Holsboer F (2008) How can we realize the promise of personalized antidepressant medicines? *Nat Rev Neurosci* 9:638–46.

Holsboer F, Barden N (1996) Antidepressants and hypothalamic-pituitary-adrenocortical regulation. *Endocr Rev* 17:187–205.

Holsboer F, Gruender G, Benkert O (2012) *Handbuch der Psychopharmakotherapie.* Heidelberg: Springer.

Hsu D (2007) The dentate gyrus as a filter or gate: A look back and a look ahead. *Prog Brain Res* 163:601–13.

Hu W, Zhang M, Czéh B, Flügge G, Zhang W (2010) Stress impairs GABAergic network function in the hippocampus by activating nongenomic glucocorticoid receptors and affecting the integrity of the parvalbumin-expressing

neuronal network. *Neuropsychopharmacology* 35:1693–707.

Iijima T, Witter MP, Ichikawa M, Tominaga T, Kajiwara R, Matsumoto G (1996) Entorhinal-hippocampal interactions revealed by real-time imaging. *Science* 272:1176–9.

Ikrar T, Guo N, He K, Besnard A, Levinson S, Hill A, Lee HK, Hen R, Xu X, Sahay A (2013) Adult neurogenesis modifies excitability of the dentate gyrus. *Front Neural Circuits* 7:204.

Jaarsma D, Postema F, Korf J (1992) Time course and distribution of neuronal degeneration in the dentate gyrus of rat after adrenalectomy: A silver impregnation study. *Hippocampus* 2:143–50.

Jackson MB, Scharfman HE (1996) Positive feedback from hilar mossy cells to granule cells in the dentate gyrus revealed by voltage-sensitive dye and microelectrode recording. *J Neurophysiol* 76:601–16.

Jacobs J, Weidemann CT, Miller JF, Solway A, Burke JF, Wei XX, Suthana N, Sperling MR, Sharan AD, Fried I, Kahana MJ (2013) Direct recordings of grid-like neuronal activity in human spatial navigation. *Nat Neurosci* 16:1188–90.

Jacobson L, Sapolsky R (1991) The role of the hippocampus in feedback regulation of the hypothalamic-pituitary-adrenocortical axis. *Endocr Rev* 12:118–34.

Jang SW, Liu X, Chan CB, Weinshenker D, Hall RA, Xiao G, Ye K (2009) Amitriptyline is a TrkA and TrkB receptor agonist that promotes TrkA/TrkB heterodimerization and has potent neurotrophic activity. *Chem Biol* 16:644–56.

Jankord R, Herman JP (2008) Limbic regulation of hypothalamo-pituitary-adrenocortical function during acute and chronic stress. *Ann N Y Acad Sci* 1148:64–73.

Joëls M (2006) Corticosteroid effects in the brain: U-shape it. *Trends Pharmacol Sci* 27:244–50.

Joëls M, Krugers HJ, Lucassen PJ, Karst H (2009) Corticosteroid effects on cellular physiology of limbic cells. *Brain Res* 1293:91–100.

Jonas P, Major G, Sakmann B (1993) Quantal components of unitary EPSCs at the mossy fibre synapse on CA3 pyramidal cells of rat hippocampus. *J Physiol* 472:615–63.

Jung MW, McNaughton BL (1993) Spatial selectivity of unit activity in the hippocampal granular layer. *Hippocampus* 3:165–82.

Kallarackal AJ, Kvarta MD, Cammarata E, Jaberi L, Cai X, Bailey AM, Thompson SM (2013) Chronic Stress Induces a Selective Decrease in AMPA Receptor-Mediated Synaptic Excitation at Hippocampal Temporoammonic-CA1 Synapses. *J Neurosci* 33:15669–15674.

Kang H, Schuman EM (1995) Long-lasting neurotrophin-induced enhancement of synaptic transmission in the adult hippocampus. *Science* 267:1658–62.

Karayiorgou M, Flint J, Gogos JA, Malenka RC, Genetic, Group NCiPW (2012) The best of times, the worst of times for psychiatric disease. *Nat Neurosci* 15:811–2.

Karst H, Berger S, Turiault M, Tronche F, Schütz G, Joëls M (2005) Mineralocorticoid receptors are indispensable for nongenomic modulation of hippocampal glutamate transmission by corticosterone. *Proc Natl Acad Sci U S A* 102:19204–7.

Karst H, Joëls M (2003) Effect of chronic stress on synaptic currents in rat hippocampal dentate gyrus neurons. *J Neurophysiol* 89:625–33.

Karst H, Joëls M (2005) Corticosterone slowly enhances miniature excitatory postsynaptic current amplitude in mice CA1 hippocampal cells. *J Neurophysiol* 94:3479–86.

Katz MM, Bowden CL, Frazer A (2010) Rethinking depression and the actions of antidepressants: Uncovering the links between the neural and behavioral elements. *J Affect Disord* 120:16–23.

Keith JR, Wu Y, Epp JR, Sutherland RJ (2007) Fluoxetine and the dentate gyrus: Memory, recovery of function, and electrophysiology. *Behav Pharmacol* 18:521–31.

Kempton MJ, Ettinger U, Foster R, Williams SC, Calvert GA, Hampshire A, Zelaya FO, O'Gorman RL, McMorris T, Owen AM, Smith MS (2011) Dehydration affects brain structure and function in healthy adolescents. *Hum Brain Mapp* 32:71–9.

Kew JN, Pflimlin MC, Kemp JA, Mutel V (2002) Differential regulation of synaptic transmission by mGlu2 and mGlu3 at the perforant path inputs to the dentate gyrus and CA1 revealed in mGlu2 -/- mice. *Neuropharmacology* 43:215–21.

Kim CS, Chang PY, Johnston D (2012) Enhancement of Dorsal Hippocampal Activity by Knockdown of HCN1 Channels Leads to Anxiolytic- and Antidepressant-like Behaviors. *Neuron* 75:503–16.

Kim JJ, Diamond DM (2002) The stressed hippocampus, synaptic plasticity and lost memories. *Nat Rev Neurosci* 3:453–62.

Kim JJ, Foy MR, Thompson RF (1996) Behavioral stress modifies hippocampal plasticity through N-methyl-D-aspartate receptor activation. *Proc Natl Acad Sci U S A* 93:4750–3.

Knable MB, Barci BM, Webster MJ, Meador-Woodruff J, Torrey EF, Stanley Neuropathology C (2004) Molecular abnormalities of the hippocampus in severe psychiatric illness: Postmortem findings from the Stanley Neuropathology Consortium. *Mol Psychiatry* 9:609–20, 544.

Kobayashi K, Ikeda Y, Haneda E, Suzuki H (2008) Chronic fluoxetine bidirectionally modulates potentiating effects of serotonin on the hippocampal mossy fiber synaptic transmission. *J Neurosci* 28:6272–80.

Köhler C (1985) A projection from the deep layers of the entorhinal area to the hippocampal formation in the rat brain. *Neurosci Lett* 56:13–9.

Kole MH, Swan L, Fuchs E (2002) The antidepressant tianeptine persistently modulates glutamate receptor currents of the hippocampal CA3 commissural associational synapse in chronically stressed rats. *Eur J Neurosci* 16:807–16.

Kopf SR, Melani A, Pedata F, Pepeu G (1999) Adenosine and memory storage:

Effect of A(1) and A(2) receptor antagonists. *Psychopharmacology (Berl)* 146:214–9.

Koponen E, Rantamäki T, Voikar V, Saarelainen T, MacDonald E, Castrén E (2005) Enhanced BDNF signaling is associated with an antidepressant-like behavioral response and changes in brain monoamines. *Cellular and Molecular Neurobiology* 25:973–980.

Kornhuber J, Schultz A, Wiltfang J, Meineke I, Gleiter CH, Zöchling R, Boissl KW, Leblhuber F, Riederer P (1999) Persistence of haloperidol in human brain tissue. *Am J Psychiatry* 156:885–90.

Kovalchuk Y, Hanse E, Kafitz KW, Konnerth A (2002) Postsynaptic Induction of BDNF-Mediated Long-Term Potentiation. *Science* 295:1729–34.

Kratzer S, Mattusch C, Metzger MW, Dedic N, Noll-Hussong M, Kafitz KW, Eder M, Deussing JM, Holsboer F, Kochs E, Rammes G (2013) Activation of CRH receptor type 1 expressed on glutamatergic neurons increases excitability of CA1 pyramidal neurons by the modulation of voltage-gated ion channels. *Front Cell Neurosci* 7:91.

Krishnan V, Nestler EJ (2008) The molecular neurobiology of depression. *Nature* 455:894–902.

Kukley M, Stausberg P, Adelmann G, Chessell IP, Dietrich D (2004) Ectonucleotidases and nucleoside transporters mediate activation of adenosine receptors on hippocampal mossy fibers by P2X7 receptor agonist 2'-3'-O-(4-benzoylbenzoyl)-ATP. *J Neurosci* 24:7128–39.

Langston RF, Ainge JA, Couey JJ, Canto CB, Bjerknes TL, Witter MP, Moser EI, Moser MB (2010) Development of the spatial representation system in the rat. *Science* 328:1576–80.

Larson J, Lynch G (1986) Induction of synaptic potentiation in hippocampus by patterned stimulation involves two events. *Science* 232:985–8.

Lega BC, Jacobs J, Kahana M (2012) Human hippocampal theta oscillations and the formation of episodic memories. *Hippocampus* 22:748–61.

Leistedt SJ, Linkowski P (2013) Brain, networks, depression, and more. *Eur Neuropsychopharmacol* 23:55–62.

Lenkey N, Karoly R, Kiss JP, Szasz BK, Vizi ES, Mike A (2006) The mechanism of activity-dependent sodium channel inhibition by the antidepressants fluoxetine and desipramine. *Mol Pharmacol* 70:2052–63.

Lépine JP, Briley M (2011) The increasing burden of depression. *Neuropsychiatr Dis Treat* 7:3–7.

Leutgeb JK, Leutgeb S, Moser MB, Moser EI (2007) Pattern separation in the dentate gyrus and CA3 of the hippocampus. *Science* 315:961–6.

Lewis CM, Lazar AE (2013) Orienting towards ensembles: From single cells to neural populations. *J Neurosci* 33:2–3.

Lichtman JW, Conchello JA (2005) Fluorescence microscopy. *Nat Methods* 2:910–9.

Linkenkaer-Hansen K, Monto S, Rytsälä H, Suominen K, Isometsä E, Kähkönen S

(2005) Breakdown of long-range temporal correlations in theta oscillations in patients with major depressive disorder. *J Neurosci* 25:10131–7.

Loew LM (1992) Voltage-sensitive dyes: Measurement of membrane potentials induced by DC and AC electric fields. *Bioelectromagnetics* Suppl 1:179–89.

Longo FM, Massa SM (2013) Small-molecule modulation of neurotrophin receptors: A strategy for the treatment of neurological disease. *Nat Rev Drug Discov* 12:507–25.

López-Muñoz F, Alamo C (2009) Monoaminergic neurotransmission: The history of the discovery of antidepressants from 1950s until today. *Curr Pharm Des* 15:1563–86.

Lowy MT, Gault L, Yamamoto BK (1993) Adrenalectomy attenuates stress-induced elevations in extracellular glutamate concentrations in the hippocampus. *J Neurochem* 61:1957–60.

Lucassen PJ, Vollmann-Honsdorf GK, Gleisberg M, Czéh B, De Kloet ER, Fuchs E (2001) Chronic psychosocial stress differentially affects apoptosis in hippocampal subregions and cortex of the adult tree shrew. *Eur J Neurosci* 14:161–6.

Luscher B, Shen Q, Sahir N (2011) The GABAergic deficit hypothesis of major depressive disorder. *Mol Psychiatry* 16:383–406.

Lynch G, Larson J, Kelso S, Barrionuevo G, Schottler F (1983) Intracellular injections of EGTA block induction of hippocampal long-term potentiation. *Nature* 305:719–21.

MacQueen G, Frodl T (2011) The hippocampus in major depression: Evidence for the convergence of the bench and bedside in psychiatric research? *Mol Psychiatry* 16:252–64.

Magariños AM, McEwen BS (1995) Stress-induced atrophy of apical dendrites of hippocampal CA3c neurons: Comparison of stressors. *Neuroscience* 69:83–8.

Maggio N, Segal M (2007) Striking variations in corticosteroid modulation of long-term potentiation along the septotemporal axis of the hippocampus. *J Neurosci* 27:5757–65.

Maggio N, Segal M (2010) Corticosteroid regulation of synaptic plasticity in the hippocampus. *ScientificWorldJournal* 10:462–9.

Makino S, Schulkin J, Smith MA, Pacák K, Palkovits M, Gold PW (1995) Regulation of corticotropin-releasing hormone receptor messenger ribonucleic acid in the rat brain and pituitary by glucocorticoids and stress. *Endocrinology* 136:4517–25.

Malberg JE, Duman RS (2003) Cell proliferation in adult hippocampus is decreased by inescapable stress: Reversal by fluoxetine treatment. *Neuropsychopharmacology* 28:1562–71.

Malenka RC, Bear MF (2004) LTP and LTD: An embarrassment of riches. *Neuron* 44:5–21.

Malenka RC, Kauer JA, Zucker RS, Nicoll RA (1988) Postsynaptic calcium is sufficient for potentiation of hippocampal synaptic transmission. *Science* 242:81–4.

Maras PM, Baram TZ (2012) Sculpting the hippocampus from within: stress, spines, and CRH. *Trends Neurosci* 35:315–24.

Marchetti C, Tafi E, Middei S, Rubinacci MA, Restivo L, Ammassari-Teule

M, Marie H (2010) Synaptic adaptations of CA1 pyramidal neurons induced by a highly effective combinational antidepressant therapy. *Biol Psychiatry* 67:146–54.

Martín ED, Buño W (2003) Caffeine-mediated presynaptic long-term potentiation in hippocampal CA1 pyramidal neurons. *J Neurophysiol* 89:3029–38.

Maya Vetencourt JF, Sale A, Viegi A, Baroncelli L, De Pasquale R, O'Leary OF, Castrén E, Maffei L (2008) The antidepressant fluoxetine restores plasticity in the adult visual cortex. *Science* 320:385–8.

McCartney H, Johnson AD, Weil ZM, Givens B (2004) Theta reset produces optimal conditions for long-term potentiation. *Hippocampus* 14:684–7.

McEwen BS (1999) Stress and hippocampal plasticity. *Annu Rev Neurosci* 22:105–22.

McEwen BS (2001) Plasticity of the hippocampus: adaptation to chronic stress and allostatic load. *Ann N Y Acad Sci* 933:265–77.

McEwen BS (2007) Physiology and neurobiology of stress and adaptation: Central role of the brain. *Physiol Rev* 87:873–904.

McEwen BS, Chattarji S, Diamond DM, Jay TM, Reagan LP, Svenningsson P, Fuchs E (2010) The neurobiological properties of tianeptine (Stablon): From monoamine hypothesis to glutamatergic modulation. *Mol Psychiatry* 15:237–49.

McEwen BS, Gianaros PJ (2011) Stress- and allostasis-induced brain plasticity. *Annu Rev Med* 62:431–45.

McEwen BS, Weiss JM, Schwartz LS (1968) Selective retention of corticosterone by limbic structures in rat brain. *Nature* 220:911–2.

Méndez P, Pazienti A, Szabó G, Bacci A (2012) Direct alteration of a specific inhibitory circuit of the hippocampus by antidepressants. *J Neurosci* 32:16616–28.

Mennerick S, Chisari M, Shu HJ, Taylor A, Vasek M, Eisenman LN, Zorumski CF (2010) Diverse voltage-sensitive dyes modulate GABAA receptor function. *J Neurosci* 30:2871–9.

Millan MJ, Marin P, Bockaert J, Mannoury la Cour C (2008) Signaling at G-protein-coupled serotonin receptors: Recent advances and future research directions. *Trends Pharmacol Sci* 29:454–64.

Miller EW, Lin JY, Frady EP, Steinbach PA, Kristan WB J, Tsien RY (2012) Optically monitoring voltage in neurons by photo-induced electron transfer through molecular wires. *Proc Natl Acad Sci U S A* 109:2114–9.

Mitchell SJ, Rawlins JN, Steward O, Olton DS (1982) Medial septal area lesions disrupt theta rhythm and cholinergic staining in medial entorhinal cortex and produce impaired radial arm maze behavior in rats. *J Neurosci* 2:292–302.

Mizuseki K, Sirota A, Pastalkova E, Buzsáki G (2009) Theta oscillations provide temporal windows for local circuit computation in the entorhinal-hippocampal loop. *Neuron* 64:267–80.

Moghaddam B, Bolinao ML, Stein-Behrens B, Sapolsky R (1994) Glucocorticoids mediate the stress-induced extracellular accumulation of glutamate. *Brain Res* 655:251–4.

Mori M, Abegg MH, Gähwiler BH, Gerber U (2004) A frequency-dependent switch from inhibition to excitation in a hippocampal unitary circuit. *Nature* 431:453–6.

Morris RG, Anderson E, Lynch GS, Baudry M (1986) Selective impairment of learning and blockade of long-term potentiation by an N-methyl-D-aspartate receptor antagonist, AP5. *Nature* 319:774–6.

Moser MB, Moser EI (1998) Functional differentiation in the hippocampus. *Hippocampus* 8:608–19.

Mott DD, Lewis DV (1992) GABAB receptors mediate disinhibition and facilitate long-term potentiation in the dentate gyrus. *Epilepsy Res Suppl* 7:119–34.

Mowla A, Mosavinasab M, Pani A (2007) Does fluoxetine have any effect on the cognition of patients with mild cognitive impairment? A double-blind, placebo-controlled, clinical trial. *Journal of Clinical Psychopharmacology* 27:67–70.

Murakami S, Imbe H, Morikawa Y, Kubo C, Senba E (2005) Chronic stress, as well as acute stress, reduces BDNF mRNA expression in the rat hippocampus but less robustly. *Neurosci Res* 53:129–39.

Myers B, McKlveen JM, Herman JP (2012) Neural Regulation of the Stress Response: The Many Faces of Feedback. *Cell Mol Neurobiol* 32:683–94.

Nakagami Y, Saito H, Matsuki N (1997) Optical recording of trisynaptic pathway in rat hippocampal slices with a voltage-sensitive dye. *Neuroscience* 81:1–8.

Nakashiba T, Young JZ, McHugh TJ, Buhl DL, Tonegawa S (2008) Transgenic inhibition of synaptic transmission reveals role of CA3 output in hippocampal learning. *Science* 319:1260–1264.

Nehlig A (2010) Is caffeine a cognitive enhancer? *J Alzheimers Dis* 20 Suppl 1:S85–94.

Nestler EJ, Hyman SE (2010) Animal models of neuropsychiatric disorders. *Nat Neurosci* 13:1161–9.

Neumeister A, Wood S, Bonne O, Nugent AC, Luckenbaugh DA, Young T, Bain EE, Charney DS, Drevets WC (2005) Reduced hippocampal volume in unmedicated, remitted patients with major depression versus control subjects. *Biol Psychiatry* 57:935–7.

Neves G, Cooke SF, Bliss TV (2008) Synaptic plasticity, memory and the hippocampus: A neural network approach to causality. *Nat Rev Neurosci* 9:65–75.

Newcomer JW, Selke G, Melson AK, Hershey T, Craft S, Richards K, Alderson AL (1999) Decreased memory performance in healthy humans induced by stress-level cortisol treatment. *Arch Gen Psychiatry* 56:527–33.

Nibuya M, Morinobu S, Duman RS (1995) Regulation of BDNF and trkB mRNA in rat brain by chronic electroconvulsive seizure and antidepressant drug treatments. *J Neurosci* 15:7539–47.

Nicoll RA, Schmitz D (2005) Synaptic plasticity at hippocampal mossy fibre synapses. *Nat Rev Neurosci* 6:863–76.

Nixon MK, Hascoet M, Bourin M, Colombel MC (1994) Additive effects of lithium and antidepressants in the forced swimming test: Further evidence for involvement of the serotoninergic system. *Psychopharmacology (Berl)* 115:59–64.

Novotný V, Faltus F (2003) First signs of improvement with tianeptine in the treatment of depression: An analysis of a double-blind study versus fluoxetine. *European Neuropsychopharmacology* 13:S230–S230.

Numakawa T, Kumamaru E, Adachi N, Yagasaki Y, Izumi A, Kunugi H (2009) Glucocorticoid receptor interaction with TrkB promotes BDNF-triggered PLC-gamma signaling for glutamate release via a glutamate transporter. *Proc Natl Acad Sci U S A* 106:647–52.

Nutt DJ (2002) The neuropharmacology of serotonin and noradrenaline in depression. *Int Clin Psychopharmacol* 17 Suppl 1:S1–12.

Olfson M, Marcus SC (2009) National patterns in antidepressant medication treatment. *Arch Gen Psychiatry* 66:848–56.

Otmakhova NA, Lewey J, Asrican B, Lisman JE (2005) Inhibition of perforant path input to the CA1 region by serotonin and noradrenaline. *J Neurophysiol* 94:1413–22.

Patton PE, McNaughton B (1995) Connection matrix of the hippocampal formation: I. The dentate gyrus. *Hippocampus* 5:245–86.

Pavlides C, Nivón LG, McEwen BS (2002) Effects of chronic stress on hippocampal long-term potentiation. *Hippocampus* 12:245–57.

Pernía-Andrade AJ, Jonas P (2014) Theta-gamma-modulated synaptic currents in hippocampal granule cells in vivo define a mechanism for network oscillations. *Neuron* 81:140–52.

Pillai AG, Anilkumar S, Chattarji S (2012) The same antidepressant elicits contrasting patterns of synaptic changes in the amygdala vs hippocampus. *Neuropsychopharmacology* .

Pittenger C, Duman RS (2008) Stress, depression, and neuroplasticity: A convergence of mechanisms. *Neuropsychopharmacology* 33:88–109.

Poo MM (2001) Neurotrophins as synaptic modulators. *Nat Rev Neurosci* 2:24–32.

Popoli M, Yan Z, McEwen BS, Sanacora G (2012) The stressed synapse: The impact of stress and glucocorticoids on glutamate transmission. *Nature Reviews Neuroscience* 13:22–37.

Porsteinsson AP, Drye LT, Pollock BG, Devanand DP, Frangakis C, Ismail Z, Marano C, Meinert CL, Mintzer JE, Munro CA, Pelton G, Rabins PV, Rosenberg PB, Schneider LS, Shade DM, Weintraub D, Yesavage J, Lyketsos CG, Cit ADRG (2014) Effect of citalopram on agitation in Alzheimer disease: The CitAD randomized clinical trial. *JAMA* 311:682–91.

Pratt AL, Brody DJ, Gu Q (2011) Antidepressant Use in Persons Aged 12 and Over: United States, 2005-2008.

Quilichini P, Sirota A, Buzsáki G (2010) Intrinsic circuit organization and theta-gamma oscillation dynamics in the entorhinal cortex of the rat. *J Neurosci* 30:11128–42.

Radley JJ (2012) Toward a limbic cortical inhibitory network: Implications for hypothalamic-pituitary-adrenal responses following chronic stress. *Front Behav Neurosci* 6:7.

Radley JJ, Sawchenko PE (2011) A common substrate for prefrontal and hippocampal inhibition of the neuroendocrine stress response. *J Neurosci* 31:9683–95.

Raison CL, Miller AH (2003) When not enough is too much: The role of insufficient glucocorticoid signaling in the pathophysiology of stress-related disorders. *Am J Psychiatry* 160:1554–65.

Rammes G, Rupprecht R (2007) Modulation of ligand-gated ion channels by antidepressants and antipsychotics. *Mol Neurobiol* 35:160–74.

Rantamäki T, Hendolin P, Kankaanpää A, Mijatovic J, Piepponen P, Domenici E, Chao MV, Männistö PT, Castrén E (2007) Pharmacologically diverse antidepressants rapidly activate brain-derived neurotrophic factor receptor TrkB and induce phospholipase-Cgamma signaling pathways in mouse brain. *Neuropsychopharmacology* 32:2152–62.

Rantamäki T, Vesa L, Antila H, Di Lieto A, Tammela P, Schmitt A, Lesch KP, Rios M, Castrén E (2011) Antidepressant drugs transactivate TrkB neurotrophin receptors in the adult rodent brain independently of BDNF and monoamine transporter blockade. *PLoS One* 6:e20567.

Refojo D, Schweizer M, Kuehne C, Ehrenberg S, Thoeringer C, Vogl AM, Dedic N, Schumacher M, von Wolff G, Avrabos C, Touma C, Engblom D, Schütz G, Nave KA, Eder M, Wotjak CT, Sillaber I, Holsboer F, Wurst W, Deussing JM (2011) Glutamatergic and dopaminergic neurons mediate anxiogenic and anxiolytic effects of CRHR1. *Science* 333:1903–7.

Remondes M, Schuman EM (2004) Role for a cortical input to hippocampal area CA1 in the consolidation of a long-term memory. *Nature* 431:699–703.

Ressler KJ, Mayberg HS (2007) Targeting abnormal neural circuits in mood and anxiety disorders: From the laboratory to the clinic. *Nat Neurosci* 10:1116–24.

Richelson E (2001) Pharmacology of antidepressants. *Mayo Clin Proc* 76:511–27.

Roozendaal B, Phillips RG, Power AE, Brooke SM, Sapolsky RM, McGaugh JL (2001) Memory retrieval impairment induced by hippocampal CA3 lesions is blocked by adrenocortical suppression. *Nat Neurosci* 4:1169–71.

Rupprecht R, Rammes G, Eser D, Baghai TC, Schüle C, Nothdurfter C, Troxler T, Gentsch C, Kalkman HO, Chaperon F, Uzunov V, McAllister KH, Bertaina-Anglade V, La Rochelle CD, Tuerck D, Floesser A, Kiese B, Schumacher M, Landgraf R, Holsboer F, Kucher K (2009) Translocator protein (18 kD) as target for anxiolytics without benzodiazepine-like side effects. *Science* 325:490–3.

Rutishauser U, Ross IB, Mamelak AN, Schuman EM (2010) Human memory strength is predicted by theta-frequency phase-locking of single neurons. *Nature* 464:903–7.

Rygula R, Abumaria N, Havemann-Reinecke U, Rüther E, Hiemke C, Zernig G, Fuchs E, Flügge G (2008) Pharmacological validation of a chronic social stress model of depression in rats: Effects of reboxetine, haloperidol and diazepam. *Behav Pharmacol* 19:183–96.

Saarelainen T, Hendolin P, Lucas G, Koponen E, Sairanen M, MacDonald E, Agerman K, Haapasalo A, Nawa H, Aloyz R, Ernfors P, Castrén E (2003) Activation of the TrkB neurotrophin receptor is induced by antidepressant drugs and is required for antidepressant-induced behavioral effects. *J Neurosci* 23:349–57.

Sanacora G, Treccani G, Popoli M (2012) Towards a glutamate hypothesis of depression: An emerging frontier of neuropsychopharmacology for mood disorders. *Neuropharmacology* 62:63–77.

Sandi C (2011) Glucocorticoids act on glutamatergic pathways to affect memory processes. *Trends Neurosci* 34:165–76.

Santarelli L, Saxe M, Gross C, Surget A, Battaglia F, Dulawa S, Weisstaub N, Lee J, Duman R, Arancio O, Belzung C, Hen R (2003) Requirement of hippocampal neurogenesis for the behavioral effects of antidepressants. *Science* 301:805–9.

Sapolsky RM, Krey LC, McEwen BS (1984a) Glucocorticoid-sensitive hippocampal neurons are involved in terminating the adrenocortical stress response. *Proc Natl Acad Sci U S A* 81:6174–7.

Sapolsky RM, Krey LC, McEwen BS (1984b) Stress down-regulates corticosterone receptors in a site-specific manner in the brain. *Endocrinology* 114:287–92.

Sapolsky RM, Krey LC, McEwen BS (1986) The neuroendocrinology of stress and aging: The glucocorticoid cascade hypothesis. *Endocr Rev* 7:284–301.

Scharfman HE (1991) Dentate hilar cells with dendrites in the molecular layer have lower thresholds for synaptic activation by perforant path than granule cells. *J Neurosci* 11:1660–73.

Scharfman HE, Kunkel DD, Schwartzkroin PA (1990) Synaptic connections of dentate granule cells and hilar neurons: Results of paired intracellular recordings and intracellular horseradish peroxidase injections. *Neuroscience* 37:693–707.

Scharfman HE, Sollas AL, Smith KL, Jackson MB, Goodman JH (2002) Structural and functional asymmetry in the normal and epileptic rat dentate gyrus. *J Comp Neurol* 454:424–39.

Schatzberg AF (2002) Pharmacological principles of antidepressant efficacy. *Hum Psychopharmacol* 17 Suppl 1:S17–22.

Schmidt B, Marrone DF, Markus EJ (2012) Disambiguating the similar: The dentate gyrus and pattern separation. *Behav Brain Res* 226:56–65.

Seidenbecher T, Laxmi TR, Stork O, Pape HC (2003) Amygdalar and hippocampal theta rhythm synchronization during fear memory retrieval. *Science* 301:846–50.

Shakesby AC, Anwyl R, Rowan MJ (2002) Overcoming the effects of stress on synaptic plasticity in the intact hippocampus: Rapid actions of serotonergic and antidepressant agents. *J Neurosci* 22:3638–44.

Sheline YI, Gado MH, Kraemer HC (2003) Untreated depression and hippocampal volume loss. *Am J Psychiatry* 160:1516–8.

Sheng H, Zhang Y, Sun J, Gao L, Ma B, Lu J, Ni X (2008) Corticotropin-releasing hormone (CRH) depresses n-methyl-D-aspartate receptor-mediated current in cultured rat hippocampal neurons

via CRH receptor type 1. *Endocrinology* 149:1389–98.

Shin LM, Liberzon I (2010) The neurocircuitry of fear, stress, and anxiety disorders. *Neuropsychopharmacology* 35:169–91.

Shirayama Y, Chen AC, Nakagawa S, Russell DS, Duman RS (2002) Brain-derived neurotrophic factor produces antidepressant effects in behavioral models of depression. *J Neurosci* 22:3251–61.

Shors TJ, Seib TB, Levine S, Thompson RF (1989) Inescapable versus escapable shock modulates long-term potentiation in the rat hippocampus. *Science* 244:224–6.

Siapas AG, Lubenov EV, Wilson MA (2005) Prefrontal phase locking to hippocampal theta oscillations. *Neuron* 46:141–51.

Simons SB, Caruana DA, Zhao M, Dudek SM (2012) Caffeine-induced synaptic potentiation in hippocampal CA2 neurons. *Nat Neurosci* 15:23–5.

Singer BH, Gamelli AE, Fuller CL, Temme SJ, Parent JM, Murphy GG (2011) Compensatory network changes in the dentate gyrus restore long-term potentiation following ablation of neurogenesis in young-adult mice. *Proc Natl Acad Sci U S A* 108:5437–42.

Skaggs WE, McNaughton BL, Wilson MA, Barnes CA (1996) Theta phase precession in hippocampal neuronal populations and the compression of temporal sequences. *Hippocampus* 6:149–72.

Slattery DA, Cryan JF (2012) Using the rat forced swim test to assess antidepressant-like activity in rodents. *Nature Protocols* 7:1009–1014.

Slattery DA, Hudson AL, Nutt DJ (2004) Invited review: The evolution of antidepressant mechanisms. *Fundam Clin Pharmacol* 18:1–21.

Smith FE, Cousins DA, Thelwall PE, Ferrier IN, Blamire AM (2011) Quantitative lithium magnetic resonance spectroscopy in the normal human brain on a 3 T clinical scanner. *Magn Reson Med* 66:945–9.

Smith MA, Makino S, Kvetnansky R, Post RM (1995) Stress and glucocorticoids affect the expression of brain-derived neurotrophic factor and neurotrophin-3 mRNAs in the hippocampus. *J Neurosci* 15:1768–77.

Smith SM, Vale WW (2006) The role of the hypothalamic-pituitary-adrenal axis in neuroendocrine responses to stress. *Dialogues Clin Neurosci* 8:383–95.

Snyder JS, Choe JS, Clifford MA, Jeurling SI, Hurley P, Brown A, Kamhi JF, Cameron HA (2009) Adult-Born Hippocampal Neurons Are More Numerous, Faster Maturing, and More Involved in Behavior in Rats than in Mice. *Journal of Neuroscience* 29:14484–14495.

Snyder JS, Soumier A, Brewer M, Pickel J, Cameron HA (2011) Adult hippocampal neurogenesis buffers stress responses and depressive behaviour. *Nature* 476:458–61.

Song L, Che W, Min-Wei W, Murakami Y, Matsumoto K (2006) Impairment of the spatial learning and memory induced by learned helplessness and chronic mild stress. *Pharmacol Biochem Behav* 83:186–93.

Sousa N, Lukoyanov NV, Madeira MD, Almeida OF, Paula-Barbosa MM (2000) Reorganization of the morphology of hippocampal neurites and synapses

after stress-induced damage correlates with behavioral improvement. *Neuroscience* 97:253–66.

Stassen HH, Angst J, Delini-Stula A (1997) Delayed onset of action of antidepressant drugs? Survey of recent results. *Eur Psychiatry* 12:166–76.

Stäubli U, Lynch G (1987) Stable hippocampal long-term potentiation elicited by 'theta' pattern stimulation. *Brain Res* 435:227–34.

Stäubli U, Xu FB (1995) Effects of 5-HT3 receptor antagonism on hippocampal theta rhythm, memory, and LTP induction in the freely moving rat. *J Neurosci* 15:2445–52.

Stepan J, Dine J, Fenzl T, Polta SA, von Wolff G, Wotjak CT, Eder M (2012) Entorhinal theta-frequency input to the dentate gyrus trisynaptically evokes hippocampal CA1 LTP. *Front Neural Circuits* 6:64.

Steward O (1976) Topographic organization of the projections from the entorhinal area to the hippocampal formation of the rat. *J Comp Neurol* 167:285–314.

Stranahan AM, Mattson MP (2010) Selective vulnerability of neurons in layer II of the entorhinal cortex during aging and Alzheimer's disease. *Neural Plast* 2010:108190.

Strauss WL, Layton ME, Hayes CE, Dager SR (1997) 19F magnetic resonance spectroscopy investigation in vivo of acute and steady-state brain fluvoxamine levels in obsessive-compulsive disorder. *Am J Psychiatry* 154:516–22.

Sugita S, Kobayashi A, Suzuki S, Yoshida T, Nakazawa K (1989) Correlative changes of serotonin and catecholamines with pharmacokinetic alterations of imipramine in rat brain. *Eur J Pharmacol* 165:191–8.

Suh J, Rivest AJ, Nakashiba T, Tominaga T, Tonegawa S (2011) Entorhinal cortex layer III input to the hippocampus is crucial for temporal association memory. *Science* 334:1415–20.

Swann JW, Le JT, Lam TT, Owens J, Mayer AT (2007) The impact of chronic network hyperexcitability on developing glutamatergic synapses. *Eur J Neurosci* 26:975–91.

Tasker JG, Di S, Malcher-Lopes R (2006) Minireview: Rapid glucocorticoid signaling via membrane-associated receptors. *Endocrinology* 147:5549–56.

Tatsumi M, Groshan K, Blakely RD, Richelson E (1997) Pharmacological profile of antidepressants and related compounds at human monoamine transporters. *European Journal of Pharmacology* 340:249–258.

Teyler TJ, Alger BE (1976) Monosynaptic habituation in the vertebrate forebrain: The dentate gyrus examined in vitro. *Brain Res* 115:413–25.

Thompson SM, Gähwiler BH (1989) Activity-dependent disinhibition. I. Repetitive stimulation reduces IPSP driving force and conductance in the hippocampus in vitro. *J Neurophysiol* 61:501–11.

Tominaga T, Tominaga Y, Yamada H, Matsumoto G, Ichikawa M (2000) Quantification of optical signals with electrophysiological signals in neural activities of Di-4-ANEPPS stained rat hippocampal slices. *J*

Neurosci Methods 102:11–23.

Toth K, Suares G, Lawrence JJ, Philips-Tansey E, McBain CJ (2000) Differential mechanisms of transmission at three types of mossy fiber synapse. *J Neurosci* 20:8279–89.

Trivedi MH, Rush AJ, Wisniewski SR, Nierenberg AA, Warden D, Ritz L, Norquist G, Howland RH, Lebowitz B, McGrath PJ, Shores-Wilson K, Biggs MM, Balasubramani GK, Fava M, Team SDS (2006) Evaluation of outcomes with citalopram for depression using measurement-based care in STAR*D: Implications for clinical practice. *Am J Psychiatry* 163:28–40.

Tsien JZ, Huerta PT, Tonegawa S (1996) The essential role of hippocampal CA1 NMDA receptor-dependent synaptic plasticity in spatial memory. *Cell* 87:1327–38.

Tsukamoto M, Yasui T, Yamada MK, Nishiyama N, Matsuki N, Ikegaya Y (2003) Mossy fibre synaptic NMDA receptors trigger non-Hebbian long-term potentiation at entorhino-CA3 synapses in the rat. *J Physiol* 546:665–75.

Ulrich-Lai YM, Figueiredo HF, Ostrander MM, Choi DC, Engeland WC, Herman JP (2006) Chronic stress induces adrenal hyperplasia and hypertrophy in a subregion-specific manner. *Am J Physiol Endocrinol Metab* 291:E965–73.

Ulrich-Lai YM, Herman JP (2009) Neural regulation of endocrine and autonomic stress responses. *Nat Rev Neurosci* 10:397–409.

van Groen T, Miettinen P, Kadish I (2003) The entorhinal cortex of the mouse: organization of the projection to the hippocampal formation. *Hippocampus* 13:133–49.

van Strien NM, Cappaert NL, Witter MP (2009) The anatomy of memory: An interactive overview of the parahippocampal-hippocampal network. *Nat Rev Neurosci* 10:272–82.

Von Frijtag JC, Kamal A, Reijmers LG, Schrama LH, van den Bos R, Spruijt BM (2001) Chronic imipramine treatment partially reverses the long-term changes of hippocampal synaptic plasticity in socially stressed rats. *Neurosci Lett* 309:153–6.

von Wolff G, Avrabos C, Stepan J, Wurst W, Deussing JM, Holsboer F, Eder M (2011) Voltage-sensitive dye imaging demonstrates an enhancing effect of corticotropin-releasing hormone on neuronal activity propagation through the hippocampal formation. *Journal of Psychiatric Research* 45:256–261.

Vouimba RM, Muũoz C, Diamond DM (2006) Differential effects of predator stress and the antidepressant tianeptine on physiological plasticity in the hippocampus and basolateral amygdala. *Stress* 9:29–40.

Vyas A, Mitra R, Shankaranarayana Rao BS, Chattarji S (2002) Chronic stress induces contrasting patterns of dendritic remodeling in hippocampal and amygdaloid neurons. *J Neurosci* 22:6810–8.

Vythilingam M, Vermetten E, Anderson GM, Luckenbaugh D, Anderson ER, Snow J, Staib LH, Charney DS, Bremner JD (2004) Hippocampal volume, memory,

and cortisol status in major depressive disorder: Effects of treatment. *Biol Psychiatry* 56:101–12.

Wagner KV, Wang XD, Liebl C, Scharf SH, Müller MB, Schmidt MV (2011) Pituitary glucocorticoid receptor deletion reduces vulnerability to chronic stress. *Psychoneuroendocrinology* 36:579–87.

Wang XD, Chen Y, Wolf M, Wagner KV, Liebl C, Scharf SH, Harbich D, Mayer B, Wurst W, Holsboer F, Deussing JM, Baram TZ, Müller MB, Schmidt MV (2011) Forebrain CRHR1 deficiency attenuates chronic stress-induced cognitive deficits and dendritic remodeling. *Neurobiol Dis* 42:300–10.

Watanabe Y, Gould E, McEwen BS (1992) Stress induces atrophy of apical dendrites of hippocampal CA3 pyramidal neurons. *Brain Res* 588:341–5.

Watanabe Y, Saito H, Abe K (1993) Tricyclic antidepressants block NMDA receptor-mediated synaptic responses and induction of long-term potentiation in rat hippocampal slices. *Neuropharmacology* 32:479–86.

Watson C, Paxinos G, Puelles L (2011) *The Mouse Nervous System* Elsevier Science.

Whitlock JR, Heynen AJ, Shuler MG, Bear MF (2006) Learning induces long-term potentiation in the hippocampus. *Science* 313:1093–7.

WHO (2004) *The global burden of disease: 2004 update.* Geneve, Switzerland: World Health Organization.

Wiegert O, Joëls M, Krugers H (2006) Timing is essential for rapid effects of corticosterone on synaptic potentiation in the mouse hippocampus. *Learn Mem* 13:110–3.

Wigström H, Gustafsson B (1986) Postsynaptic control of hippocampal long-term potentiation. *J Physiol (Paris)* 81:228–36.

Winson J (1978) Loss of hippocampal theta rhythm results in spatial memory deficit in the rat. *Science* 201:160–3.

Witter MP (2007) Intrinsic and extrinsic wiring of CA3: indications for connectional heterogeneity. *Learn Mem* 14:705–13.

Worrall EP, Moody JP, Peet M, Dick P, Smith A, Chambers C, Adams M, Naylor GJ (1979) Controlled studies of the acute antidepressant effects of lithium. *Br J Psychiatry* 135:255–62.

Wrobel S (2007) Science, serotonin, and sadness: The biology of antidepressants: A series for the public. *FASEB J* 21:3404–17.

Xu L, Anwyl R, Rowan MJ (1997) Behavioural stress facilitates the induction of long-term depression in the hippocampus. *Nature* 387:497–500.

Xu L, Holscher C, Anwyl R, Rowan MJ (1998) Glucocorticoid receptor and protein/RNA synthesis-dependent mechanisms underlie the control of synaptic plasticity by stress. *Proc Natl Acad Sci U S A* 95:3204–8.

Yamada M, Yasuhara H (2004) Clinical pharmacology of MAO inhibitors: Safety and future. *Neurotoxicology* 25:215–21.

Yang YC, Kuo CC (2002) Inhibition of Na^+ current by imipramine and related compounds: Different binding kinetics as an inactivation stabilizer and as an open channel blocker. *Molecular Pharmacology* 62:1228–1237.

Ying SW, Futter M, Rosenblum K, Webber MJ, Hunt SP, Bliss TV, Bramham CR (2002) Brain-derived neurotrophic factor induces long-term potentiation in intact adult hippocampus: Requirement for ERK activation coupled to CREB and upregulation of Arc synthesis. *J Neurosci* 22:1532–40.

Zola-Morgan S, Squire LR, Amaral DG (1986) Human amnesia and the medial temporal region: Enduring memory impairment following a bilateral lesion limited to field CA1 of the hippocampus. *J Neurosci* 6:2950–67.

Chapter 8

Appendix

8.1 Chemicals

Tab. 8.1. *Chemicals*

Substance	Chemical Name	Supplier	Solving Medium
ANA-12	N-[2-[[(hexahydro-2-oxo-1H-azepin-3-yl)amino]carbonyl]phenyl]benzo[b]thiophene-2-carboxamide	Tocris	Aqua dest.
BDNF	Brain derived neurotrophic factor, human recombinant (rHuBDNF)	Biomol	Aqua dest.
Amitriptyline hydrochloride	3-(10,11-Dihydro-5H-dibenzo[a,d]cyclohepten-5-ylidene)-N,N-dimethyl-1-propanamine hydrochloride	Sigma-Aldrich	ACSF
1(S),9(R)-(-)-Bicuculline methiodide	[R-(R*,S*)]-5-(6,8-Dihydro-8-oxofuro[3,4-e]-1,3-benzodioxol-6-yl)-5,6,7,8-tetrahydro-6,6-dimethyl-1,3-dioxolo[4,5-g]isoquinolinium iodide	Sigma-Aldrich	ACSF
Caffeine	1,3,7-Trimethylxanthine	Sigma-Aldrich	ACSF
Citalopram hydrobromide	1-[3-(Dimethylamino)propyl]-1-(4-fluorophenyl)-1,3-dihydro-5-isobenzofurancarbonitrile hydrobromide	Sigma-Aldrich	ACSF
Corticosterone	11β,21-Dihydroxy-4-pregnene-3,20-dione,11β,21-Dihydroxyprogesterone	Sigma-Aldrich	Ethanol
Clomipramine hydrochloride	3-Chloro-10,11-dihydro-N,N-dimethyl-5H-dibenz[b,f]azepine-5-propanamine hydrochloride	Sigma-Aldrich	ACSF
CRH	Corticotropine-releasing hormone	Abcam	ACSF
D-APV	D-(-)-2-Amino-5-phosphonopentanoic acid	Abcam	ACSF
DMSO	Dimethyl sulfoxide	Sigma-Aldrich	-
DCG-IV	(2S,2'R,3'R)-2-(2',3'-dicarboxycyclopropyl)glycine	Tocris bioscience	ACSF
Di-4-ANEPPS	4-(2-(6-(Dibutylamino)-2-naphthalenyl)ethenyl)-1-(3-sulfopropyl)pyridinium hydroxide inner salt	Sigma-Aldrich	DMSO
Diazepam	7-Chloro-1-methyl-5-phenyl-3H-1,4-benzodiazepin-2(1H)-one	Sigma-Aldrich	DMSO
Fluvoxamine maleate	(E)-5-methoxy-1-[4-(trifluoromethyl)phenyl]-1-pentanone-O-(2-aminoethyl)oxime maleate	Sigma-Aldrich	ACSF
FLUO	Fluoresceine	Sigma-Aldrich	ACSF
Fluoxetine hydrochloride	(±)-N-Methyl-y-[4-(trifluoromethyl)phenoxy]benzenepropanamine hydrochloride	Sigma-Aldrich	Aqua dest.
Haloperidol	4-[4-(4-Chlorophenyl)-4-hydroxy-1-piperidinyl]-1-(4-fluorophenyl)-1-butanone	Sigma-Aldrich	DMSO
Isoflurane	(±)-Difluormethoxy-1-chlor-2,2,2-trifluorethan	Abbott	-
Ketamine	S-(+)-ketamine hydrochloride	Sigma-Aldrich	Aqua dest.
Lithium chloride	-	Sigma-Aldrich	Aqua dest.
NBQX disodium salt	2,3-Dioxo-6-nitro-1,2,3,4-tetrahydrobenzo[f]quinoxaline-7-sulfonamide disodium salt	Abcam	ACSF
Ponceau S	3-Hydroxy-4-(2-sulfo-4-[4-sulfophenylazo]phenylazo)-2,7-naphthalenedisulfonic acid sodium salt	Sigma-Aldrich	Aqua dest.
Tranylcypromine hydrochloride	Trans-2-phenylcyclopropylamine hydrochloride	Sigma-Aldrich	ACSF
ACSF salts	-	Sigma Aldrich	Aqua dest.
Tianeptine sodium salt	7-[(3-Chloro-6,11-dihydro-6-methyl–5,5-dioxidodibenzo[c,f][1,2]thiazepin-11-yl)amino]heptanoic acid sodium salt	Tocris bioscience	Aqua dest.
Venlafaxine hydrochloride	(+/-)-1-[2-(Dimethylamino)-1-(4-methoxyphenyl)ethyl]cyclohexanol hydrochloride	Sigma-Aldrich	ACSF

(Abcam, Cambridge, UK; Abbott, Chicago, USA; Biomol, Hamburg, Germany; Sigma-Aldrich, St. Louis, USA; Tocris, Bristol, UK)